Tunneling times and excited state interactions between chromophores

Promotor: prof.dr. T.J. Schaafsma, hoogleraar Moleculaire fysica
Copromotoren: dr. G. van der Zwan, universitair docent,
Analytische chemie en toegepaste spectroscopie
dr. J.B.M. Uffink, universitair docent,
Geschiedenis en grondslagen van de wiskunde en de natuurwetenschappen

Samenstelling promotiecommissie: prof.dr. D.G.B.J. Dieks (Universiteit Utrecht)
prof.dr. M. Cohen-Stuart (Wageningen Universiteit)
prof.dr. E.J.H. Südtholter (Wageningen Universiteit)
dr. W.M. de Muijnck (Technische Universiteit Eindhoven)
dr. J.T. Zuilhof (Wageningen Universiteit)

Tunneling times and excited state interactions between chromophores

Regien Stomphorst

Proefschrift
ter verkrijging van de graad van doctor
op gezag van de Rector Magnificus
van Wageningen Universiteit
prof.dr.ir. L. Speelman,
in het openbaar te verdedigen
op 27 April 2001
des namiddags te 16.00 in de aula

Stomphorst, Regien G.
Tunneling times and excited state interactions between chromophores
Thesis, Wageningen Universiteit
ISBN 90-5808-395-0

Stellingen

1. De visualiseerbaarheid van het kwantummechanische tunnelproces laat zien dat de causale of Bohm interpretatie superieur is aan de orthodoxe interpretatie met betrekking tot tunneltijden.
   (Dit Proefschrift, Hoofdstuk 2)

2. Het spectrale profiel voor statistische paren veronderstelt een isotrope omgeving van de paarvormende moleculen. Om spectrale veranderingen als gevolg van deze paarvorming te kunnen waarnemen, moet de afstand tussen de moleculen in de statistische paren zo klein zijn dat hun omgeving ten gevolge van sterische hindering anisotroop is.
   (Dit Proefschrift, Hoofdstuk 4, R. Knox, Spectral effects of exciton splitting in 'statistical pairs', J. Chem. Phys., 98, 7270-7273, 1994)

3. God does not play dice but hide and seek.
   (Naar aanleiding van A. Pais, Subtle is the Lord..., The science and the life of Albert Einstein, Oxford University Press, 1982 p. 440)

4. Toen de jonge Max Planck in 1875 naar de universiteit ging, zei zijn hoogleraar dat hij niet natuurkunde moest gaan studeren omdat er in de natuurkunde niets meer was te ontdekken. Ongeveer 100 jaar later zei Stephen Hawking tijdens zijn inaugurele rede in Cambridge dat het einde van de theoretische natuurkunde in zicht is. Deze opvatting is gebaseerd op het geloof in het bestaan van een 'theorie van het alles'. Dit geloof draagt niet bij tot de vooruitgang van de wetenschap.

5. In de afgelopen jaren is het 'aangeleerd-aangeboren' debat door de tegenvallende resultaten van de maakbare samenleving naar de 'aangeboren' kant opgeschoven.
   (Naar aanleiding van de verlening van een eredoctoraat aan L. Eaves aan de Vrije Universiteit Amsterdam oktober 2000)

6. Het huwelijk is een instelling om problemen samen op te lossen die je niet gehad zou hebben als je alleen gebleven was.
   (Ter nagedachtenis aan George J. Coppens)

7. Als we de verwantschap van de toekomstige koningin niet in ogenschouw nemen, zouden we dat voor onze toekomstige koning ook niet moeten doen.

8. De eis van 'good governance' voor het verlenen van ontwikkelingshulp is net zoiets als kapotte auto's alleen te willen repareren als ze goed rijden.

Regien Stomphorst
Tunneling times and excited state interactions between chromophores
Wageningen, 27-04-01

Contents

VOORWOORD: samenvatting voor niet-specialisten

Voorwoord: samenvatting voor niet-specialisten

Einstein had gelijk toen hij zei
'God dobbelt niet':
Ze speelt verstoppertje!

Al keuvelend bij een drankje doemt soms zomaar de vraag op 'waar gaat jouw proefschrift eigenlijk over?' Ik stamel dan 'iets met kwantummechanica'. Meestal wordt hiermee iedere verdere discussie vermoord. Hoewel ik natuurlijk weleens, al dan niet aangemoedigd, dieper op de zaak ben ingegaan, heb ik veelal het gevoel gehad dat ik niet goed wist waar te beginnen om uit te leggen waar mijn proefschrift over gaat. Daarom heb ik me in dit voorwoord ten doel gesteld een poging te doen op bovengenoemde vraag een antwoord te geven.

Planten hebben in hun bladeren miniatuurfabriekjes. Met behulp van bepaalde kleurstoffen leggen deze 'vluchtige' zonneënergie, vast in 'duurzame' chemische energie. Zonneënergie wordt omgezet in suikers. Deze kleurstoffen zijn de reden dat vrijwel alle planten groen zijn. Bovenstaand proces wordt fotosynthese genoemd en staat aan de basis van alle leven op aarde. Een van de basismechanismen van de fotosynthese is de verhuizing van electronen tussen de verschillende kleurstoffen, de zogenaamde ladingsscheiding. Dit proces is vergelijkbaar met het chemische proces dat in batterijen optreedt, maar dan in tegengestelde richting. Het zou voor het wereld-energievraagstuk natuurlijk ontzettend handig zijn als we dit proces na konden bouwen om zo zonneënergie te gebruiken voor de opwekking van electriciteit (het opladen van batterijen). Het fotosynthetisch proces is nog steeds niet volledig begrepen. Daarom houd ik me in dit proefschrift bezig met de verhuizing (overdracht of transport) van electronen onder invloed van licht en met de wisselwerking van licht en de kleurstoffen, waartoe de verhuislustige electronen behoren.

In het eerste deel van mijn proefschrift behandel ik electronentransport onder invloed van licht. Daarbij gebruik ik de kwantumtheorie om deze electronenoverdracht te beschrijven en kijk ik vooral naar de tijdsduur van de overdracht van electronen. Omdat tijd een lastig begrip is in de kwantumtheorie vergelijk ik de betekenis van dit begrip 'tijd' binnen twee verschillende interpretaties van de kwantumtheorie. Ik maak gebruik van een eenvoudig model om de kleurstofmoleculen te beschrijven. In het tweede deel leg ik de nadruk op de wisselwerking van licht en de kleurstoffen omdat de electronen onderdeel uitmaken van deze kleurstoffen. Met behulp van spectroscopie (wat letterlijk betekent 'kijken met licht') kan de interactie tussen kleurstoffen en licht bestudeerd worden. Dit deel verbindt theorie en experiment en is soms wat gedetailleerd. Het doel van deel 2 was om met de aldus opgedane informatie een betere beschrijving te geven voor het eenvoudige kleurstofmodel uit deel 1. Dat bleek echter niet haalbaar.

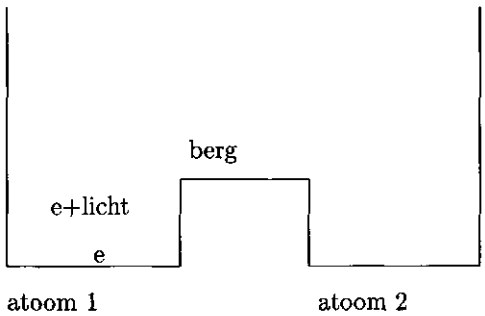

Figure 1: Iedere put stelt een atoom voor. Het systeem wordt door licht in de aangeslagen toestand gebracht (e+licht). De energie van e is dan hoger maar nog niet hoog genoeg om over de (energie)berg heen te gaan. Het electron kan wel van atoom één naar atoom twee tunnelen (door de (energie)berg heengaan).

Deel 1

Electronenoverdracht

Om electronenoverdracht uit te leggen, ga ik even terug naar de middelbare-schoolstof. Een molecuul bestaat uit atomen (die van het periodiek systeem in het scheikundelokaal) en deze atomen op hun beurt bestaan uit positief geladen kernen en negatief geladen electronen, die om die kernen heen draaien. De lichte electronen en de zware kernen voelen zich tot elkaar aangetrokken en blijven daarom in elkaars buurt. Als zich naast dit atoom nog een atoom bevindt, wordt een electron ook door die kern aangetrokken. Onder bepaalde omstandigheden kan het electron van atoom één naar atoom twee gaan, dat heet dan electronenoverdracht. Maar het electron ondervindt op zijn weg van atoom één naar atoom twee touwtrekkerij van beide kernen en dat vindt het niet prettig. De afstand tussen het electron en kern één wordt groter terwijl de afstand tot kern twee nog niet klein genoeg is om daarvoor te compenseren en dat is energetisch ongunstig. Het overbruggen van de ruimte tussen atoom één en twee heet daarom het passeren van een (energie)berg. Het electron moet voldoende energie hebben om over de berg heen te gaan. Dit kun je je voorstellen als een knikker, die over een berg heen moet. Een knikker moet genoeg snelheid (energie) hebben om over de berg heen te komen anders rolt hij terug. In Fig. 1 heb ik dat getekend. Atoom één is een putje en atoom twee ook. In het eerste putje ligt een electron, die heb ik e genoemd. Het is duidelijk dat e niet over de berg heen kan. Dit betekent geen electrontransport. Ik ga het electron helpen met behulp van licht. Het systeem wordt door licht in de aangeslagen toestand gebracht. Het licht zorgt ervoor dat het electron een beetje extra energie krijgt.
In de Fig. 1 heb ik dat weergegeven door e+licht. Als het electron met licht nu wel

genoeg energie heeft om de berg te passeren en naar atoom twee te gaan, spreken we over gewoon electronen transport. Als de energie van dit electron niet voldoende is, zou het electron nog steeds niet in staat moeten zijn om naar atoom twee te gaan omdat het de energieberg niet over kan. In mijn kleurstoffen is de energieberg te hoog voor het electron. Er zou dus geen electronentransport moeten plaatsvinden, toch zijn sommige electronen wel in staat om de berg te passeren. Het lijkt wel alsof ze door de berg heen gegaan zijn. Dat noemen we tunnelen. (Dit tunnelen kan in zeer zeldzame gevallen ook vanuit de toestand zonder licht plaatsvinden.) Het aardige is dat we met behulp van de kwantummechanica dit gedrag kunnen beschrijven. We kunnen zelfs voorspellen hoe groot de kans is dat een electron gaat tunnelen. Omdat tunneling alleen maar binnen de kwantumtheorie gedefinieerd is, vertel ik nu iets over de kwantumtheorie.

De kwantumtheorie

De kwantumtheorie is een wiskundig bouwwerk. De basis van deze theorie is een set afspraken. Dit alles is bedacht om uitkomsten van experimenten te beschrijven en te voorspellen. En de theorie is daar goed in geslaagd. Maar de fysische wereld die de kwantumtheorie ons voorschotelt is bijzonder bizar. Een fysisch systeem ontwikkelt zich in de tijd volgens een wiskundige formule. Als we meten vinden we niet een continue verdeling van resultaten maar een beperkt aantal uitkomsten. Het electron lijkt als het ware in één van de mogelijke uitkomsten te springen. De kans om een bepaalde uitkomst te meten is nauwkeurig bekend maar het valt met geen mogelijkheid te zeggen welke uitkomst gevonden zal worden. Het lijkt dus alsof het electron in een heleboel toestanden tegelijk zit en op het moment dat je meet vind je één discrete uitkomst. De volgende keer dat je meet vind je een andere uit de verzameling discrete mogelijkheden (vandaar kwantumtheorie). De theorie is statistisch: alleen kansen op een bepaalde uitkomst kunnen voorspeld worden. Het electron (e+licht in Fig. 1) wordt beschreven met een wiskundige formule. Als ik na verloop van tijd meet is er een kleine kans dat het electron bij atoom twee zit en dat er dus tunneling is opgetreden. In het dagelijks leven hebben we weinig weet van dit soort kleinschalige effecten. Het is een bizar idee dat je door een muur heen zou kunnen tunnelen naar de andere kant (of door andere auto's heen in de file).
Het doel van de filosofie van de kwantumtheorie is om te bestuderen hoe de fysische wereld eruit ziet als de kwantumtheorie waar is [1]. In de volgende paragraaf zal ik twee richtingen (interpretaties) binnen de filosofie van de kwantummechanica uiteenzetten.

Twee belangrijke natuurkundigen, Niels Bohr en Albert Einstein hebben heel wat over de kwantumtheorie afgediscusieerd [2]. Ze zijn er nooit uitgekomen. Het grappige is dat

[1] Om de bizarre wereld van de kwantumtheorie te beschrijven zijn er vele mooie boeken verschenen. Paul Davies probeerde met een boekje getiteld 'the ghost in the atom' een groot publiek iets te vertellen over de kwantummechanica [1]. George Gamow laat zijn Mr. Tompkins avonturen beleven in de kwantum wereld [2]. Ook het boek 'the emperor's new mind' van Roger Penrose is prachtig maar vraagt wat meer doorzettingsvermogen om het helemaal uit te lezen [3].

[2] Een belangrijke discussie tussen Einstein en Bohr over de kwantumtheorie vond plaats tijdens een conferentie in 1927. Paul Pourveur heeft over deze conferentie een toneelstuk 'Noorderlicht' geschreven

veel natuurkundigen (waaronder ook veel tekstboek-schrijvers) denken dat Bohr gewonnen heeft en daarmee ook de interpretatie van de kwantumtheorie voor eens en altijd heeft vastgelegd. De interpretatie van hem en zijn aanhangers wordt niet voor niets de orthodoxe interpretatie genoemd. Er zijn wel andere interpretaties maar het vergt een filosofische bril om die te zien. De interpretatie doet er niet zoveel toe wanneer je alleen maar geinteresseerd bent in het resultaat van een meting (dat wat wij kunnen waarnemen), die is namelijk onafhankelijk van de manier waarop dat resultaat tot stand komt. In mijn proefschrift bespreek ik zowel de algemeen erkende orthodoxe als de causale interpretatie van de kwantumtheorie.

Twee verschillende interpretaties van de kwantumtheorie

De kwantumtheorie zegt iets over wat de uitkomsten van experimenten (zullen) zijn. Volgens de orthodoxe interpretatie kan er niets gezegd worden over de eigenschappen van het systeem als we niet meten. Volgens deze interpretatie bestaat er geen onafhankelijke wereld buiten ons maar is zij onlosmakelijk verbonden met onze waarneming. In deze wereld kunnen we de zaken niet langer visualiseren omdat de boel te abstract is. De rigoureuze toepassing van causaliteit (=verband tussen oorzaak en gevolg) is niet langer geldig (indeterminisme). De wereld is als het ware wazig totdat je een experiment doet, dan is er iets reëels namelijk de uitkomst van het experiment.

De causale interpretatie kiest voor een visie waarin beide, visualisatie en determinisme behouden blijven. In de causale interpretatie wordt een voorschrift gegeven om vast te stellen langs welk pad een electron zich beweegt, gegeven dat het op dat pad zit. De paden geven de plaats van het electron in de tijd weer. Er valt dus zonder te meten te zeggen waar het electron zich op ieder moment bevindt. De wisselwerking tussen dit deeltje en een meetapparaat geeft een experimentele uitkomst. Omdat het deeltje zich op een bepaald pad bevindt, onafhankelijk van een meting, geldt hier causaliteit, vandaar de naam causale interpretatie. Er zijn echter een heleboel mogelijke paden van de knikker in put één naar put twee te trekken maar we weten niet op welk pad de knikker zit (en dat kunnen we principieel ook niet weten). Kwantumtheorie blijft statistisch onafhankelijk van de interpretatie. Als de causale interpretatie van de theorie consequent wordt doorgevoerd blijkt dat in deze interpretatie localiteit wordt opgegeven. Localiteit wil zeggen dat bij fysische systemen die ruimtelijk gescheiden zijn, een verandering bij één systeem geen onmiddellijke reactie in een ander teweeg kan brengen. Bij niet-localiteit is het mogelijk dat een systeem op de maan instantaan weet als er op aarde een meting aan een ander systeem verricht wordt. In de fysische, klassieke, dus voorkwantumwereld golden zowel causaliteit als localiteit. De kwantumtheorie geeft dus tenminste één van de

[4]. Michael Frayn heeft een toneelstuk geschreven over de ontmoeting tussen de bovengenoemde Niels Bohr en Werner Heisenberg (een Duitse grondlegger van de quantummechanica) in 1941. De voormalige vrienden zijn door de oorlog vijanden geworden. Hun ontmoeting wordt een fiasco en de vraag blijft: 'waarover spraken zij die twee daar onderweg¿ De kwantumtheorie is op kunstige wijze verweven met het beantwoorden van die vraag [5].

twee prijs.

De eerste vorm van de causale interpretatie is al bijna net zo oud als de orthodoxe interpretatie, maar de bedenker ervan, de Borglie, is uitgelachen en heeft hem in 1927 opgegeven. Pas 25 jaar later is de interpretatie weer uit de kast gehaald en toen heeft het nog tot ongeveer 1980 geduurd voordat ze serieus genomen werd. Met behulp van de computer kunnen er mooie plaatjes gemaakt worden van de paden. Dat hielp om de causale interpretatie onder de aandacht te brengen. Cushing, een grote voorvechter van de causale interpretatie beweert in zijn boek [6] dat de orthodoxe interpretatie in het verleden alleen maar standaard geworden is omdat ze betere 'public relations' hadden dan de causale interpretatie. (Het boek ademt wel erg een sfeer van een verdrukte minderheid uit en is evangeliserend van toon.) Of het argument van Cushing waar is, valt nog te bezien. In de volgende paragraaf zal blijken dat de causale interpretatie voor het berekenen van tunneltijden superieur is, maar de interpretatie is zeker niet vrij van problemen als het over andere kwantumvraagstukken gaat. Ze kan dus niet zomaar de orthodoxe interpretatie vervangen.

Tunneltijd en twee interpretaties van de kwantumtheorie

De kwantumtheorie weet niet goed raad met het begrip tijd omdat haar voorschriften geen methode geven voor het meten van tijd. Dat is natuurlijk jammer omdat tijd nu eenmaal een belangrijk concept is. Maar omdat ieder nadeel ook een voordeel kan zijn, kan ik het begrip tijd en met name 'tunneltijd' gebruiken om twee interpretaties met elkaar te vergelijken. Met andere woorden ik wil graag weten of er iets te zeggen valt over de tijd dat een knikker in de berg zit op zijn reis naar de andere kant. Daarom is het interessant te kijken wat de twee verschillende interpretaties te zeggen hebben over de verblijf tijd van de knikkers in de berg. De orthodoxe interpretatie kan de vraag hoe lang het tunnelend electron in de energieberg zit niet beantwoorden omdat er geen meetvoorschrift is. Toch probeerde men binnen de orthodoxe interpretatie wel allerlei formules te geven met de dimensie tijd, maar strikt genomen hebben die geen betekenis. In tegenstelling tot de orthodoxe interpretatie kan de causale interpretatie paden uitrekenen, die de plaats van het electron in de tijd weergeven. Omdat we niet weten volgens welk pad het electron zich beweegt, kunnen we alleen een gemiddelde tunneltijd uitrekenen. Ik concludeer dat de causale interpretatie tunnel tijden beter kan definiëren dan de orthodoxe interpretatie.

Deel 2

Wisselwerking licht en kleurstof

In het eerste deel heb ik de electronen opgevat als knikkers die in een put liggen en die over een berg heen moeten. Het electron wordt welliswaar naar een iets hoger gedeelte getild door lichtenergie, maar dat is nog steeds lager dan de berg. In dit deel ga ik gedetailleerder naar de put kijken. Ik kijk naar de wisselwerking tussen kleurstofmoleculen en licht met behulp van spectroscopie. De put wordt gevormd door een kleurstofmolecuul, een

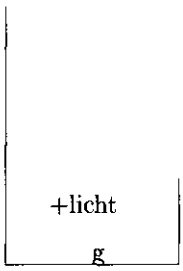

Figure 2: Het electron is onderdeel van een ingewikkeld kleurstofmolecuul. De wisselwerking tussen de grondtoestand (g) en de aangeslagen toestand (+licht) geeft informatie over de relatie tussen de verschillende putjes.

ingewikkeld systeem bestaande uit atomen en electronen die niet langer bij één atoom horen, maar over het molecuul zweven. Licht bestaat volgens de kwantummechanica uit pakketjes, de fotonen. De wisselwerking tussen kleurstofmoleculen en licht geeft een heleboel indirecte informatie over het systeem. Vòòr de licht opname spreekt men van de grondtoestand. Na de lichtopname is het molecuul in een aangeslagen toestand. Dit putje-electron complex bepaalt hoe er lichtpakketjes worden opgenomen. Het pakketje energie dat de knikkers opnemen, moet dus aan allerlei eisen voldoen. Die eisen geven informatie over de putten, de kleurstoffen waar de electronen onderdeel vanuit maken. In dit tweede deel kijk ik dus niet meer naar electronenoverdracht maar naar de wisselwerking tussen putten en lichtenergie. Ik concentreer me dus op het linker deel van het putje zoals weergegeven in Fig. 2.

De kleurstof experimenten

Ik heb twee experimenten uitgevoerd om de wisselwerking tussen kleurstoffen en licht te bestuderen.
In het eerste experiment heb ik de kleurstof erythrosine b opgelost in een smerig organisch goedje (DMSO genaamd) en dat samen met plastic korrels gekookt. Nadat alles goed gemengd was, heb ik dat DMSO eruit gedampt. Het plastic vormt daardoor een laagje met daarin de kleurstof. De verschillende plastic filmpjes bevatten verschillende concentraties kleurstoffen. Ik heb toen gekeken wat de invloed is van de concentratie op de manier waarop de kleurstoffen licht opnemen (en weer afstaan). Eerst zitten de kleurstofmoleculen ver uit elkaar, ze zijn dan éénlingen. Naarmate de concentratie hoger wordt, moeten ze steeds dichter bijelkaar gaan zitten door ruimte gebrek, het zijn dan meerlingen.
In het tweede experiment zijn pannekoekvormige kleurstofmoleculen, porfyrines genaamd met behulp van kleine moleculen op 4 verschillende manieren aan elkaar gesmeed. Deze

tweelingen (dimeren) zijn opgelost in tolueen. Ik heb gekeken naar de manier waarop de 4 verschillende dimeren licht absorberen. Ik heb dus in feite allerlei verschillende putjes met knikkers gemaakt.

Invloed van kleurstof concentratie in films op spectroscopie

Bij hele lage concentraties van de langgerekte kleurstoffen (erythrosine b) in een film, zitten de moleculen bijna allemaal ver bij elkaar vandaan. Ze zijn éénlingen (monomeren). Maar omdat ze willekeurig ten opzichte van elkaar zitten, zijn er op grond van de statistiek zo nu en dan twee die wel dicht bij elkaar zitten. Die twee vormen dan een concentratie paar. Als we nu een éénling kleurstofmolecuul extra energie geven met behulp van licht komt het dus in de aangeslagen toestand. Er kunnen dan 3 dingen gebeuren.

1. Deze extra energie kan weer afgestaan worden, dat kun je zien als fluorescentie.
2. Het licht kan ook aan een andere éénling geven worden en die kan dan gaan fluoresceren.
3. De lichtenergie kan ook aan een concentratie paar geven worden, je ziet dan geen fluorescentie, want er is geen éénling om te fluoresceren.

Het gaat hier om het doorgeven van lichtenergie, dus niet het doorgeven van electronen. Hier is sprake van energietransport niet van tunneling. De drie manieren waarop een opgenomen lichtpakketjes weer wordt afgestaan aan de buitenwereld zegt iets over de afstand tussen de putjes met electronen.
Bij hogere kleurstof concentraties zitten de moleculen zo dicht bij elkaar dat er geen éénlingen meer zijn om licht op te nemen (en dus ook niet om het weer af te staan) maar dat er alleen meerlingen zijn om licht op te nemen. Er valt in het experiment te zien dat meerlingen licht op een andere manier opnemen dan éénlingen. De putjes met knikkers zitten zo dicht bij elkaar dat geen afzonderlijke putjes met knikkers meer zijn ten opzichte van lichtpakketjes. Ik heb toen met behulp van een groot computer programma laten uitrekenen hoe die langgerekte meerlingen ten opzichte van elkaar het liefst zitten. Deze oriëntaties heb ik in de theorie over licht opname voor meerlingen gestopt en vergeleken met de experimentele gegevens. De conclusie van dit hoofdstuk is dat de concentratie van de kleurstoffen van invloed is op de manier waarop er licht opgenomen wordt. Als de putjes met knikkers dicht bij elkaar zitten heeft dat dus invloed op de grootte van de lichtpakketjes die ze opnemen.

Spectroscopie van dimeren

In het tweede experiment is gebruik gemaakt van porphyrine kleurstofmoleculen. De orientaties van de éénlingen binnen een tweeling (dimeer) is van groot belang voor de manier waarop de tweelingen licht opnemen. De oriëntatie van een putje ten opzichte van een ander putje waarmee het een eenheid vormt is van belang voor de grootte van de opgenomen lichtpakketjes. Ik heb met spectroscopie gekeken hoe de 4 verschillende

dimeren (van de porphyrine kleurstof) licht opnemen. Om een verklaring te vinden voor de experimentele gegevens, moest de bestaande theorie uitgebreid worden omdat die niet geschikt was voor pannekoekvormige moleculen. De theorie was bedoeld voor langerekte moleculen waarbij, alleen de lengterichting van belang was voor het opnemen van lichtpakketjes. Voor pannekoekvormige porphyrine moleculen zijn er twee loodrecht op elkaar staande richtingen waarin licht opgenomen kan worden. De bewegingsvrijheid van de monomeer eenheden ten opzichte van elkaar binnen de dimeren heb ik op grond van hoe ze elkaar hinderen, beredeneerd en toen uitgerekend hoe de spectroscopische gegevens er theoretisch uit zouden moeten zien. In Fig. 6.3 kun je zien hoe goed experiment en theorie op elkaar aansluiten.

Tenslotte

Het bleek ondoenlijk in het tijdsbestek van dit proefschrift om de resultaten uit het spectroscopisch onderzoek terug te vertalen naar een betere beschrijving van de aangeslagen toestand in een tunnelprobleem. De uitwerking daarvan is toekomstmuziek.

Voor degene die het om de knikkers gaat:
In deel 1 heb ik knikkers in putjes gelegd en ze toen sprongetjes laten maken door er lichtpakketjes op af te sturen. Ik ben toen gaan kijken hoe lang de knikkers er (gemiddeld) over doen om kwantummechanisch door de berg heen te gaan. In deel 2 heb ik me bezig gehouden met de relatie van putten met de knikkers en de lichtpakketjes.

Chapter 1

INTRODUCTION

1.1 THE ORIGINS OF QUANTUM MECHANICS AND ITS INTERPRETATION

It is told that when the young Max Planck entered the University of Munich in 1875, the physics professor strongly urged him not to study science. In his opinion there was little left to be discovered [7]. Fortunately, Planck disregarded this advice. Instead, he went his own way and made a great contribution to the development of quantum mechanics which, in the decades to follow, turned physics upside down. In the philosophy of science the occasions when scientists adopt theories that are radically different from their predecessors have been coined scientific revolutions. Quantum theory definitely qualifies for this status [8, 9]. The quantum theory had a shocking impact on the scientific and philosophical view of the physical world surrounding us. Even outside the scientific community, the world never looked the same anymore [10].

The components of the mature formulation of the quantum theory were assembled in the period around 1925-1933. A crucial episode in this development was the 5th Solvay Conference in 1927. The founders of quantum mechanics, in particular Planck, Einstein, Bohr, Heisenberg, Schrödinger, Dirac and de Broglie, all attended this Conference which is often referred to as the starting point of the Einstein-Bohr debate [11] about the interpretation of quantum theory. In this Thesis, many aspects of the original work of each of the founding fathers return in some form. The disagreement between Einstein and Bohr is one of the major controversies in modern scientific history. The debate is about what a physical theory ought to be, in other words: about what kind of description of the universe we should regard satisfactory [12]. In particular, the question was whether the existing quantum theory provided a complete account of the microphysical phenomena or whether the analysis should and could be carried further to a more detailed level. Bohr relied heavily on the indeterminacy relations, formulated by Heisenberg [13]. Einstein, on the other hand, basically disagreed with this view and set out at demonstrating that an exact space-time path of an individual system can be specified, together with a detailed specification of the momentum [14]. Although the controversy was never solved, even today many (in particular experimental) physicists believe that Bohr solved the basic problems and even that his interpretation is the only existing one. The views of Bohr and his school are commonly referred to as 'the orthodox' or Copenhagen interpretation, although this school never reached full agreement on a single consistent interpretation, resulting in quite significant variations in its point of view. We will rely on the most commonly used interpretation, which is mainly based on the work of the mathematician Von Neumann [15].

The pilot wave theory of de Broglie, another participant of the Solvay Conference, was the forerunner of the so-called causal interpretation of quantum mechanics. Ironically, de Broglie's ideas were received with despises [16], and he withdrew his proposal. Twenty five years after the Solvay conference Bohm revived the idea of the Broglie, forming the present basis of the causal interpretation [17], which in this Thesis is compared with the

orthodox interpretation of quantum mechanics.

Other interpretations like many worlds [18], many minds [19], consistent histories [20, 21], pure ensemble interpretations [22] and their variations and combinations are beyond the scope of this Thesis and therefore will not be discussed.

The quantum theory has been experimentally very successful in explaining and predicting a variety of phenomena at the microscopic and even at the macroscopic level. As a working theory, it does not make any statements about the system unless an experiment is performed. The theory only explains and predicts outcomes of experiments. Despite its experimental success, the philosophical foundations of the quantum theory are nevertheless controversial. Physicists and philosophers disagree about what quantum mechanics can says about the physical world and what is real or what exists or what we think there exists in the physical world.

It is generally accepted that according to quantum mechanics the seemingly simple physical world surrounding us is actually very odd. Accordingly, the purpose of studying the philosophical and physical consequences of quantum theory is to define the various options of how the physical world could look like, assuming the validity of quantum mechanics. One result is already clear: we may adopt a world view with a loss of visualization, i.e. a high level of abstractness and indeterminism, i.e. the non-validity of rigorous causality. We can also choose for a view which retains visualization and determinism, but sacrifices locality. This view is the causal interpretation of quantum mechanics. Non-locality in this theory has the effect that measurements at a particular position have instantaneous effects on other systems, even when their spatial positions are far apart.

In Chapter 2 of this Thesis, the orthodox interpretation and causal interpretation are compared with respect to tunneling times. In contrast to the orthodox view, the causal interpretation provides an unambiguous way to define tunneling times.

1.2 THE CAUSAL INTERPRETATION

In the causal interpretation [23] of quantum theory a particle has a well-defined position and velocity at each instant of time. Its motion is causally determined by a so-called guidance field [24]. Integration of the velocity subject to initial conditions yields the particle trajectories. In this Thesis the relation between position and time, shown by the trajectories, is investigated, because this relation contains information about the duration and velocity of the process. In 1952 when Bohm presented these ideas [25], a hidden variable theory, to the outside world, Einstein and others did not pay much attention. Bell was impressed, however, and wrote a paper [26] in which he questioned the relevance of von Neumann's proof for the non- existence of hidden variables. Because the relevance of this proof had not been interrogated for more than 30 years, this was such a courageous deed

that Bell managed to attract attention (Although not at the time he handed in his paper, because it got lost and was only published two years later). In the eighties and nineties the theory received finally ample attention.

1.3 ELECTRON TRANSPORT AND TUNNELING TIME

So far the two different interpretations of quantum mechanics have remained rather abstract. The next part of this Thesis focuses on the non-classical phenomenon of electron tunneling, for which the two interpretations are highly relevant. Electron tunneling is also at the basis of one of the most important biological processes on earth, i.e. photosynthesis. The primary steps of this process are [27]: (i) absorption of solar photons in the visible spectral region by a specialized antenna system containing different photosynthetic pigments, organized in complexes with proteins; (ii) very efficient transport of the excitation energy through this system to a so- called reaction center, where (iii) electron transfer takes place from a photo-excited donor molecule in the reaction center to an acceptor molecule.

As long as the electrons possess enough kinetic energy to pass the potential barrier formed by the protein between the donor and acceptor molecules, a classical model can be used to calculate the transfer rate [28]. Without sufficient kinetic energy to overcome this barrier tunneling models are necessary to calculate the electron transfer rate. Although some critical remarks were made [29], it is generally believed that tunneling may play a role in biological systems even at physiological temperatures [30]. Tunneling is associated with temperature-independent reaction rates. Indeed, below $\approx 150K$ electron transfer in photosynthetic reaction centers still occurs, and its rate becomes independent of temperature. Note however that one can not infer that tunneling does not occur when the rate is temperature dependent [31].

In this Thesis the process of photosynthesis is modelled by isolated chromophores. To study the behavior of these isolated chromophores, they are dissolved in liquids or polymer matrices [32]. Just as the proteins in photosynthesis, these media are isolating substances and hence function as high potential barriers between the chromophores. The electrons need to tunnel through these high potential barrier to travel from one chromophore to another. Hence, in this Thesis the electron transfer process is described by tunneling. The chromophores are modelled as low energy areas for the electrons, while the gap is the potential barrier between the molecules. This model provides the possibility to describe the electron wave functions analytically. Both the ground state and the excited state wave functions can be determined.

Tunneling is a purely quantum mechanical phenomenon. Although it is discussed in any

quantum theory text book, its implications are still subject of conferences [33]. One of these implications concerns the time it takes to tunnel through a potential barrier. In fact time is a complicated subject in quantum mechanics because time is not an operator but enters the Schrödinger equation as a parameter. In quantum mechanics every observable corresponds to an Hermitian operator and a series of measurements of an ensemble of systems is predicted to yield the expectation value of the dynamical variables. Wave functions yield probabilities for the results of suitable measurements. Because time lacks an operator, the orthodox approach does not provide a clear-cut answer for the question about the duration of tunneling processes. In the causal interpretation a particle has a well-defined position and velocity at each instant of time. Therefore, this interpretation can be applied to the problem of tunneling time and provides a well-defined answer to the question how long each particle takes to cross the barrier. The question has been raised whether the tunneling time problem could serve as a crucial test to demonstrate an alleged superiority of the causal interpretation above the orthodox interpretation. Superficially the fact that the causal interpretation offers a clear-cut answer, where the orthodox approach is as yet unable to provide an unambiguous meaningful analysis seems to provide a clear advantage. However, in Chapter 3 we argue that conceptually clear definitions are not necessarily experimentally measurable.

1.4 EXCITED STATE INTERACTIONS

As implied by the results in Chapter 3, for the calculation of electron- and energy transfer rate constants the wave function describing the initial and final states, as indicated below, must be known. These interactions are controlling two different processes:

Process	Initial state		Final state
Electron transfer	D^*A	$\rightarrow$	D^+A^-
Energy transfer	D^*A	$\rightarrow$	DA^*

where D and A represent the donor and the acceptor for both processes. As is evident from the above mentioned equations the initial state for both processes is the same. For particular combinations of the highest occupied molecular orbital energy (HOMO) of D and the lowest unoccupied molecular orbital (LUMO) energy of A electron- and energy transfer may be competing decay channels of the excited state.

In Chapters 4, 5, and 6 the interactions between a chromophore in the lowest excited state with neighboring chromophores in the ground state, including energy transfer, are therefore explored using optical spectroscopy. A description of the optical spectra in terms of an excitonic model is used to explain the experimental results.

Following absorption of a photon by a monomeric chromophore, the excitation energy can

be transferred to other neighboring monomeric chromophores in their electronic ground state. The excited chromophore might also return to the ground state, releasing the excitation energy as fluorescence. If the energy is transferred to dimeric chromophores, no fluorescence is observed, hence the process is often referred to as fluorescence quenching. While the dimeric structures were called statistical pairs by Knox [34], the name quenching pairs is preferred in this Thesis. The name 'statistical pairs' suggests, that the dimeric structures are formed by randomly orientated chromophores. However, at sufficiently high concentration, the shape of the chromophores causes the monomers in these structures to occur only in preferential mutual orientations.

This Thesis treats the interactions between an excited dye molecule and its neighboring molecules of the same type in the ground state (homo-molecular interactions). By embedding the dyes in polymer matrices they are immobilized within the fluorescence life time [32]. Although the polymer matrices resemble in this sense the protein environment of the pigments in the photosynthetic systems, other properties of the proteins are lacking: the proteins dictate the positions and orientations of the chromophores, whereas in the polymer matrices the positions and orientations of the chromophores are more flexible. Also the protein environment of photosynthetic antenna pigments favors fast and efficient excitation energy transport, whereas the chromophores in polymer matrices loose their energy easily. This energy loss is studied in this Thesis by fluorescence and fluorescence quenching of chromophores.

1.5 CHROMOPHORES AND ABSORPTION SPECTROSCOPY

The transition of chromophore molecules from the ground state to an excited state only occurs when light is absorbed with a preferential polarization. This preference is determined by the angle of the transition dipole moment(s) $\vec{\mu}$ of the dye molecules with respect to the electric field vector of the incident light. The transition dipole moments transform as vectors and are intrinsic properties of the dye molecule: the length of the vector, representing the transition dipole moment, determines the maximum absorption intensity of the corresponding transition and the direction of the vector the sensitivity of the absorption intensity to the polarization direction of the incident light. When monomers are present in abundance, fluorescence of the monomers occurs. However, on statistical grounds some molecules are close enough together to form interacting pairs, which generally quench the fluorescence. Note that the presence of these quenching pairs cannot be observed by absorption spectroscopy. The absorption spectra of dilute solutions are monomeric, since at sufficiently low concentration the chromophore electron clouds do not interact.

When dye molecules are sufficiently close in space, their electron clouds and nuclear charges interact thereby modifying the spectral and dynamic properties of the chro-

mophores [27]. The wave functions, describing the initial and final states of the new interacting systems, needed for the calculation of the energy and electron transfer rate constants are very complicated. These initial states are studied by absorption spectroscopy since new bands appear if the coupling between the dye molecules is strong enough.

The spectral shifts of the new bands compared to the original one(s) can be predicted by a point dipole model. As long as the distance between the molecules is larger than the size of their size the excitonic interactions between dyes can be expressed as:

$$\hat{V} = \frac{1}{4\pi\epsilon R^3}\hat{\vec{\mu}}_n \cdot \left(1 - 3\frac{\vec{R}\vec{R}}{R^2}\right) \cdot \hat{\vec{\mu}}_m \tag{1.1}$$

where ϵ is the dielectric constant of the medium, $\vec{R}$ is the distance between the chromophores and $\vec{\mu}$ the above mentioned transition dipole moments of the chromophores m and n. These interaction energies form the off-diagonal elements of a $(n \times m)$ matrix with the diagonal elements as the excited state monomer energies. The eigen energies of the diagonalized matrix yield the spectral shifts, whereas the relative intensities for the various transitions can be obtained from the corresponding eigen vectors. Note that in equation (1.1) the intermolecular distance R has a fixed value, whereas in reality the distance is distributed and a distance distribution function must be included To incorporate the variations in excited state monomer energies, we also include inhomogeneous broadening by adding disorder to the diagonal matrix elements. Homogeneous broadening is accounted for by dressing each of the sticks in the stick spectrum, which result from solving the eigen values and eigen vectors of the matrix with a Gaussian lineshape.

The so-called Kasha model [35] often referred to in spectroscopic literature [36] is a simplified version of eqn. (1.1). The model applies to two interacting chromophores, each with a single dominant transition dipole moment each and hence is not suitable for porphyrines and their derivatives, containing two mutually perpendicular transition dipole moments. These are included in eqn. (1.1).

1.6 MAIN QUESTIONS ADDRESSED IN THIS THESIS

1. How can we define tunneling time?

   In Chapter 2 various definitions for tunnelling times are compared and their meaning within the orthodox and causal interpretations of quantum mechanics investigated. The focus of this Chapter is on the so-called transmission time, i.e. the average time electrons stay inside the barrier given that the tunnelling process takes place. It is argued that the use of stationary wave functions to obtain the transmission times

creates more problems than they solve. Therefore, we have to rely on time dependent wave packets incident on a barrier. The conclusion of the analysis carried out in this Chapter is that transmission time can be unambiguously defined within the causal interpretation of quantum mechanics, whereas the above mentioned definition of transmission time does not have any meaning in the orthodox interpretation of the quantum theory.

2. How can we make a simple model to mimic electron tunneling between dye molecules?

In Chapter 3 the trajectories of the electrons in a double potential well are calculated using the causal interpretation. The two wells correspond to the dye molecules and the potential barrier represents the medium between these molecules. The energy levels of the potential barrier are assumed to be higher than those of the electrons, accounting for the isolating properties of the medium. An electron in a state localized in one well can move to the other. The depth of the wells is assumed to be equal corresponding to identical molecules.

3. How can we make our model more realistic?

The model in Chapter 3 is oversimplified. The representation of dye molecules by wells is obviously not adequate. Hence, in this Thesis we investigate the initial state of chromophores.

In photosynthetic reaction centers the energy levels of the donor and acceptor molecules are different. The energy level of the electron acceptor is lower than that of the donor in order assisting the excitation energy from returning. We could mimic this situation by inclusion of unequal well depths but a double potential well with a deeper well at the acceptor side does not represent the situation in real systems since back-flow is not prevented in this way. Back-flow in real systems is prevented by dissipation to the environment. Dissipation is not included in the model. Coupling quantum systems to dissipation using the causal interpretation has been explored by several authors [37, 38, 39].

In Chapter 3 the pigment molecules have been treated as immobile wells, whereas in reality the molecules exhibit inter- and intramolecular vibrations. The limiting cases of very fast and very slow modes, as compared to the time needed by the wave functions to adjust to the vibrations, have been explored in Chapter 3. This can be done by adjusting the widths of the wells. For fast intermolecular vibrations of the wells, the wave packet of the tunneling electron cannot adjust to the time

dependent well width and the wave packets see an average well width. For slow vibrations, the wave packets have sufficient time to adjust to the intermolecular vibration. The middle regime is the most interesting regime because tunneling might be enhanced or inhibited by these vibrations. The inclusion of intermolecular vibrations, resulting in vibrationally assisted tunneling models has not been further explored in this Thesis.

4. How can we explore the wave functions of electrons in chromophores?

The electronic wave functions of chromophores are far more complicated than those of the energy wells in our model, and can definitely not be obtained by simple analytical methods. In order to describe electron transport between chromophores, one of which is an electron donor and the other an acceptor, intermolecular interactions should be included in the description of the system by wave functions. We used spectroscopic techniques to determine these interactions resulting in excitonic spectral shifts and fluorescence quenching.

5. Which mechanism underlies fluorescence quenching?

Following excitation, chromophores in matrices or liquid solutions loose their excitation energy easily to the surrounding medium by radiative (fluorescence) or non-radiative decay (heat). Also, energy transfer from the excited chromophore to non-fluorescent chromophore dimers (quenchers), may result in fluorescence quenching. In Chapter 4 a model is presented, to give an estimate of the number of potential quenchers in the neighborhood of an excited chromophore. A perfectly ordered dimer with a dark lower excitonic state could potentially act as a quencher. The number of these ordered dimers, however is low due to statistical distribution of distances between the pigments and homogeneous and inhomogeneous broadening. Although increasing the concentration of chromophores, increases the number of potential quenchers, the number of ordered dimers is reduced by the interaction with other nearby pigments.

6. Which interactions of chromophores can be measured with absorption spectroscopy?

Fluorescence quenching already occurs at concentrations too low to show any visible effect on the absorption spectra. So, absorption spectroscopy is not an useful tool to explain intermolecular behavior at low concentrations ($\leq 10^{-}5$ mol/g in experiments of Erythrosin B chromophores in PVA films). At sufficiently high concentration, i.e. $5 \times 10^{-}5$ mol/g, the absorption spectra reveal excitonic interactions

between the chromophores and the experimental spectral shifts can be explained by an exciton model. This model requires: (i) information about the dielectric constant of the medium and (ii) about the positions and orientations of the chromophores with respect to each other (see eqn.(1.1)).

In Chapter 5 the exciton model is used to explain the interactions of Erythrosin B chromophores at different concentrations in PVA films. The positions and orientations of the Erythrosin B chromophores with respect to each other are dependent on the concentration and subsequent steric hindrance between the chromophores. In Chapter 6 the experimental absorption spectra of porphyrin dimers, consisting of two porphyrin monomers linked by small molecules, are compared with the theoretically predicted spectra. The dimers have their conformational freedom partly restricted by steric effects and the position of the covalent link. The remaining rotational freedom is modeled to predict the dimeric absorption spectra. The model describes the experimental data quite well.

1.6.1 Final remarks

This Thesis deals with electrons and photons, which both require quantum theory to explain the phenomena. However, the interpretations of the quantum theory are controversial. In this Thesis, a long forgotten but recently fervently discussed, causal interpretation, is applied to describe the tunneling time of electrons. The visualization of the tunnelling process is appealing and shows that conceptually this causal or Bohm interpretation is superior to the orthodox interpretation, at least with respect to tunneling times.

Chapter 2

TUNNELING TIMES IN THE ORTHODOX AND CAUSAL INTERPRETATIONS OF QUANTUM MECHANICS

2.1 ABSTRACT

In this paper we analyze the concept of tunneling time from the perspective of the orthodox and causal interpretation of quantum mechanics. For this purpose we compare various definitions of tunneling times, to wit dwell time, transmission and reflection times, for stationary wave functions and wave packets. We address the question whether or not the causal interpretation is superior, conceptually or empirically to the orthodox interpretation. We show that the values of tunneling times are critically dependent on whether stationary wave functions or moving wave packets are used. We argue that the stationary waves are ill-suited for the study of tunneling times. We argue that for wave packets neither dwell time nor the reflection and transmission times can be given a well-defined meaning in the orthodox interpretation. The expressions proposed for these times in the literature rely on a sort of pseudo-orthodox interpretation. By contrast, in the causal interpretation these definitions are conceptually clear. Average dwell times have equal expressions in the pseudo-orthodox and causal interpretation. The expressions for average transmission and reflection times in the pseudo-orthodox interpretation are different from the expressions in the causal interpretation. For average dwell times, the interpretations are empirically equivalent. Experimental superiority of the causal interpretation with respect to average transmission and reflection times has so far not been established. Whether (and if how) an experimental set-up to measure average transmission and reflection times can actually be devised remains an open question.

2.2 INTRODUCTION

Tunneling is the quantum mechanical phenomenon that a particle can cross a barrier with potential V, even if its energy is strictly less than V. Particles penetrate the barrier and can be either transmitted or reflected. The transmitted particles cross the barrier. It is a natural question to ask how long it takes on average for particles to cross this barrier. One would expect that quantum theory provides a suitable prescription for a time operator, whose expectation value for a given wave packet can be compared with experiment. However, the pursuit of such a prescription is fraught with difficulties. Indeed, the literature abounds with proposals for various time operators or other mathematical constructions, intended to capture the notion of tunneling time and with discussions pointing out defects and objections to such proposals. Hence, definitions of tunneling times are not unambiguously available. Because of all its difficulties the debate is nicely characterized by Steinberg as: a not-so-brief history of tunneling times [40].

There is a non-orthodox interpretation of quantum mechanics, the so-called causal interpretation, which has been advocated by de Broglie and Bohm. It is well known that under certain assumptions the causal interpretation is empirically equivalent to the orthodox Copenhagen interpretation [41, 42]. However, there are a number of physical problems where the orthodox approach provides no clear-cut answers. One of such problems is the question of a time observable for a tunneling process. In the causal interpretation of quantum mechanics, a particle, e.g. an electron, has a well-defined position and velocity at each instant of time. Therefore, this interpretation can be applied to the problem of tunneling time and provides a well-defined answer to the question how long each particle takes to cross the barrier.

The question has been raised whether the tunneling time problem could serve as a crucial test to demonstrate an alleged superiority of the causal interpretation above the orthodox interpretation [43]. At first sight, the fact that the causal interpretation offers a clear-cut answer, where the orthodox approach is as yet unable to provide an unambiguous meaningful analysis seems to provide a clear advantage. However, there are several issues, which complicate this issue. First of all, there are different kinds of tunneling processes, which call for a different treatment. They may be classified in two types: scattering type, when a wave is initially incident on a barrier, and then partly transmitted and partly reflected; and decay type when, the particle is initially in a bound state, surrounded by a barrier, and subsequently leaks out of this confinement. Another problem is that one has to distinguish between various, closely related, definitions of tunneling times. The most important distinction is that between dwell time, transmission time, reflection time and arrival time. Finally, we shall see that the well-defined picture offered in the causal interpretation looks very different, depending on whether the tunneling process is described by a model with stationary waves or with moving wave packets.

Electron transfer and other physical and chemical processes such as radio-active decay

are tunneling processes of decay type. Our final aim of describing electron transfer, we leave for a subsequent paper. In this paper we only consider the scattering case.

The purpose of this paper is to analyze the above mentioned tunneling time problems in detail. In particular, we will address the question whether or not the causal interpretation is superior, either conceptually or empirically, to the orthodox interpretation with respect to tunneling times. The paper is structured as follows: In section 2.3 we review some aspects of the orthodox interpretation of quantum mechanics. In section 2.4 a brief review of the causal interpretation of quantum mechanics is given. In section 2.5 tunneling time concepts in the orthodox interpretation are discussed, while in section 2.6 tunneling time concepts in the causal interpretation are discussed. In section 2.7 we apply these concepts to concrete examples. In section 2.8 we discuss the question whether or not the causal interpretation is either conceptually or empirically superior to the orthodox interpretation with respect to tunneling times.

2.3 SOME ASPECTS OF THE ORTHODOX INTERPRETATION OF QUANTUM MECHANICS

In the orthodox interpretation, quantum mechanics is conceived of as a theory which refers only to concrete phenomena occurring in well-defined measurement context. This interpretation refuses to say anything about the properties of systems as long as no measurements have taken place. It is assumed that each such measurement context corresponds to some self-adjoint operator or a set of (commuting) self-adjoint operators, which represent(s) the observable(s) measured in that particular measurement contexts. Non-commuting observables correspond to mutually exclusive measurement contexts. Hence, the choice of a particular measurement context dictates the visibility of particular phenomena. A series of measurements on an ensemble of systems of the same observable give the expectation value of the observable.

Now, measurements of time are regularly performed in the laboratory. One would therefore expect that quantum mechanics provides an appropriate time operator, whose expectation value can be compared to the experimental data. However, the definition of such time operators is fraught with difficulties. Pauli showed already in 1933 that if a time operator exists that is canonically conjugate to the Hamiltonian, the latter must necessarily have a continuous spectrum without lower bound. This implies that the system would not possess a stable ground state [44]. The problem has since been addressed by many authors [45, 46, 47, 48, 49, 50, 51]. But although no time operator, canonically conjugate to the Hamiltonian seems possible, the question about the duration of quantum mechanical processes remains legitimate. Hence, there is a contradiction between the wish to define tunneling times, and the orthodox interpretation, which tells us that there does

not exist a straightforward way to define this time. Because experiments are performed to measure times related to tunneling times, it seems natural to ask whether the orthodox interpretation might be too strict to solve the tunneling times problems.

2.4 A BRIEF REVIEW OF THE CAUSAL INTERPRETATION OF QUANTUM MECHANICS

In this section we review some basic elements of the causal interpretation or, as it is called by P. Holland [23]: the quantum theory of motion. The basic postulates are discussed in [23]. We consider a one-dimensional case for a one-body problem and we emphasize the aspects, that will be important in the remainder of this paper:

- An individual physical system comprises a wave, propagating in space and time, together with a point particle which moves continuously under the guidance of the wave.
- The wave ($\Psi(x,t)$) is a solution to the Schrödinger wave equation.
- The particle motion is obtained as the solutions $x(t)$ to the equation:

$$\dot{x} = \frac{\frac{\hbar}{m} Im(\Psi^*(x,t)\frac{\partial}{\partial x}\Psi(x,t)}{|\Psi(x,t)|^2} \tag{2.1}$$

  where the right-hand side denotes the probability current density over the probability density function. To solve this equation we have to specify the initial condition x_0. The trajectory is then given by $x(x_0,t)$. The specification of x_0 constitutes extra information not contained by the wave function. An ensemble of possible trajectories associated with the same wave is generated by varying x_0. All these trajectories are weighted by the initial particle density $\rho(x,0) = |\Psi(x,0)|^2$.

Another way to obtain these trajectories is by considering a quantum Hamilton-Jacobi equation:

$$\frac{\partial S(x,t)}{\partial t} + \frac{(\frac{\partial}{\partial x}S(x,t))^2}{2m} + V(x,t) + Q(x,t) = 0 \tag{2.2}$$

S the phase of the complex wave function when the wave function is written in the form of $\Psi(x,t) = R(x,t)\exp(\frac{iS(x,t)}{\hbar})$, $V(x,t)$ is the classical potential and $Q(x,t)$ the quantum potential defined by $Q(x,t) = -\frac{\hbar^2}{2m}\frac{\frac{\partial^2}{\partial x^2}R(x,t)}{R(x,t)}$.
The possible trajectories can again be obtained by integration of the velocity [17]:

$$\dot{x} = \frac{\frac{\partial}{\partial x}S(x,t)}{m} \tag{2.3}$$

We highlight a few points about eqn. (2.2):

- The quantum potential has the strange feature that its effects does not always fall off with distance, as would be the case for any classical potential.

- If the initial position x_0 is specified, the initial velocity is uniquely given by:

$$\dot{x_0} = \frac{\partial}{\partial x} S_0(x)|_{x=x_0} \tag{2.4}$$

  So, no specification of initial velocity is required to determine the trajectory.

- The trajectories do not cross, which implies that the total probability at the right (or left) of any trajectory is constant for all times [52].

In the causal interpretation, the electron, moving under the influence of a quantum potential, travels along a particular trajectory. The time evolution of the system is determined by the first-order differential equation and the initial position. Thus, when the electron is on a particular position its future is determined along this trajectory. The probability density function describes the probability that a particle actually is at a specific location at a particular time. This stands in contrast to the usual interpretation according to which this function determines the probability of finding a particle if a suitable measurement is carried out. The causal theory does not assign a special role to the observer. Nevertheless, the standard quantum theory and the causal interpretation of quantum mechanics are regarded as empirically equivalent [41]. The big difference between the theories lies in their interpretation. This interpretation difference refers to what the theory tells us about the underlying structure of quantum phenomena.

2.5 TUNNELING TIME CONCEPTS IN THE ORTHODOX INTERPRETATION

To study the tunneling time concepts in the orthodox interpretation, we use a simple one-dimensional scattering processes, with a potential $V(x)$ inside and $V(x) = 0$ outside a barrier of arbitrary shape [1]. The wave functions encounter a barrier, located around the origin from $-b$ to b.

The question about the duration of tunneling processes of scattering type has been discussed by many authors (see the following review articles [53, 54, 55]). Hauge et al. [53] argue that all tunneling times suffer from one flaw or other. Some of the times are even imaginary, which makes them difficult to compare with experimental results. In this paper we will not attempt to repeat this discussion, instead we concentrate on dwell times,

[1] For tunneling in the strict sense the energy levels of the wave functions should be lower than the barrier. However, the tunneling time concepts are not restricted to this condition.

which seem the most well-known times, and their derivatives, i.e. transmission and reflection times.

Average dwell time is intended to represent the time a particle on average remains inside the barrier area. A formal definition of quantum mechanical dwell time has been proposed by Büttiker [56], inspired by collision theory [57], in which a "collision time" for scattering events was given. This collision time is defined as the ratio of the number of particles within the barrier to the incident flux. By analogy the quantum mechanical average dwell time, the average Büttiker dwell time $\langle \tau_{d_B} \rangle$, is the probability to find the electron in the barrier area ($\int dx \, |\Psi(x)|^2$) divided by the incident flux (k)

$$\langle \tau_{d_B} \rangle = \frac{\int_{-b}^{b} dx \, |\Psi(x)|^2}{k} \tag{2.5}$$

Unfortunately, this definition is only applicable for the special case of stationary wave functions. However, it still remains the most generally accepted member of the tunneling time family.

A generalization of the Büttiker dwell time, to cover the case in which wave packets are used, is proposed by Hauge et al. [53]). They define average dwell time $\left\langle \tau_{d_{B_g}} \right\rangle$ by the probability to encounter the particle inside the barrier and integrating over time.

$$\left\langle \tau_{d_{B_g}} \right\rangle = \int_0^\infty dt \int_{-b}^{b} dx |\Psi(x,t)|^2 \tag{2.6}$$

Hauge et al [53] mention this formula in the appendix of their paper but they warn the reader that this definition is not universally accepted. The assumption behind this formula is that the probability of finding a particle within the barrier at time t, integrated over time, gives the average time spend in the barrier [53].
It can be shown that the Büttiker dwell time (2.5) is obtained, when an appropriate limit is taken, as a limiting case of (2.6) for a stationary state $\Psi(x;k)$.

Average dwell times ignore the question how particles leave the barrier, i.e. whether they are transmitted or reflected. Many authors introduce two other time scales, namely average transmission time and reflection times. These are interpreted as the average time spent inside the barrier by those particles which are ultimately transmitted and ultimately reflected, respectively. There is also a proposal for a relation between average transmission and average reflection times, which gives a time, again called average dwell time. We indicate this average dwell time as $\langle t_d \rangle$. We will discuss the differences between the different average dwell times shortly. The relation is [58]:

$$\langle t_d \rangle = |T|^2 \langle t_T \rangle + |R|^2 \langle t_R \rangle \tag{2.7}$$

where $|T|^2$ and $|R|^2$ are the transmission and reflection coefficients respectively, $\langle t_T \rangle$ is the average transmission time (sometimes referred to as traversal time), $\langle t_R \rangle$ is the average

reflection time. This relation is not limited to either stationary wave functions or wave packets but is supposed to cover both. For wave packets this relation assumes that barrier is empty at the beginning and at end of the tunneling process.

However, the validity and generality of this relation (2.7) is controversial [54, 55]. Landauer et al. [55] argue that both the Bütiker$\langle t_{d_B} \rangle$ dwell time and the generalized Bütiker $\left\langle t_{d_{B_g}} \right\rangle$ are not necessarily equal to $\langle t_d \rangle$.
For example, this can easily be seen for stationary wave functions. The equality of these dwell times would mean that the probability to encounter the particle inside the barrier is equal to $k|T|^2 \langle t_T \rangle + k|R|^2 \langle t_R \rangle$ (see eqn. (2.5)). This means that the probability density decomposes into two non- interfering additive terms corresponding to the reflected and transmitted parts. But this assumption is dubious.

Even if eqn. (2.7) would hold the relation does not provide definitions for average transmission and reflection times because these two values cannot be deduced from this formula. Hence, we need separate definitions for average transmission and reflection times. Such definitions have been proposed by Olkhovsky et al. [54] and Muga et al. [59]. We will indicate these times, for reasons that will become clear later, as pseudo-orthodox (po). Their definitions are based on right-going and left-going components of the probability current density ($j(x,t)$), ($j_+(x,t)$ and $j_-(x,t)$) respectively.

$$j_+(x,t) = \begin{cases} j(x,t) & \text{if } j(x,t) \geq 0 \\ 0 & \text{otherwise} \end{cases} \tag{2.8}$$

$$j_-(x,t) = \begin{cases} j(x,t) & \text{if } j(x,t) \leq 0 \\ 0 & \text{otherwise} \end{cases} \tag{2.9}$$

The average transmission times $\langle \tau_T \rangle_{po}$ can be defined as:

$$\langle \tau_T \rangle_{po} = \frac{\int dt\, t j_+(b,t)}{\int dt\, j_+(b,t)} - \frac{\int dt\, t j_+(-b,t)}{\int dt\, j_+(-b,t)} \tag{2.10}$$

and the reflection time:

$$\langle \tau_R \rangle_{po} = \frac{\int dt\, t j_-(-b,t)}{\int dt\, j_-(-b,t)} - \frac{\int dt\, t j_+(-b,t)}{\int dt\, j_+(-b,t)} \tag{2.11}$$

Average transmission and reflection times were interpreted as the time spent inside the barrier by those particles which are ultimately transmitted and ultimately reflected, respectively. To see whether the definitions of $\langle \tau_T \rangle_{po}$ and $\langle \tau_R \rangle_{po}$ are equal to the intended definition, we analyze $\langle \tau_T \rangle_{po}$ and $\langle \tau_R \rangle_{po}$ in terms of arrival time distributions.

Arrival time distributions are popular in the literature about the problems of time in quantum mechanics [60, 61, 62, 63]. They are intended to represent the probability that a particle arrives at a certain location x_1. When applied to particles interacting with barriers, they can be used to extract information about tunneling times. An expression for these arrival time distributions $P_a(x,t)$, in case the probability current is unidirectional, is proposed by Dumont [64] using the probability current density:

$$P_a(x,t)dt = \frac{j(x,t)dt}{\int_0^\infty dt\, j(x,t)} \tag{2.12}$$

The average arrival time ($t_a(x_1)$) at a particular point x_1 is then:

$$\langle t_a(x_1)\rangle = \int dt\, t P_a(x_1,t) = \frac{\int_0^\infty dt\, t j(x_1,t)}{\int_0^\infty dt\, j(x_1,t)} \tag{2.13}$$

We now analyze the average transmission and reflection times in eqns. (2.10) and (2.11) from the point of view of average arrival times.

- The first term of the right-hand side of eqn. (2.10) is the average arrival time of transmitted particles at the exit of the barrier. At the exit of the barrier all particles are transmitted. All probability current is unidirectional, corresponding to j_+
- In the second term of the right-hand side of eqn. (2.10) all right-going probability current at the entrance of the barrier is taken into account. However, it seems plausible that part of the particles, that enter the barrier are not transmitted but reflected as will be shown clearly in the case of Gaussian wave packets in section 2.7.
- In the first term of the right-hand side of eqn. (2.11) all left-going probability current density is taken into account, which gives the average arrival time of returning particles.
- In the second term of the right-hand side of eqn. (2.11) all right going probability current at the entrance of the barrier is taken into account. This term is equal to the second term of the right-hand side of eqn. (2.10). Again, however, it seems plausible that part of this current is not reflected but transmitted.

In the second terms of the right-hand side of eqns.(2.10) and (2.11) no distinction is made between the to-be transmitted and to-be reflected components of the positive current density. This means that these terms do not describe the average arrival of the to-be-transmitted and to-be- reflected particles separately, but that they give an average time of all right-going particles. Whether these terms are over- or underestimating of the average arrival times at the entrance of the barrier, and hence under- or overestimate $\langle\tau_T\rangle_{po}$ and $\langle\tau_R\rangle_{po}$ is, without further assumptions hard to say. But it is clear that $\langle\tau_T\rangle_{po}$ and $\langle\tau_R\rangle_{po}$ do not correspond to the intended meaning of time spent inside the barrier by those particles which are ultimately transmitted or reflected. We will see later that the non-crossing

assumption provides a clear answer to the question about under- or overestimation.

This discussion shows that there are attempts to propose definitions for tunneling times in scattering events. We gave definitions of average dwell time (2.5) and (2.6) and average transmission (2.10) and reflection (2.11) times and their proposed relation (2.7). However, the question about transmission and reflection times of particles asks for a simultaneous answer to the question whether the particle is transmitted or reflected and its presence inside the barrier, which are two non-commuting variables. It is impossible to specify the position in the barrier of a particle and at the same time the direction of its velocity, which forms the basis of the distinction between transmission and reflection times [64]. Hence, in the orthodox interpretation there is no possibility to talk about transmission and reflection times and therefore also not about relation (2.7).

In fact, if the orthodox interpretation is followed in the strict sense then even dwell time does not belong to the orthodox interpretation because dwell time is not described by a self-adjoint operator and is not related to a well-defined measurement context. However, to interpret quantities with dimension time, the so-called Positive Operator Valued (POV) measurements can be included as an extension of the orthodox interpretation. The measurement context is no longer related to a self-adjoint operator but to a POV measure. These POV measures are bilinear functionals of the wave function. Average dwell time is a bilinear functional of the wave function, and hence, it might be possible to find a way to relate average dwell times to well-defined measurement contexts. Such an attempt is made for stationary wave functions by Leavens et al. [65]. However, most definitions of dwell times are given without a measurement context and hence they do not, strictly speaking, belong to the orthodox interpretation.

Neither average dwell times, nor transmission and reflection times can be defined in the orthodox interpretation. Hence, the orthodox interpretation is too strict to define these times. We will refer to these times as belonging to the pseudo-orthodox interpretation. In this pseudo-orthodox interpretation the properties of a system are assumed to be represented by the wave function independent of the measurement context e.g. the wave functions represent something real. More specifically, in many attempts to define tunneling times, the probability current density is assumed to be something real, analogue to classical currents.

In the next section we will show that the causal interpretation avoids these problems by assuming that particles deterministically follow trajectories.

2.6 TUNNELING TIME CONCEPTS IN THE CAUSAL INTERPRETATION

We now study the tunneling time concepts in the causal interpretation for the situation described in section 2.5.

In the causal interpretation, the trajectories give information about average dwell time of particles inside the barrier. This average dwell time is the average time spent inside the barrier subsequent to $t = 0$ by particles following trajectories $x(x_0, t)$, averaging over the initial positions [66]:

$$\langle \tau_d \rangle_{causal} = \int_0^\infty dx_0 |\Psi(x_0, 0)|^2 \int_0^\infty dt \int_{-b}^{b} dx\, \delta(x - x(x_0, t)) \tag{2.14}$$

where $\int_{-b}^{b} dx\delta(x - x(x_0, t))$ is 1 or 0 depending on whether the particles are inside or outside the barrier. After interchanging the order of integration, $\langle \tau_d \rangle_{causal}$ is equal to [58, 66]:

$$\langle \tau_d \rangle_{causal} = \int_0^\infty dt \int_{-b}^{b} dx |\Psi(x, t)|^2 \tag{2.15}$$

Note that this expression is equal to the generalized Büttiker dwell time eqn. (2.6). As we shall see in the concrete examples trajectories in general are either reflected and transmitted, depending on the starting position inside the packet [67] . Because of the non-crossing property, particles starting in the front part of the wave packet are transmitted, the ones at the back reflected. The special trajectory $x(x^c_{(0)}, t)$, implicitly defined by

$$|T|^2 = \int_{x(x_0^c, t)}^{\infty} dx\, |\Psi(x, t)|^2 \tag{2.16}$$

separates transmitted and reflected trajectories. Transmission ($\langle \tau_T \rangle_{causal}$) and reflection ($\langle \tau_R \rangle_{causal}$) times are defined by Leavens [66]:

$$\langle \tau_T \rangle_{causal} = \frac{1}{|T|^2} \int_0^\infty dt \int_{-b}^{b} dx\, |\Psi(x, t)|^2\, \Theta(x - x(x_0^c, t)) \tag{2.17}$$

$$\langle \tau_R \rangle_{causal} = \frac{1}{|R|^2} \int_0^\infty dt \int_{-b}^{b} dx\, |\Psi(x, t)|^2\, \Theta(x(x_0^c, t) - x) \tag{2.18}$$

where Θ is the Heaviside function and $|\Psi(x,t)|^2\,\Theta(x - x(x_0^c, t))$ is the to-be-transmitted component and $|\Psi(x,t)|^2\,\Theta(x(x_0^c - x, t))$ the to-be-reflected component of the probability density. These expressions are unambiguous definitions. In the next section we want to compare them to the pseudo-orthodox tunneling times and therefore we connect the trajectory approach to the probability current density. This connection can be established

via the concept of arrival time distributions.

The trajectories provide information about the position (x) at each instant of time (t) via the function $x(t)$, which, under the assumption that each trajectory passes x only once, can be inverted to give the function $t(x)$. To calculate the arrival time distributions at a particular location (x_1), we need each point in time (t) that a trajectory, starting in a particular initial position (x_0) passes x_1. Averaging over the probability density $|\Psi(x_0,0)|^2$, that a particle starts at $t=0$ in x_0, we obtain the arrival time distributions ($\Pi_{x_1}(t)$):

$$\Pi_{x_1}(t) = \frac{\int_{x_0^c}^{\infty} dx_0 |\Psi(x_0,0)|^2 \delta(t - t(x_0;x_1))}{\int_{x_0^c}^{\infty} dx_0 |\Psi(x_0,0)|^2} \tag{2.19}$$

Leavens [68] showed that under the assumption of no recurrence, which means that the probability current density is unidirectional:

$$\int dx_0 |\Psi(x_0,0)|^2 \delta(t - t(x_0;x_1)) = j(x_1, t(x_1)) \tag{2.20}$$

where ($j(x_1,t)$) is the probability current density.

Hence, the average arrival time ($t_a(x_1)$) at point x_1 is (see eqn. (2.19)):

$$\langle t_a(x_1) \rangle = \frac{\int dt\, t j(x_1,t)}{\int dt\, j(x_1,t)} \tag{2.21}$$

In the causal interpretation of quantum mechanics dwell times, average transmission and reflection times are based on trajectories, which provide a straightforward way to define them.

2.7 APPLICATIONS TO EXAMPLES

In this section, we narrow the situation from sections 2.5 and 2.6 by using a simple rectangular barrier $V(x) = V$, $|x| < b$. The wave functions will be either described by stationary wave functions or by Gaussian wave packets.

2.7.1 Dwell, transmission and reflection times for stationary wave functions

The average time a particle stays inside the barrier is called average dwell time. According to textbook quantum mechanics stationary wave functions approaching a square potential are reflected or transmitted. The stationary wave function can be given as:

$$\begin{aligned} \Psi(x) &= \exp(ikx) + R\exp(-ikx) && x \le -b \\ \Psi(x) &= C_1 \exp(-\alpha x) + D_1 \exp(\alpha x) && |x| < b \\ \Psi(x) &= T\exp(ikx) && x \ge b \end{aligned} \tag{2.22}$$

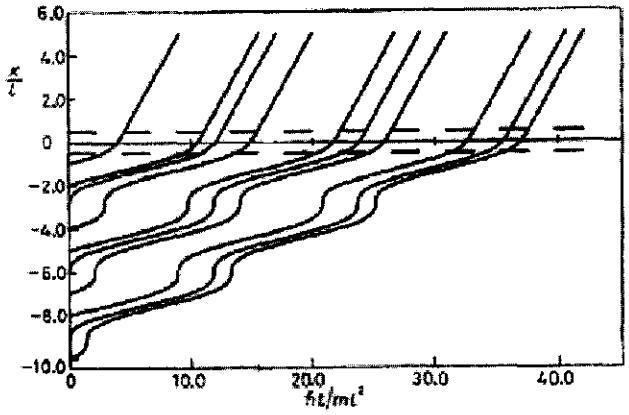

Figure 2.1: An ensemble of trajectories, calculated by Spiller. Time is along the x-axe and the position along the y-axe. The barrier energy is double the wave function energy. The transmission coefficient is 0.42. The barrier is shown dashed. For actual numerical values see [69]. Reproduced with permission of T. Spiller and [69]

Where (in atomic units and scaled to $m = 1$) $k^2 = 2E$ and E is the energy of the wave function and $\alpha^2 = 2(V - E)$, α is real and $E < V$. $|T|^2$ and $|R|^2$ are the transmission and reflection coefficient respectively. C_1 and D_1 are constants.

The average Büttiker dwell time $\langle \tau_{d_B} \rangle$ for the stationary wave function is (for explanations of symbols see equation (2.22):

$$\langle \tau_{d_B} \rangle = \frac{k}{\alpha}\left(\frac{2b\alpha(\alpha^2 - k^2) + (\alpha^2 + k^2)\sinh(2\alpha b))}{4k^2\alpha^2 + (\alpha^2 + k^2)^2\sinh^2(\alpha b)}\right) \tag{2.23}$$

In the causal interpretation, dwell time for stationary wave functions were calculated Spiller et al. [69]. These calculations gave some remarkable results because no reflected trajectories were found (see Fig. (2.1)). The dwell time is well defined and independent of the starting position of the particle. All trajectories (and so all particles) pass the barrier, and thus the transmission coefficients in the causal interpretation $|T_c|^2 = 1$ and the reflection coefficients $|R_c|^2 = 0$. Thus, transmission and reflection coefficients have different values in the different interpretations.
This is a somewhat awkward result. In the causal interpretation, the average time the particles stay inside the barrier is equal to the time consumed by ultimately transmitted particles. Average dwell time is equal to average transmission time (or in Spiller's vocabulary: traversal time) and average reflection times do not exist.

This dwell/transmission time can be given analytically [69]:

$$t_{causal} = \frac{2\alpha b(\alpha^2 - k^2) + (\alpha^2 + k^2)\sinh(2\alpha b)}{4k\alpha^3} \tag{2.24}$$

The Büttiker dwell time ($\langle \tau_d \rangle$) and the causal dwell/transmission time (t_{causal}) are not equal but there exists a relation between them. The Büttiker time is the probability to encounter a particle inside the barrier over the incident flux (k)

$$\langle \tau_{d_B} \rangle = \frac{\int_{-b}^{b} dx\, |\Psi|^2}{k} \tag{2.25}$$

while the dwell/transmission time calculated by Spiller is the probability to encounter a particle inside the barrier over the causal flux ($(1 - |R|^2)k$):

$$t_{causal} = \frac{\int_{-b}^{b} dx\, |\Psi|^2}{(1 - |R|^2)k} \tag{2.26}$$

So, it is clear that the description of the orthodox interpretation and the causal interpretation are not consistent for stationary wave functions. However, it is not clear whether these problems are caused by differences in interpretations because of two interfering factors.

The greatest complication is that in the stationary wave description, there are no incoming waves, which are temporally prior to the transmitted and reflected waves. Rather, they all exist everywhere in space at the same time. Thus there is no basis for the view that one precedes the other, or the interpretation that the reflected and transmitted waves are caused by a reflection and transmission respectively of the incident wave. Hence, attempts to define average transmission and reflection times for stationary wave functions are questionable.

An additional complication is that these stationary wave functions are not square integrable. They are not normalizable vectors in Hilbert space. Postulate 1 of quantum mechanics demands this property, so if we take quantum mechanics seriously, these wave function are in the strict sense not allowed as representations of a quantum state. In fact, these stationary wave functions can be seen as limiting cases, delta functions in k-space. Let us for a moment consider a delta function in x-space. This delta function is a single position point. Because in the causal interpretation the trajectories do not cross, they obviously cannot start in a single point. We see that the causal interpretation treats the limiting case of delta functions more critically than the orthodox interpretation does.
Based on these weaknesses of the stationary wave description we agree with Leavens and Oriols that the stationary states do not provide a fully satisfactory description of the quantum state [52, 70]. Therefore, we stop the pursuit to obtain definition of transmission and reflection times for stationary wave functions in the pseudo- orthodox interpretation.

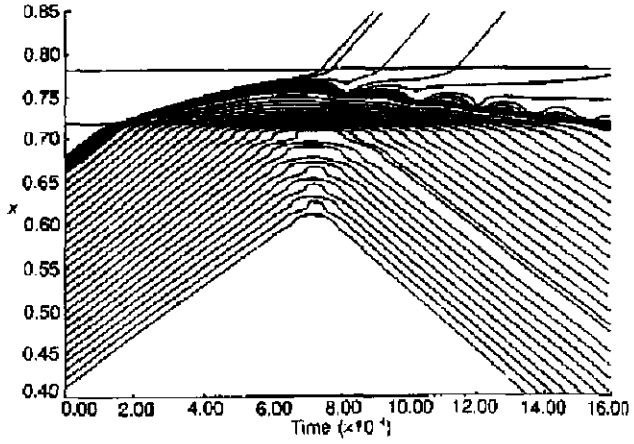

Figure 2.2: An ensemble of trajectories, calculated by Dewdney. Time is along the x-axe and the position along the y-axe. The barrier is indicated. The high concentrations of lines, starting around 0.67 serve a didactical purpose. The transmission coefficient is ± 0.01. For actual numerical values see [67]. Reproduced with permission of C. Dewdney, [67], A. Whitaker and [12]

2.7.2 Dwell, transmission and reflection times for wave packets

We now turn to a discussion of Gaussian wave packets. Consider a well-localized wave packet moving in the direction of the barrier. When it arrives at the barrier, part is reflected and part is transmitted. The average dwell time for the pseudo-orthodox interpretation eqn. (2.6) is equal to average dwell time for the causal interpretation eqn. (2.15). In the causal interpretation, average dwell time can also be deducted from trajectories. These trajectories for Gaussian wave packets have been given by Dewdney et al [67] (see Fig. (2.2)).

In the pseudo-orthodox interpretation, average transmission and reflection times are given by eqn. (2.10) and (2.11). To apply these formulae to Gaussian wave packets we use Fig. 2.3. In Fig. 2.3 the integrated probability current density ($\int_0^t dt^* j(x,t^*)$) for Gaussian wave packets at each instant of time (t) is given for the entrance $-b$ and the exit b of the barrier [2]. This figure can be used to investigate the integration limits of the integrals of the definitions of transmission and reflection times.

- The integrated probability current density at the exit of the barrier increases till

[2]We used the same wave packet as Dewdney et al. [67] (see Fig. (2.2). However, we decreased the width of the barrier to increase the transmission probability.

the transmission probability value is reached. Hence, in the first term of the right hand-side of eqn. (2.10) $j_+(b,t)$ can be replaced by $j(b,t)$ and the integration limits are 0 to infinity.

- The integrated probability current density at the entrance of the barrier has a maximum at t_2. At this time the sign of the probability current density changes and hence, this is the upper limit of of the integral in the second term of the right-hand side of eqn. (2.10).
- The first term of the right-hand side of eq. (2.11) depends on left-going probability current density j_- at the entrance of the barrier. This $j_-(-b,t)$ can be replaced by $j(-b,t)$ with the integration limit starting at t_2 and going to infinity.
- The second term of the right-hand side of eq. (2.11) is equal to the second term of the right-hand side of eqn. (2.10)

Hence, the average transmission and reflection times are:

$$\langle \tau_T \rangle_{po} = \frac{\int_0^\infty dt\, tj(b,t)}{\int_0^\infty dt\, j(b,t)} - \frac{\int_0^{t_2} dt\, tj(-b,t)}{\int_0^{t_2} dt\, j(-b,t)} \tag{2.27}$$

$$\langle \tau_R \rangle_{po} = \frac{\int_{t_2}^\infty dt\, tj(-b,t)}{\int_{t_2}^\infty dt\, j(-b,t)} - \frac{\int_0^{t_2} dt\, tj(-b,t)}{\int_0^{t_2} dt\, j(-b,t)} \tag{2.28}$$

We will now compare $\langle \tau_T \rangle_{po}$ and $\langle \tau_R \rangle_{po}$ to the definitions for average transmission and reflection times in the causal interpretation. For this purpose we will analyze these times in a similar fashion as above.
Fig. 2.2 shows trajectories of reflected and transmitted particles. According to the non-crossing property, particles starting in the front part of the wave packet are transmitted, the ones at the back reflected. In Fig. 2.3 time t_1 is indicated. This time is given by:

$$\int_0^{t_1} dt\, j(-b,t) = |T|^2 \tag{2.29}$$

and distinguishes between the positive current of to-be-transmitted and to-be-reflected probability current densities [52]. At t_1 all particles, that are eventually transmitted have passed at the entrance of the barrier because the non-crossing property states that the first particles entering the barrier are the ones that are transmitted.

The average transmission time is the time difference between the average arrival time of the to-be-transmitted particles at the exit and the entrance.:

- Reflected particles do not reach the exit of the barrier and hence, the average arrival time at the exit is:

$$\langle t_a(b) \rangle = \frac{\int_0^\infty dt\, tj(b,t)}{\int_0^\infty dt\, j(b,t)} \tag{2.30}$$

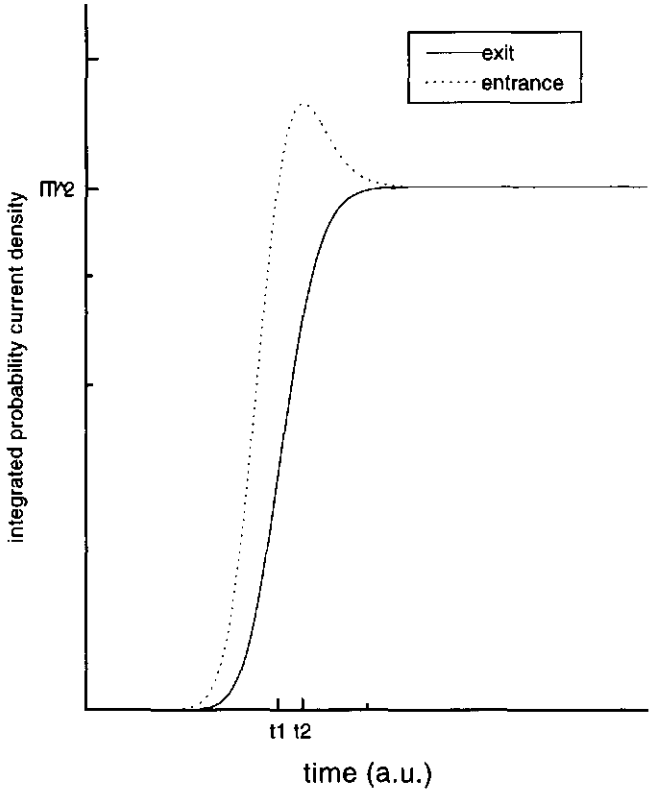

Figure 2.3: The integrated probability current density, $\int_0^t dt^* j(x,t^*)$, at each instance of time, t, at the entrance $(-b)$ and the exit (b) of the barrier (see text). The transmission coefficient, $|T|^2$ at the entrance is reached at time t_1. At t_2 the positive current at $-b$ has passed.

- The arrival time of the to-be-transmitted particles at the entrance of the barrier lies between 0 and t_1 and hence, the average arrival time, (t_{a_t}), at the entrance of the barrier is:

$$\langle t_{a_t}(-b)\rangle = \frac{\int_0^{t_1} dt\, tj(-b,t)}{\int_0^{t_1} dt\, j(-b,t)} \tag{2.31}$$

The average reflection time is the time difference between the average arrival time of the left-going particles and the right- going, to-be-reflected particles at the entrance of the barrier.

- The average arrival time for the negative probability current density $(t_{a_{r2}})$ at the entrance is:

$$\langle t_{a_{r2}}(-b)\rangle = \frac{\int_{t_2}^{\infty} dt\, tj(-b,t)}{\int_{t_2}^{\infty} dt\, j(-b,t)} \tag{2.32}$$

- For the positive probability current density, the average arrival time of the to-be reflected particles $(t_{a_{r1}})$ at the entrance is:

$$\langle t_{a_{r1}}(-b)\rangle = \frac{\int_{t_1}^{t_2} dt\, tj(-b,t)}{\int_{t_1}^{t_2} dt\, j(-b,t)} \tag{2.33}$$

These expressions can now be used to obtain average transmission and reflection times for Gaussian wave packets in the causal interpretation in terms of probability current density.

$$\langle \tau_T\rangle_{causal} = \langle t_a(b)\rangle - \langle t_{a_t}(-b)\rangle = \frac{\int_0^{\infty} dt\, tj(b,t)}{\int_0^{\infty} dt\, j(b,t)} - \frac{\int_0^{t_1} dt\, tj(-b,t)}{\int_0^{t_1} dt\, j(-b,t)} \tag{2.34}$$

$$\langle \tau_R\rangle_{causal} = \langle t_{a_{r2}}(-b)\rangle - \langle t_{a_{r1}}(-b)\rangle = \frac{\int_{t_2}^{\infty} dt\, tj(-b,t)}{\int_{t_2}^{\infty} dt\, j(-b,t)} - \frac{\int_{t_1}^{t_2} dt\, tj(-b,t)}{\int_{t_1}^{t_2} dt\, j(-b,t)} \tag{2.35}$$

These expressions give the average time spent inside the barrier by ultimately transmitted (reflected) particles.

Comparison of the pseudo-orthodox and causal average transmission and reflection times reveals the following:
The first terms of the right-hand sides of average transmission times eqns. (2.27) and (2.34) and of reflection times eqns. (2.28) and (2.35) are equal. However, the second term of the right-hand side of eqn. (2.27) takes all probability current entering $-b$ into account and hence the subtracted term is larger as compared to the causal average transmission times, which only takes the time till all ultimately to-be-transmitted particles have passed. Hence, average transmission times in the pseudo-orthodox interpretation are smaller than in the causal interpretation. The second term in eqn. (2.28) is smaller than the second

term of eqn. (2.35) and hence the average reflection time is larger in the pseudo-orthodox interpretation as compared to the causal interpretation.[3].

In section 2.5 we concluded that, in the pseudo-orthodox interpretation, the average transmission times $\langle\tau_T\rangle_{po}$ and reflection $\langle\tau_R\rangle_{po}$ do not define the intended meaning of time spent inside the barrier by those particles which are ultimately transmitted or reflected. We could not resolve whether these terms were an over- or underestimating of the average transmission and reflection times. As shown above the non-crossing assumption shows clearly that $\langle\tau_T\rangle_{po}$ is an underestimation and $\langle\tau_R\rangle_{po}$ an overestimation of the intended times as compared to the causal times.

2.8 DISCUSSION AND CONCLUSIONS

Is the causal interpretation superior, conceptually or empirically, to the orthodox interpretation with respect to tunneling times?

Our analysis shows, that dwell time and transmission and reflection times give very different values in the orthodox and causal interpretations when stationary wave functions are used. However, due to the lack of time dependence these wave functions are not suitable to describe the tunneling process. Therefore, it is not clear whether the differences between tunneling times in the orthodox and causal interpretations can be blamed on the interpretations. Hence, the question about the conceptual or empirical superiority of one interpretation over the other cannot be answered in this case.

The use of wave packets avoids this problem. As we have seen, the expressions for average dwell time, using wave packets, are equal in the causal and (pseudo-)orthodox interpretation (see (2.6) and (2.15)). However, their foundations are different. Average dwell times are defined without a measurement context and hence there is no proper foundation for these definitions in the orthodox interpretation. In the literature one often adopts a pseudo-orthodox view to define average dwell times, in which the probability current density represents a flow through space analogous to a classical flow. Challinor et al. [71] go even further. They calculate streamlines, which follow the flow of probability current density through space and argue in favor of the non-crossing property of these streamlines. They specifically mention that their approach is based on the assumption that the dynamics of the probability current density directly describes the temporal aspects of tunneling. However, the question about the justification of this assumption remains unanswered. On the other hand, the causal interpretation gives a conceptually unproblematic way to define dwell times because it provides definite trajectories without measurements and hence, the average time they spend in a barrier region or that they arrive at a particular point can be unambiguously determined. Therefore, the answer to the question about conceptual

[3]Leavens [42] mentioned already these under- and overestimation of the average transmission and reflection times in the pseudo-orthodox interpretation as compared to the causal interpretation.

superiority of the causal interpretation over the pseudo-orthodox interpretation with respect to dwell time is 'yes'.

Let us now consider the experimental status of the average dwell time. Although this time is defined without reference to a measurement context, and does not take the form of an expectation value of a self-adjoint operator, the average dwell time provided in eqn. (2.6) is still a bilinear functional of the wave function. This implies that it may still be possible to relate this average dwell time to a well-defined observable as demanded by the orthodox interpretation by means of the extended formalism of POV measures. However, in comparison, we see that expressions for average dwell time are identical in the orthodox and causal interpretations (eqns. (2.6) and (2.15)). Therefore, even if a concrete measurement context for dwell time can be realized, such an experiment will not provide a crucial test between the two interpretations. Hence, the causal and orthodox interpretations are empirically equivalent with respect to average dwell times.

We now turn to a discussion of transmission and reflection times. We have seen that according to the strict orthodox viewpoint the concepts of transmission and reflection times are meaningless, because it would require the simultaneous determination of incompatible quantities. On the other hand, the definitions for average transmission and reflection times proposed by Olkhovsky and Muga et al. (eqns. (2.10) and (2.11)), rely on a pseudo-orthodox viewpoint. However, since this view does not provide a clear criterion for a distinction between the the to-be transmitted and to-be reflected probability current density, these definitions do not correspond to their intended meaning. By contrast, in the causal interpretation this problem does not arise. Here, one can specify exactly which trajectories are transmitted or reflected and a clear-cut determination of the associated average times is straightforward. Moreover we have seen that the values obtained for these times are numerically different in the causal and pseudo-orthodox interpretation. Based on these findings the answer to the question about the conceptual superiority of the causal average transmission and reflection times over the pseudo-orthodox one is 'yes'.

However, if we compare the strict orthodox and causal interpretation the situation becomes more involved. The fact that it is impossible to define average transmission and reflection times in the orthodox interpretation raises the question whether these times are at all meaningful. If one answers in the negative, one can argue that the orthodox interpretation is more appropriate by providing no definitions for these times. Whereas the the causal interpretation aims to answer a superfluous question. The weakness of this argument is of course that the orthodox and causal interpretations differ in their assessment of what is physically meaningful. Hence, from the causal point of view transmission and reflection times are physically real, and the fact that a clear definition is available is seen as a sign of superiority of the causal view. Clearly, there is no way to settle this dispute on the conceptual superiority between the causal and orthodox interpretation.

Let us now turn to the experimental issue. The question whether average transmission

and reflection times are experimentally accessible is a factual one. It might be that these times are not measurable, as assumed by the orthodox interpretation. The fact that the causal interpretation nevertheless gives definite values for them is then comparable to other non-testable predictions of the causal interpretation, such as the prediction that particles in a box in an eigen state do not move. If average transmission and reflection times are not measurable, one might argue that the orthodox interpretation is superior due to the economically principle: the less unanswerable questions, the better the theory. However, if we disregard the causal interpretation, we also lose the advantages of the theory. For example, the causal interpretation offers a useful visualization of quantum phenomena. Whether the advantages outweigh the disadvantages seems a matter of taste. Nevertheless, the fact that within the orthodox interpretation a reasonable number of articles appear about tunneling times shows that the desire to answer questions which are officially meaningless does not disappear by outlawing them.

However, this assumes that average transmission and reflection times are not measurable. What if they are measurable? If so, it would provide a crucial test for the causal interpretation. This issue was raised in an interesting discussion between Cushing [43] and Bedard [72]. Cushing raised the question whether or not tunneling times experiments could serve as a crucial test for the causal interpretation. In response, Bedard argued that any experiment purporting to measure a tunneling time according to the causal interpretation can always be reinterpreted in the orthodox interpretation, due to the fact that tunneling times in the causal interpretation are always functionals of the wave function, and can hence, be also regarded as characteristic values of the wave function in the orthodox interpretation. So, Bedard concluded that experiments cannot distinguish between the orthodox and causal interpretation.

In reply to Bedard's claim, Cushing agreed and pointed to an article by Leavens et al. [65], which states that the average transmission and reflection times, eqns. (2.17) and (2.18) depend implicitly on the special trajectory, which separates transmitted from reflected trajectories. Because this trajectory $x(x_c^{(0)}, t)$ is an implicit functional of $\Psi(x,t)$, its appearance in the integrands of eqns. (2.17) and (2.18) means that $|T|^2 \langle \tau_T \rangle_{causal}$ and $|R|^2 \langle \tau_R \rangle_{causal}$ unlike their sum, the dwell time, are not bilinear functionals of $\Psi(x,t)$.
In the orthodox interpretation every expectation value of an operator or POV measurement is a bilinear functional of the wave function. The causal interpretation does not directly state that all expectation values of measurements are bilinear functional of the wave function. However, if one adopts, like Cushing [6], the viewpoint that all measurements are position measurements, than the expectation values of all measurable observables should be bilinear functionals of the wave function in the causal interpretation. Hence, Cushing's belief, that all measurements are position measurements, made him renounce the project of showing the causal view to be superior with respect to tunneling times [73].

The assumption that in the causal interpretation all measurements are position measurements is not as rigid as sometimes posed. For example, Holland [23] leaves room for

the possibility to accommodate other measurements. However, the lack of linearity is a serious problem. As said before, in quantum mechanics every expectation value of an observable corresponds to a bilinear functional of the wave function, independent of the actual state of the system. However, it might be possible that quantum mechanics allows a procedure which can be interpreted as a measurement of transmission and reflection times for a limited class of wave functions, whereas another procedure would be needed for this purpose for other (classes of) wave functions. The collection of such measurement procedures, for each class of wave functions could then correspond to a non-linear functional. The question whether (and if how) an experimental set-up to realize this remains open. Because of this open question, it seems too early to follow Cushing and give up on the project to show that the measurement of tunneling times may provide a crucial test for the causal interpretation.

Chapter 3

TUNNELING IN A DOUBLE POTENTIAL WELL: DOING IT THE BOHMIAN WAY

3.1 ABSTRACT

In this paper, the causal or Bohm interpretation of quantum mechanics is applied to a tunneling process in a double potential well. This can be regarded as a simplified model for electron transport in chemical processes. We consider a time dependent periodic wave function and study its behavior during half a period. The particle trajectories during the tunneling process are analyzed. We discuss the meaning of transmission and reflection coefficients. Special attention is paid to the average time a particle stays inside the barrier, given that the tunneling process (transmission from one side to another) takes place. This average transmission times can be unambiguously defined in a double potential well. Hence, the causal interpretation provides a conceptually clear way to define average transmission times. The question remains whether average transmission time can be experimentally measured.

3.2 INTRODUCTION

After a long hibernation, the causal or Bohm interpretations of quantum theory are back in the picture. In the mid-1920s the pilot wave version of a causal interpretation suggested by de Broglie was rejected in favor of the orthodox Copenhagen interpretation. In 1952 Bohm reformulated this causal interpretation, in which, a particle, e.g. an electron, has a well-defined position and velocity at each instant of time. Its motion is causally determined by a guidance field. Integration of the velocity subject to initial conditions yields the particle trajectories. At that time Bohm's ideas received very limited attention by the physics community. According to Holland [23] interest in the Bohm program only came more than 25 years later. It was the availability of personal computers that worked as the starting shot of an umpire for the causal theory. Obtaining trajectories involves lengthy numerical calculations, which were effortlessly done by computers and hence, trajectories easily emerged on a computer screen. These trajectories even serve as a cover illustration of the book on the foundations of quantum mechanics written by Whitaker in 1996 [12]. In the eighties and nineties the theory received a booming interest (see for instance [74]).

It is well known that (under certain circumstances) the causal interpretation is empirically equivalent to the orthodox Copenhagen interpretation [41, 42]. However, there are a number of physical problems for which this orthodox approach provides no clear-cut answers. One of such problems is the question of a time observable for a tunneling process.

Tunneling is the quantum mechanical phenomenon that a particle can cross a barrier with potential V, even if its energy is strictly less than V. It is a natural question to ask how long it takes on average for particles to cross such a barrier. Unfortunately the quantum theory does not provide a suitable time operator, whose expectation value for a given wave packet can be compared with experiment. Time enters quantum mechanics as a parameter, not as an operator. Therefore, this question about tunneling time is not an easy one.

Tunneling processes may be classified in two types: scattering type, where a wave packet is initially incident on a barrier, and then partly transmitted; and decay type when, the particle is initially in a bound state, surrounded by a barrier, and subsequently leaks out of this confinement. Many authors have addressed the question about the duration of tunneling processes, in case of scattering processes [53, 54, 55].

In the causal interpretation of quantum mechanics various concepts of tunneling times for scattering processes can be distinguished. The most well-known time is dwell time, i.e. the time particles spend inside the barrier. For an ensemble of particles, we can determine the average dwell time. This average dwell time ($\langle t_d \rangle$) can be decomposed into an average transmission times ($\langle t_t \rangle$), i.e. the time spent inside the barrier by those particles, which eventually cross the barrier, and average reflection time ($\langle t_r \rangle$), i.e. the time consumed by those particles, which penetrate the barrier but re-emerge on the same side, according to

[42]:

$$\langle t_d \rangle = |T|^2 \langle t_t \rangle + |R|^2 \langle t_r \rangle \tag{3.1}$$

where $|T|^2$ and $|R|^2$ are the transmission and reflection probabilities respectively. This relation assumes that particles are either transmitted or reflected, i.e. they do not remain inside the barrier.

It appeared to be convenient to obtain the average transmission time by means of the concept of the average arrival time. The average arrival times at particular places is defined. Particles on trajectories arrive somewhere at a particular time. Average arrival time at a particular point x_1 ($\langle t_a(x_1) \rangle$) is given by [68]:

$$\langle t_a(x_1) \rangle = \frac{\int dt\, t j(x_1, t)}{\int dt\, j(x_1, t)} \tag{3.2}$$

where $j(x_1, t)$ is the probability current density. This equation is only valid under the condition that the probability current density is unidirectional (see section 2.6 of Chapter 2).

In this paper, we consider decay type tunneling, because tunneling processes of the decay type are important in certain chemical processes. For example, electron transfer between molecules (in biological structures) occurs even at very low temperatures [75, 76]. This transfer process cannot be explained classically, it is commonly thought to be due to tunneling [77]. Nowadays, it is assumed that even at physiological temperatures, tunneling plays an important role in biological electron transfer processes [30]. A simple model to describe electron transfer processes is by a double potential well. Here, the two wells correspond to the molecules (or molecular groups) and the potential barrier represents the gap between these molecules. Most reactions take place under the absorption of light hence, the molecules in our model are in an excited state. This electron in an excited molecular orbital, localized in one well can move to the other.

The decomposition of the dwell time into average transmission and reflection time according to relation (3.1) in a decay type of tunnelling is not as straightforward as for the scattering cases. Definitions for transmission and reflection probabilities are not common for this decay type of tunneling. However, we shall propose natural definitions for these concepts and use these to define average transmission and reflection time. It will again appear to be convenient to obtain the average transmission time by using the concept of the average arrival time.

The aim of this paper is firstly, to investigate whether the causal interpretation of quantum mechanics provides a straightforward way to define transmission times in double potential wells. For simplicity, we will study periodic wave functions. Because we are interested in tunneling from one side to another, we consider only half a period time ($t_{\frac{1}{2}}$).

Secondly, the question whether it is necessary to adopt the causal interpretation to give meaning to the thus obtained transmission times is addressed.
This paper is organized as follows:
In section 3.3 a brief review of the causal interpretation of quantum mechanics is given. In section 3.4 we apply the causal interpretation method to tunneling in a double potential well. The last section is devoted to a discussion about the question whether or not the causal interpretation provides a clear way to define transmission times in a double potential well and about the necessity to rely on the causal interpretation for this definition and about the usefulness of the definition of average transmission times in the description of duration of electron transfer processes.

3.3 A BRIEF REVIEW OF THE CAUSAL INTERPRETATION OF QUANTUM MECHANICS

In this section we review some basic elements of the causal interpretation or, as it is called by P. Holland [23]: the quantum theory of motion. The basic postulates are in summary discussed in [25, 23]. We consider for a one body problem, a one-dimensional case and we emphasize the aspects, that will be important in the remainder of this paper:

- An individual physical system comprises a wave, propagating in space and time, together with a point particle which moves continuously under the guidance of the wave.
- The wave ($\Psi(x,t)$) is a solution to the Schrödinger wave equation.
- The particle motion is obtained as the solution $x(t)$ to the equation:

$$\dot{x} = \frac{\frac{\hbar}{m} Im(\Psi^*(x,t)\frac{\partial}{\partial x}\Psi(x,t)}{|\Psi(x,t)|^2} \tag{3.3}$$

  where the right-hand side denotes the probability current density over the probability density function. To solve this equation we have to specify the initial condition $x(0)$ (indicated as x_0). This specification constitutes extra information not contained by the wave function. An ensemble of possible trajectories associated with the same wave is generated by varying x_0. All these trajectories are weighted by the initial particle density $\rho(x,0) = |\Psi(x,0)|^2$.

In the causal interpretation, the electron, moving under the influence of a quantum potential, travels along a particular trajectory. The time evolution of the system is determined by the first-order differential equation and the initial position. Thus, when the electron is on a particular position its future is determined along this trajectory. The trajectories do not cross, which means that the total probability presence at the right (or left) of any trajectory is constant for all times [52]. The probability density function describes the probability that a particle actually is at a specific location at a particular time. This

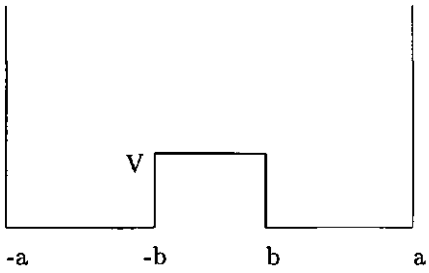

Figure 3.1: The system under consideration: a double potential well. The total length of the box is $2a$, the potential at a and $-a$ is infinite. The barrier is situated from $-b$ to b and has a constant height V.

stands in contrast to the usual interpretation according to which this function determines the probability of finding a particle if a suitable measurement is carried out. The causal theory does not assign a special role to the observer. Nevertheless, the standard quantum theory and the causal interpretation of quantum mechanics are regarded as empirically equivalent [41]. The big difference between the theories lies in their interpretation. This interpretation difference refers to what the theory tells us about the underlying structure of quantum phenomena.

3.4 THE CAUSAL INTERPRETATION APPLIED TO A DOUBLE POTENTIAL WELL

In this section, the causal interpretation described in the previous section is applied to tunneling in a double potential well. We study the possibilities to define transmission and reflection coefficients, average dwell time, average transmission time and reflection time according to this method.

3.4.1 Description of the double potential well

Electron transfer takes place from an electron donor molecule (in an excited state) to an electron acceptor molecule. Hence, the electron is initially in a bound state, surrounded by a barrier, and subsequently leaks out of this confinement into another enclosure.

To model this tunneling process we consider a wave packet in a double potential well. The potential well is described by a one-dimensional box, defined from $-a$ to a. At these points, the walls are infinitely high. In the middle of the box a barrier from $-b$ to b is

situated ($b < a$).

$$V(x) = \begin{cases} \infty & \text{if } |x| \geq a, \\ 0 & \text{if } b \leq |x| \leq a, \\ V & \text{if } 0 \leq |x| \leq b \end{cases} \tag{3.4}$$

See Fig. 3.1.
We consider a wave packet which is, initially, concentrated on one side of the barrier only, and in the course of time moves to the other side of the well[1].

To create wave packets, we calculate, according to standard procedure (see Appendix 3.7.1) the energy eigen values and eigen functions for this double potential well. A linear combination of the lowest even energy eigen function ($f_e^{(0)}(x,t)$) and the lowest odd energy eigen function ($f_o^{(0)}(x,t)$) will be treated as a wave function of the ground state of the donor molecule, while the linear combination of the next two, even ($f_e^{(1)}(x,t)$) and odd ($f_o^{(1)}(x,t)$) energy eigen states is called the excited state wave function.
Electron transfer in biological processes takes place mainly from an excited state of the donor molecule. Hence, in our model, electron transfer is better described by excited state wave functions than by the ground state functions. However, the wave functions in the ground state are mathematically simpler. Fortunately, the method we follow to define average transmission times is equal for excited state and ground states. So, we study both states and we indicate them as $\Psi^{(0)}(x,t)$ and $\Psi^{(1)}(x,t)$ respectively:

$$\Psi^{(0,1)}(x,t) = c_e^{(0,1)} f_e^{(0,1)}(x,t) + c_o^{(0,1)} f_o^{(0,1)}(x,t) \tag{3.5}$$

We choose the weight factors a follows:

$$\begin{aligned} c_e^{(0,1)} &= \frac{\exp(-ik_o^{(0,1)}a)}{\sqrt{2}} \\ c_o^{(0,1)} &= \frac{\exp(-ik_e^{(0,1)}a)}{\sqrt{2}} \end{aligned} \tag{3.6}$$

where $(k_o^{(0,1)})^2$ are proportional to odd energy eigenvalues and $(k_e^{(0,1)})^2$ to the even energy eigenvalues. The choice of these constants assures a high probability of finding the electron at $t = 0$ between $-a$ and $-b$. [2]

Although eqn. (3.5) provides wave packets with (approx.) maximum extinction at one side, this extinction is not complete and can never be complete. Thus, our description is in that sense not an ideal description of a chemical reaction. We could enhance this

[1]Note that in the causal interpretation a particle described by a stationary wave function does not move, and hence no tunneling occurs.

[2]In our examples choosing optimalized coefficients enhances the probability to find our electron at one side of the barrier with a negligible value of approx. 0.002 percent

extinction by using a linear combination of more than two eigen functions. But this might introduce recurrent trajectories, which we want to avoid.

All energy levels are chosen to be lower than the barrier potential in order to make sure that the passage is due to tunneling.
Our wave packet shows periodic behavior, and tunneling from one side to the other takes place in half a period. The tunneling period is inversely proportional to $(k_o^{(0,1)})^2 - (k_e^{(0,1)})^2$.

From the wave packets we can calculate trajectories. Analytical expressions of the velocity $(\dot{x})$ can be obtained by using the expressions given in Appendix 3.7.1. To obtain the trajectories $x(t)$ the differential equation (eqn. 3.3) should be solved after a starting value (x_0) is chosen (see section 3.3). We solved this differential equation numerically [78]. The trajectories are given in Figs. 3.2 ($\Psi^{(0)}(x,t)$, the ground state) and 3.3 ($\Psi^{(1)}(x,t)$, excited state).

3.4.2 A classification of the trajectories

Let us first note some salient aspects of the form of the possible trajectories. Fig. 3.2 shows trajectories of the ground state ($\Psi^{(0)}(x,t)$). The various trajectories are generated by varying the choice of an initial position (x_0).
One clearly sees their periodic behavior, and that the trajectories do not cross. Note that at any given time, all trajectories move in the same direction, i.e., to the right during the first half period, and towards the left during the second half. The figure shows that at very left and at the very right there are trajectories, which remain on the same side of the barrier. This occurs for all trajectories with a starting point left of point s_1 and to the right of s_3. The area indicated with R (returners) contains trajectories, which reach inside the barrier but do not pass it, they return to their original area. Their starting positions at $t = 0$ is between s_1 and s_2. These trajectories correspond to reflection. The trajectories starting in area T (travelers) are trajectories, which pass the barrier and end up, after half a period, at the other side of the barrier. At $t = 0$ the starting point of the travelers is between s_2 and $-b$. This behavior corresponds to transmission. The trajectories between $-b$ and b are already inside and between b and s_3 already past the barrier at $t = 0$.

3.4.3 Definitions of transmission and reflection coefficients

In view of the above classification, the most straightforward way to define transmission and reflection seems to reserve the term transmission for travelers (T) and reflection for returners (R). Indeed, only travelers are actively involved in the tunneling process. A probability for transmission, the transmission coefficient $|T|^2$, can then be defined as:

$$|T|^2 = \int_{s_2}^{-b} dx\, |\Psi(x,0)|^2 \tag{3.7}$$

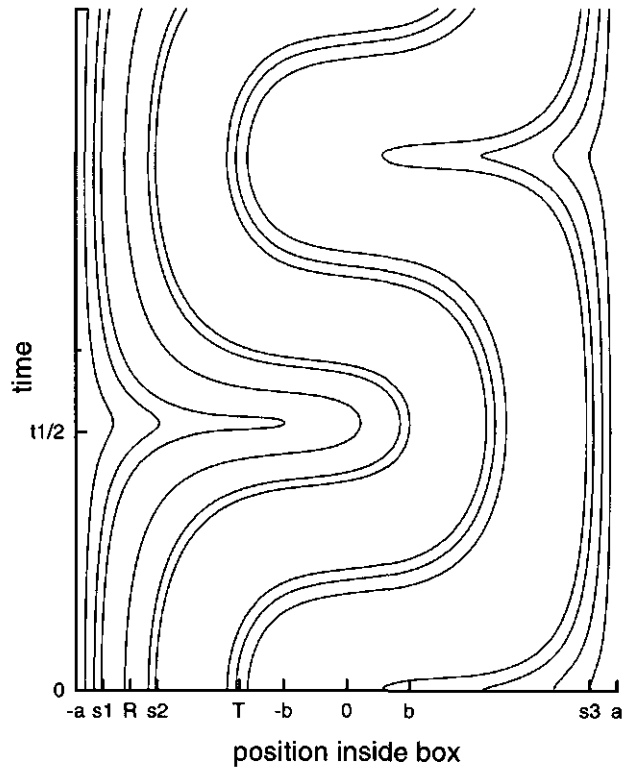

Figure 3.2: Bohm trajectories to show the different starting point x_0 possibilities at $t = 0$. Left of s_2 and right of s_3 trajectories do not leave their own area. R=reflection area, starting positions between s_1 and s_2. T=transmission area starting positions between s_2 and $-b$.

The reflection coefficient can be defined likewise:

$$|R|^2 = \int_{s_1}^{s_2} dx\, |\Psi(x,0)|^2 \tag{3.8}$$

Note that in this definition the transmission and reflection coefficients do not add up to unity: $|T|^2 + |R|^2 \neq 1$. Of course, this is due to the fact that there is a finite probability that trajectories always remain on the same side of the barrier or that the trajectories are already inside or past the barrier. These possibilities are usually excluded in discussions of tunneling in one-dimensional scattering processes [79].

3.4.4 Definitions of dwell time, transmission and reflection times

To define dwell time, transmission and reflection time, we need to consider not only the form of the trajectories but also the probability density $|\Psi(x,0)|^2$ according to the wave functions (3.5). In Fig. 3.3 the trajectories are depicted for the excited state $\Psi^{(1)}(x,t)$. We see that the concentrations of trajectories (in two packets) at the left hand side of the barrier (between $-a$ and $-b$) reflect the double sine and cosine belonging to the first excited states (the meaning of the symbols a, b, s_1, s_2 and $t_{\frac{1}{2}}$ are given in Figs. 3.2 and 3.3). Along the time axis we marked some special times, t_p t_m and t_n. Time t_p is the instant at which the trajectory, starting at $t = 0$ in s_2 passes at $-b$. This trajectory marks the bifurcation between the reflection and transmission area. Time t_m indicates the time the trajectory starting at $t = 0$ in $-b$ arrives at b. This is the time needed to deliver the trajectories, which at $t = 0$ already are inside the barrier, to the right hand side of the barrier. Although time t_n lies outside half a period of time, we marked this time because it gives information about reflection times. All trajectories starting at $t = 0$ between s_1 and s_2 are at $t = t_{\frac{1}{2}}$ inside the barrier. Between $t = t_{\frac{1}{2}}$ and $t = t_n$ they leave the barrier and hence, reflected particles are inside the barrier between time t_p and time t_n.

Average dwell time is the average time that particles spend inside the barrier region:

$$\langle t_d \rangle = \int dt \int_{-b}^{b} dx\, |\Psi(x,t)|^2 \tag{3.9}$$

The probability to encounter a particle inside the barrier ($\int_{-b}^{b} dx\, |\Psi(x,t)|^2$) is independent of time (see Appendix 3.7.2) and hence, the average dwell time inside the barrier in half a period is the probability to encounter a particle inside the barrier multiplied by half a period:

$$\langle t_d \rangle = t_{\frac{1}{2}} \int_{-b}^{b} dx\, |\Psi(x,t)|^2 \tag{3.10}$$

To define average transmission and reflection times, we have to go back to the trajectories because trajectories provide information about the position (x) at each instant of time

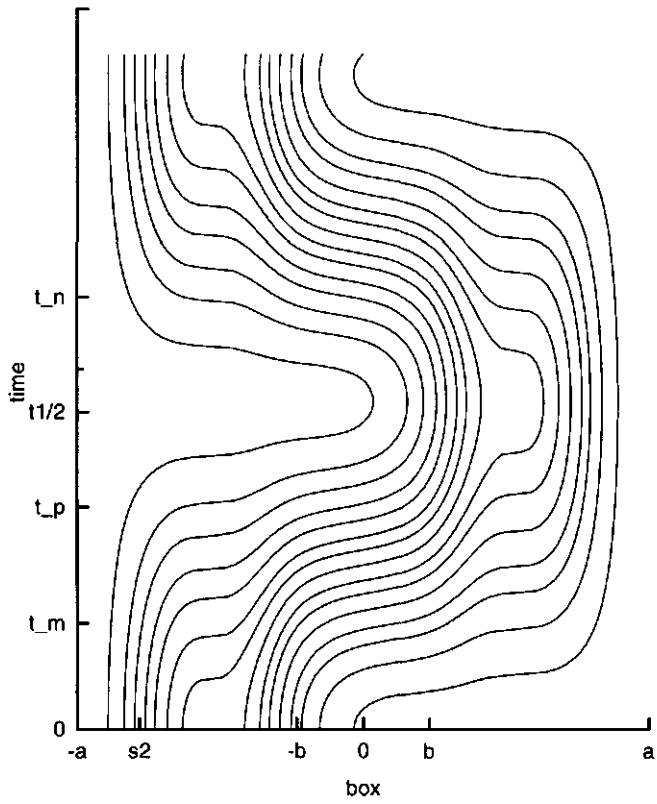

Figure 3.3: Bohm trajectories for a one dimensional double potential well with the even and odd eigen functions in the first excited state. We represent the probability density function $t = 0$ by N points. These points are spaced with equal probability density intervals. $\int_{-a}^{x_N} dx\,|\Psi(x,t_0)|^2 = \frac{N-\frac{1}{2}}{N_{tot}}$. x_N is the position of x_0 dependent on N. N_{tot} is the total number of points. The value of $-\frac{1}{2}$ is arbitrarily chosen. Any other valuė (between 0 and 1) gives an equally valid description. t_p is the time the trajectory, starting at $t = 0$ in s_2, passes at $-b$. $t_m = t_{\frac{1}{2}} - t_p$ and $t_n = t_{\frac{1}{2}} + t_m$. In this example $N = 15$.

(t), which, under the assumption that each trajectory passes x only once, can be inverted to give the function $t(x)$. Similar to the scattering case, transmission and reflection times can be conveniently expressed in terms of arrival time distributions. The time that a trajectory, starting in x_0 at $t = 0$, arrives at x_1, can be notated as $t(x_0; x_1)$. Averaging over the probability density $|\Psi(x_0, 0)|^2$ that a particle starts at x_0, we obtain the arrival time distributions $(\Pi(t))$:

$$\Pi_{x_1}(t) = \frac{\int dx_0 |\Psi(x_0,0)|^2 \delta(t - t(x_0; x_1))}{\int dx_0 |\Psi(x_0,0)|^2} \tag{3.11}$$

where the integration limits should be chosen to fulfill the assumption that each trajectory passes x_1 only once.
Hence, the arrival time distribution of the to-be-transmitted particles at the exit of the barrier (b) is:

$$\Pi_b(t) = \frac{\int_{s_2}^{-b} dx_0 |\Psi(x_0,0)|^2 \delta(t - t(x_0; b))}{\int_{s_2}^{-b} dx_0 |\Psi(x_0,0)|^2} \tag{3.12}$$

The denominator is the transmission coefficient (see formula 3.7). The starting points x_0 are within the transmission area, between $-b$ to s_2.
Similarly, he arrival time distribution of the to-be-transmitted particles at the entrance of the barrier $(-b)$ is:

$$\Pi_{-b}(t) = \frac{\int_{s_2}^{-b} dx_0 |\Psi(x_0,0)|^2 \delta(t - t(x_0; -b))}{\int_{s_2}^{-b} dx_0 |\Psi(x_0,0)|^2} \tag{3.13}$$

As long as the trajectories cross a particular point (x_1) only once, Leavens [68] showed that:

$$\int dx_0 |\Psi(x_0,0)|^2 \delta(t(x_1) - t(x_1; x)) = j(x_1, t(x_1)) \tag{3.14}$$

which gives us the arrival time distributions in term of probability current densities. Hence, the average arrival time at point x_1 $(\langle t_a(x_1) \rangle)$ under the same conditions, is:

$$\langle t_a(x_1) \rangle = \frac{\int dt\, t j(x_1, t)}{\int dt\, j(x_1, t)} \tag{3.15}$$

In the double potential well, the probability current density is unidirectional for half a period and hence, we can determine the average arrival time at the entrance and the exit of the barrier. Taking the time boundaries from Fig. 3.3 in consideration the average arrival time at the entrance of the barrier is:

$$\langle t_a(-b) \rangle = \frac{\int_0^{t_p} dt\, t j(-b, t)}{\int_0^{t_p} dt\, j(-b, t)} \tag{3.16}$$

and at the exit:

$$\langle t_a(b)\rangle = \frac{\int_{t_m}^{t_{\frac{1}{2}}} dt\, tj(b,t)}{\int_{t_m}^{t_{\frac{1}{2}}} dt\, j(b,t)} \tag{3.17}$$

and hence, the average transmission time, the average arrival time at the exit of the barrier minus the average arrival time at the entrance of the barrier, reads:

$$\langle t_t\rangle = \langle t_a(b)\rangle - \langle t_a(-b)\rangle = \frac{\int_{t_m}^{t_{\frac{1}{2}}} dt\, tj(b,t)}{\int_{t_m}^{t_{\frac{1}{2}}} dt\, j(b,t)} - \frac{\int_0^{t_p} dt\, tj(-b,t)}{\int_0^{t_p} dt\, j(-b,t)} \tag{3.18}$$

To determine reflection times, we have to extend the observation time to t_n (see Fig. 3.3). To-be reflected particles enter the barrier between time t_p and $t_{\frac{1}{2}}$, they pass the barrier again on their way back between time $t_{\frac{1}{2}}$ and t_n. Hence, the average reflection time is:

$$\langle t_r\rangle = \frac{\int_{t_{\frac{1}{2}}}^{t_n} dt\, tj(-b,t)}{\int_{t_{\frac{1}{2}}}^{t_n} dt\, j(-b,t)} - \frac{\int_{t_p}^{t_{\frac{1}{2}}} dt\, tj(-b,t)}{\int_{t_p}^{t_{\frac{1}{2}}} dt\, j(-b,t)} \tag{3.19}$$

In this definition we use time t_n, which does not fall inside the range defined as half a period (from t_0 to $t_{\frac{1}{2}}$). This might seem in contradiction to eqn (3.10), the definition of average dwell time, which uses $t_{\frac{1}{2}}$ as its upper bound limit. However, the time taken by the reflecting particles on their way back to their original place ($t_{\frac{1}{2}}$ to t_n) is equal to the time taken by particles already inside the barrier at $t = 0$, to leave the barrier. The last mentioned time was not accounted for as belonging to average transmission time. Hence, the integration limits of the addition of average transmission and reflection times and the total average dwell times are consistent.

3.4.5 Transmission time in terms of probability density of the wave function

In the previous section, the definitions of the average transmission and reflection times, using the average arrival time distribution were based on trajectories from the causal interpretation of quantum mechanics. However, the final expressions (eqns. 3.18 and 3.19) do no longer depend on the trajectories but on probability current densities. This suggests the possibility to define average transmission (and reflection times) without explicit use of the trajectories. In this section, we will show, that average transmission times can, indeed be obtained without explicit reference to trajectories. Instead we only rely on the non-crossing property of the causal interpretation and the unidirectionality between $t = 0$ and $t = t_{\frac{1}{2}}$ of the current density flow and the periodicity of the wave functions. Average reflection times will not be considered, because we are interested in the transmission process. The question whether, the fact that the trajectories are not needed explicitly in

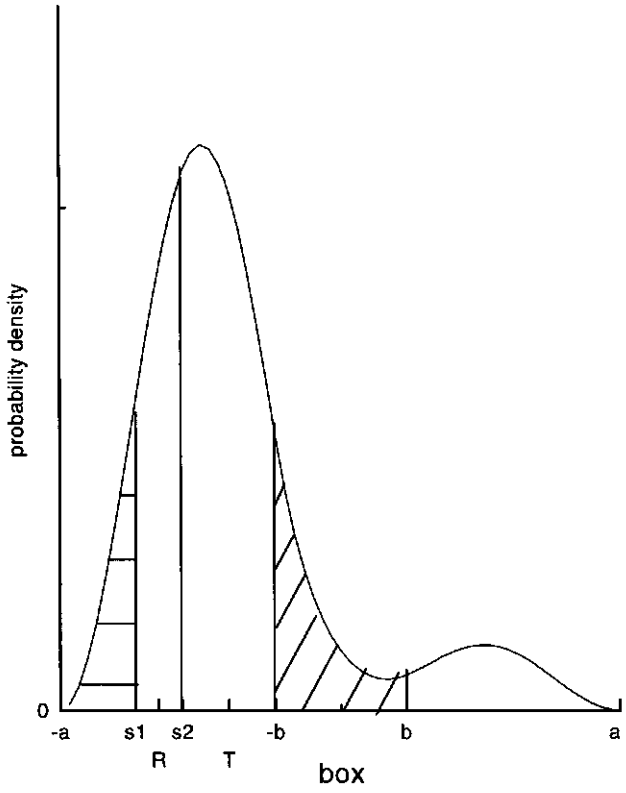

Figure 3.4: Probability density at $t = t_0$. The transmission area (T) and reflection area (R, between s_1 and s_2) are indicated. Their destinations are given in Fig. 3.5. $-a$ and a are box boundaries and $-b$ and b the barrier boundaries.

order to determine the transmission times implies that the causal interpretation is superfluous for this purpose is left for the next section.

In order to show how average transmission times for a periodic wave function can be determined from the probability density, we refer to Figs. 3.4 and 3.5 [3]. Here we have partitioned the interior of the double well in 5 areas, as shown in the figures. In Fig. 3.4 the probability densities at $t = 0$ and in Fig. 3.5 at $t = t_{\frac{1}{2}}$ are given. One can see that the probability density goes from left to right during half a period. The probability densities in Figs. 3.4 and 3.5 are mirror images. We will exploit this symmetry in our calculations.

The 5 areas indicated in Figs. 3.4 and 3.5 have the following meaning:

- The probability in area at the utmost left-hand side, between $-a$ and s_1, remains in its own domain. s_1 can be found by the condition that the probability between $-a$ and s_1 should be equal to the probability between $-a$ and $-b$ in Fig. 3.5. Because of symmetry the probability density between $-a$ and s_1 is equal to the probability density between b and a at $t = 0$ (Fig. 3.4). Hence,

$$\int_{-a}^{s_1} dx \, |\Psi(x,0)|^2 = \int_{b}^{a} dx \, |\Psi(x,0)|^2 \tag{3.20}$$

- The area which is indicated with an R in Fig. 3.4 is the reflection area (between s_1 and s_2). In Fig. 3.5 the probability within that area has moved inside the barrier. The probability density inside the barrier is constant at all times (see Appendix 3.7.2) and hence is the same as the probability inside the barrier at $t = 0$:

$$\int_{s_1}^{s_2} dx \, |\Psi(x,0)|^2 = \int_{-b}^{b} dx \, |\Psi(x,0)|^2 \tag{3.21}$$

- We indicated a T in Fig. 3.4 for the transmission area (between s_2 and $-b$). The probability density from this area arrives at $t = t_{\frac{1}{2}}$, Fig. 3.5, at the opposite side of the barrier. Because the probability density of all other areas are known, this probability density can be determined by:

$$\int_{s_2}^{-b} dx \, |\Psi(x,0)|^2 = 1 - 2\int_{-b}^{a} dx \, |\Psi(x,0)|^2 \tag{3.22}$$

To determine the average transmission time, we need the average arrival time of the to-be transmitted particles at the entrance of the barrier and at the exit of the barrier. We use the assumption that the flux is unidirectional between $t = 0$ and $t = t_{\frac{1}{2}}$.

[3] Actually, we took the ground state wave function, $\Psi^{(0)}(x,t)$, and chose the constants (see eqn. (3.6) in such a way that the probability to encounter particles at $t = 0$ at the right-hand side of the barrier is large enough to be visible in graphical presentations.

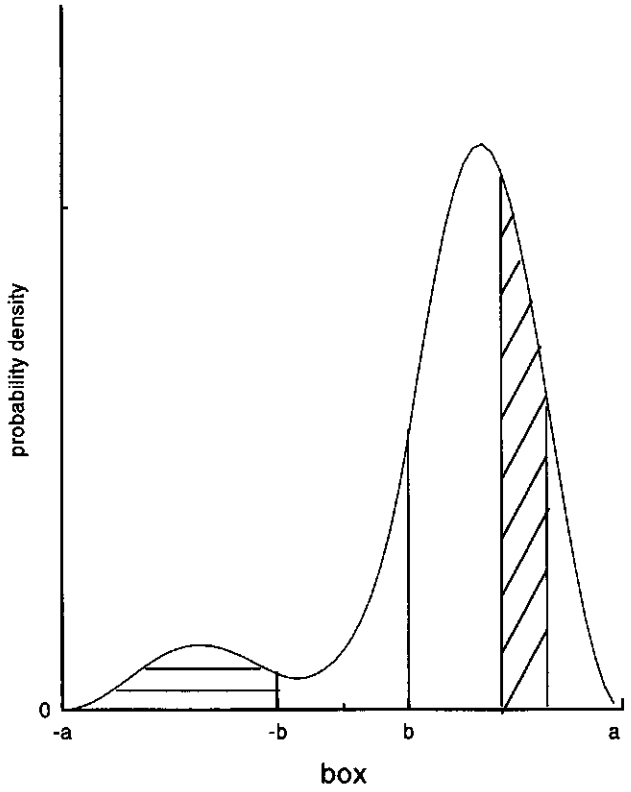

Figure 3.5: Probability density at $t = t_{\frac{1}{2}}$. Compare to Fig. 3.4: T is past the barrier and R inside the barrier.

- At the entrance of the barrier the transmission flux starts at $t = 0$ and should be stopped at the time, when the left-hand side of the barrier is emptied of all traveling probability. The probability left behind at the left-hand side of the barrier at $t = t_p$ is equal to the probability between $-a$ and s_2 at $t = 0$. Hence, this time, t_p, can be found implicitly by:

$$\int_{-a}^{-b} dx \, |\Psi(x, t_p)|^2 = \int_{-a}^{s_2} dx \, |\Psi(x, 0)|^2 \tag{3.23}$$

- At the exit of the barrier, we must wait until all the probability initially inside the barrier has passed before the traveling part arrives. This happens between time $t = 0$ and $t = t_m$. After half a period the traveling part is inside the right-hand side well. Between time t_m to $t_{\frac{1}{2}}$ the transmission part passes at the exit of the barrier. t_m starts when the right hand side of the barrier contains the probability of the right-hand side and the probability under the barrier:

$$\int_{b}^{a} dx \, |\Psi(x, t_m)|^2 = \int_{-b}^{a} dx \, |\Psi(x, 0)|^2 \tag{3.24}$$

  The right-hand side terms of eqns. (3.23) and (3.24) are equal. The half period evolution ($t_{\frac{1}{2}}$) is $\frac{\pi}{E_o - E_e}$ (see for symbols Appendix 3.7.1) [4].

Now, eqn. (3.18) can be filled in, which gives us the average transmission time of the double potential well, without using the trajectories.

3.5 DISCUSSION AND CONCLUSIONS

In this section, we discuss the question whether or not the causal interpretation provides an unambiguous way to define average transmission times in a double potential well. Secondly, we discuss the necessity to adopt the causal interpretation to define this transmission time. Lastly, we discuss usefulness of the definition of average transmission time to describe electron transfer duration processes.

3.5.1 Does the causal interpretation provide an unambiguous way to define average transmission time in a double potential well?

In the causal interpretation of quantum mechanics, the position of an individual particle traveling along a particular trajectory is determined at each instant of time. The tra-

[4] Using the probability current density the times t_p and t_m can also be found by:

$$|T|^2 = \int_0^{t_p} dt \, j(-b, t) = \int_{t_m}^{t_{\frac{1}{2}}} dt \, j(b, t) \tag{3.25}$$

jectories show the possible behavior of particles inside the barrier and hence, the causal interpretation creates the possibility (at least numerically) to discriminate between trajectories inside the barrier, whose fate is transmission and whose fate is reflection. Although definitions for transmission and reflection coefficients are not common practice in a double potential well, the definitions, given in eqns. (3.7) and (3.8) provide a useful tool to differentiate between these two possibilities. The trajectories show that the current density flow, between $t = t_0$ and $t = t_{\frac{1}{2}}$, is unidirectional. Similar to the more well- known case of scattering processes, the transmission times can be conveniently expressed in terms of the arrival time distributions. Average arrival times at the entrance and exit of the barrier are used to express the transmission time. Hence, the average time spent inside the barrier by eventually transmitted particles can unambiguously be defined and hence the answer to the question whether the causal interpretation can give an unambiguous definition of average transmission time in a double potential well is "yes".

3.5.2 Is the causal interpretation of quantum mechanics needed to define transmission times?

In this section the question is addressed whether or not the causal interpretation of quantum mechanics is needed to define transmission time?

Transmission times for a double potential well are unambiguously defined in the causal interpretation of quantum mechanics. However, the causal interpretation also implies a different world view than the standard, orthodox interpretation. The trajectories describe the way particles move. The initial position of the particle, although unknown to us, fixes its future path completely and hence, in contrast to the orthodox interpretation, the causal interpretation theory is a deterministic theory.

In section 3.4.5 we showed how the definition of transmission times could be obtained, without trajectories, from the probability density of the wave function. This may suggest that the causal interpretation is superfluous for the determination of transmission times. However, transmission times are obtained under the assumption that the flow of probability density follows the non-crossing property of the trajectories of causal interpretation (see Chapter 2 of this Thesis). Outside the causal interpretation, the justification for this assumption is not clear. Hence, our discussion of the definition of average transmission time in a double potential is dependent on this aspect of the causal interpretation of quantum mechanics for its justification.

3.5.3 Transmission times and electron transfer

How useful is the definition of average transmission times to describe the duration of electron transfer processes? We divide the section into 3 subsections. We discuss two

limitations of the model and pose an open question whether or not average transmission times are experimentally accessible.
To describe electron transfer, our model should be able to have a well-localized wave packet at the electron-donating molecule at $t = 0$ and a high transmission probability for reasonable heights of the barrier. However, the barrier height and the localization and the transmission probability are related. When a wave packet is well localized $t = 0$, then it is equally well localized at the opposite side half a period later and hence the transmission probability is high. But the higher the barrier, the better the localization and the larger the probability of transmission. This seems counter-intuitive. The explanation is found by realizing that the energy eigen values are not freely chosen. They are dependent on the barrier height. When the barrier is higher, the energy levels are less separated and the wave packet is more strongly concentrated at one side at $t = 0$. However, a high barrier also makes the period time large and hence, tunneling is very slow. Neither the high barrier nor the slow tunneling process give realistic descriptions of an electron transfer process. Hence, our model is limited in its ability to have a reasonable height of the barrier and a well localized wave packet.

The second limitation of our model is that we do not take into account that electron transfer in chemical reactions is a one-way process. The electron is transported from one molecular group to another. Our model lacks the possibility of a one-way process, although by continuing the process only to half a period, we suggested a decay process. However, subsequently the periodic behavior causes the electron to tunnel back to its original place. So in our model, although it was chosen to resemble processes in chemistry (biology) closely, the dissipative character of the process is not incorporated. To obtain more realistic models other descriptions, which include dissipation, should be used [80].

Finally, we pose the question of the experimental accessibility of average transmission times. For scattering processes this question has been discussed in a previous paper (Chapter 2 of this Thesis). For a double potential well model, a definition for the average transmission time is offered in this paper but the question whether an experimental set-up to measure average transmission times can be devised is open and hence, the question remains whether the average transmission time for a double potential well can be verified by experiments. The usefulness of the definition of average transmission times would be greatly enhanced if average transmission times can be experimentally measured.

3.6 Acknowledgement

Frank Vergeldt was of great help in performing programming acrobatics.

3.7 Appendix

3.7.1 Calculation of energy eigenvalues and construction of the wave functions

We take atomic units, i.e. we put $m = 1$ and $\hbar$=1. General solutions for the Schrödinger equation for the double potential well are:

$$\Psi(x) = \begin{cases} A\exp(ikx) + B\exp(-ikx) & \text{if } -a \le x \le -b, \\ C\exp(-\alpha x) + D\exp(\alpha x) & \text{if } -b \le x \le b, \\ F\exp(ikx) + G\exp(-ikx) & \text{if } b \le x \le a \end{cases} \tag{3.26}$$

$k^2 = 2E$ en $\alpha^2 = 2(V - E)$ α is real and $E < V$. Taking the boundary conditions in consideration gives us even (symmetric) and odd (asymmetric) solutions. For the even solutions we find:

$$f_e(x,t) = \begin{cases} N_e i\sin(k_e(x+a))\exp(-i(k_e a + E_e t)) & \text{if } -a \le x \le -b, \\ N_e i\sin(k_e(b-a))\exp(-i(k_e a + E_e t))\frac{\cosh(\alpha_e x)}{\cosh(\alpha_e b)} & \text{if } -b \le x \le b, \\ -N_e i\sin(k_e(x-a))\exp(-i(k_e a + E_e t)) & \text{if } b \le x \le a \end{cases} \tag{3.27}$$

where a, b and V are explained in Fig 3.1
N_e =normalising factor (even case)
$k_e = \sqrt{2E_e}$
$\alpha_e = \sqrt{2(V - E_e)}$
and E_e is the solution of the equation:

$$\arctan\left(\frac{\sqrt{E_e}}{\sqrt{V - E_e}}\coth(b\sqrt{2(V - E_e)})\right) = n\pi - (a - b)\sqrt{2E_e} \tag{3.28}$$

n is a positive integer
and for the odd solutions:

$$f_o(x,t) = \begin{cases} N_o i\sin(k_o(x+a))\exp(-i(k_o a + E_o t)) & \text{if } -a \le x \le -b, \\ N_o i\sin(k_o(b-a))\exp(-i(k_o a + E_o t))\frac{\sinh(\alpha_o x)}{\sinh(\alpha_o b)} & \text{if } -b \le x \le b, \\ N_o i\sin(k_o(x-a))\exp(-i(k_o a + E_o t)) & \text{if } b \le x \le a \end{cases} \tag{3.29}$$

where N_o =normalizing factor (odd case)
$k_o = \sqrt{2E_o}$
$\alpha_o = \sqrt{2(V - E_o)}$
and E_o can be found by solving:

$$\arctan\left(\frac{\sqrt{E_o}}{\sqrt{V - E_o}}\tanh(b\sqrt{2(V - E_o)})\right) = n\pi - (a - b)\sqrt{2E_o} \tag{3.30}$$

To create the total wave function we use as coefficients (see formula 3.6):

$$c_e = \frac{\exp(-ik_o a)}{\sqrt{2}} \tag{3.31}$$
$$c_o = \frac{\exp(-ik_e a)}{\sqrt{2}}$$

The total wave function is (see formula 3.5):

$$\Psi(x,t) = c_e f_e(x,t) + c_o f_o(x,t) \tag{3.32}$$

3.7.2 Proof that probability to encounter the particle between $-b$ and b is independent of time

To prove that the probability to encounter a particle between $-b$ and b is independent of time, we have to prove that $\int_{-b}^{b} dx\,|\Psi(x,t)|^2$ is independent of time.

$$\int_{-b}^{b} dx\,|\Psi(x,t)|^2 \quad = \tag{3.33}$$

$$\int_{-b}^{b} dx(\frac{1}{2}(|f_e(x,t)|^2 + |f_e(x,t)|^2) + c_e^* c_o f_e^*(x,t) f_o(x,t) + c_e c_o^* f_e(x,t) f_o^*(x,t))$$

The last two terms become zero and hence

$$\int_{-b}^{b} dx\,|\Psi(x,t)|^2 \quad = \tag{3.34}$$

$$\frac{1}{2}(N_e^2(\frac{\sin^2(k_e(b-a))}{\cosh^2(\alpha_e b)})(b + \frac{\sinh(2\alpha_e b)}{2\alpha_e}) +$$

$$N_o^2(\frac{\sin^2(k_o(b-a))}{\sinh^2(\alpha_o b)})(-b + \frac{\sinh(2\alpha_o b)}{2\alpha_o}))$$

(see Appendix 3.7.1 for the definition of the symbols) This expression is independent of time.

Chapter 4

SPECTRAL EFFECTS OF EXCITONIC INTERACTIONS IN DISORDERED SOLID FILMS

Regien G. Stomphorst, Tjeerd J. Schaafsma, and G. van der Zwan, J. Phys. Chem., in press.

4.1 ABSTRACT

This paper describes the absorbance properties of pigments in disordered films. The fluorescence quenching of pigment systems at low concentrations are usually attributed to the presence of so–called statistical pairs. We show that, if line broadening mechanisms are taken into account such as homogeneous and inhomogeneous broadening, and statistical distribution of distances between the pigments, the number of potential quenchers decreases dramatically, since all these effects lead to an increase of the dipole strength of the lowest excitonic state of a dimer. We also show, on the basis of Monte Carlo calculations on assemblies of pigments, that spectral effects beyond a general broadening of the spectrum will not be observed, even for concentrated systems, where a larger number of these statistical pairs may assumed to be present.

4.2 INTRODUCTION

One of the interesting questions of photosynthesis is how antenna systems are able to keep an excited state from degrading or losing its energy by fluorescence, before the excitation is delivered to the reaction center, where it can effectively be used for initializing electron transfer reactions.

In natural photosynthetic systems the chromophores are usually embedded in a protein. One of its effects is that the pigments are held in place, at specific positions and orientations. The concentration of chromophores in such systems can be quite high. In LHCII for instance with 12 chlorophyll (Chl) pigments in a box of approximately 4 nm size, the average distance between the pigments ranges from 1 to 2 nm [81]. This amounts to a concentration of ≈ 0.2 M, whereas concentration quenching in dye [82], and chlorophyll solutions [83, 84] starts to play an important role at the much smaller concentrations of 10^{-3}–10^{-4} M. Nevertheless LHCII is capable of preserving the excited state on Chla for periods up to several nanoseconds [85].

Embedding the pigments in a polymer matrix mimics the protein pigment complexes. These systems can be used profitably to study energy transfer [86, 87], since the clustering behavior that chromophores such as chlorophylls or porphyrins often display in water and organic solvents can be avoided. However, matrices like polyvinylalcohol do not influence the relative positions and orientations of the chromophores, while in photosynthesis the proteins do. As a consequence fluorescence quenching at higher concentrations cannot be avoided.

In these random systems, the mechanism of fluorescence quenching remains fundamentally a mystery [84, 34]. It is generally assumed that excitations are transferred to so–called "statistical pairs", excitonically coupled dimers with random relative orientation, by a Förster transfer mechanism, and that these dimers somehow avoid fluorescence, and back–transfer of the excitation.

Since the initial steps in photosynthesis, the harvesting of light, and the subsequent transfer of the excitation to a reaction center are extremely important in reaching its high overall efficiency, a thorough understanding of the underlying mechanisms would be very helpful in the construction of artificial antenna systems [88].

In a recent paper Knox [34] argued that on average a statistical pair has a smaller oscillator strength for the lowest excitonic transition than for the highest, leading to a blueshifted spectrum for a collection of statistical pairs. This is not observed, in general the absorption spectrum changes little even for relatively high concentrations, and if larger changes are observed it is most likely due to ground state interaction effects at higher concentrations [89] (Chapter 5 of this Thesis).

In this paper we argue that the effect is even smaller than Knox calculated, for two reasons: the inclusion of inhomogeneous broadening as diagonal disorder in the exciton Hamiltonian leads to an increase of the oscillator strength of the lowest excitonic state, even for a completely dark state, and secondly taking a distribution of positions for the monomer comprising a dimer also has a broadening effect. Together these effects lead to a slightly broadened absorption spectrum, and not to a blueshifted spectrum.

Inclusion of a distribution of distances does, however, point to a possible mechanism for fluorescent concentration quenching. On the basis of the nearest neighbor distribution function derived by Hertz [90] we argue that around every pigment there is likely to be at least one pigment pair of which the pigments are closer than 1 nm within a sphere determined by the Förster radius R_F. Such a dimer will not likely be a dimer in which the pigments have random orientations, since due to steric hindrance a more parallel configuration will be favored. For chlorophylls, bacteriochlorophylls and porphyrins such parallel relative orientations can easily lead to close lying charge transfer (CT) states. Evidence for this can be found in large positive first order contributions (red shifts) to the Stark spectrum of for instance the special pair in the reaction center or LH antenna systems [91, 92, 93]. Although CT states are usually slightly higher in energy than the covalent states due to the "Coulomb penalty", that has to be paid for putting an extra electron on a pigment [94], in polar media this is offset by the lowering in energy such a system can get by means of its own reaction field [95, 96, 97, 98, 99]. These CT states are obviously dark, since they have no transition dipole moment to the ground state, and for the same reason they cannot transfer their energy to another chromophore by means of a Förster type transfer mechanism. Hence they can effectively quench the fluorescence of a concentrated solution of pigments.

In this paper we present a theoretical study of the absorption spectrum due to excitonic interactions between pigment molecules located at random positions and with random orientation. In the first part of the paper we will follow Knox [34], and consider dimers only, but we do include inhomogeneous as well as homogeneous broadening, and allow for random positions as well. We will give an analytic derivation of Knox's result, and show that inclusion of the above broadening mechanisms decrease the blueshift effect alluded to above. We will also show explicitly that even for a dimer with a dark low excitonic state diagonal disorder will make the lowest transition allowed.

In the second part of the paper we will consider the absorption spectrum that results if we take a large, random collection of pigments. It can then be showed that only a general broadening of the absorption spectrum will be observed at higher concentrations, but that even at moderate concentrations a large enough concentration of quenchers is present, so that every pigment is close enough to such a quencher to lose its energy by Förster transfer, rather than fluorescence. Observable effects in the absorption spectrum only occur when the pigments get so close that the assumption of random orientations is no longer justified.

4.3 DESCRIPTION OF THE SYSTEM

The dimeric system consists of two two-level monomers, of which we only consider the relative position and orientation of the transition dipole moments. The vector connecting the positions of the transition dipoles is denoted by $\vec{R}$, and we define a dimer frame by letting the z-axis point along the $\vec{R}$ direction. Furthermore we choose the dimer frame such that the transition moment of pigment 1 is in the xz-plane. The polar angle of pigment 1 is given by θ_1, its azimuth is by definition zero, the polar angle and azimuth of the transition dipole of pigment 2 are given by θ_2 and ϕ respectively. The structure is displayed in Fig. 4.1.

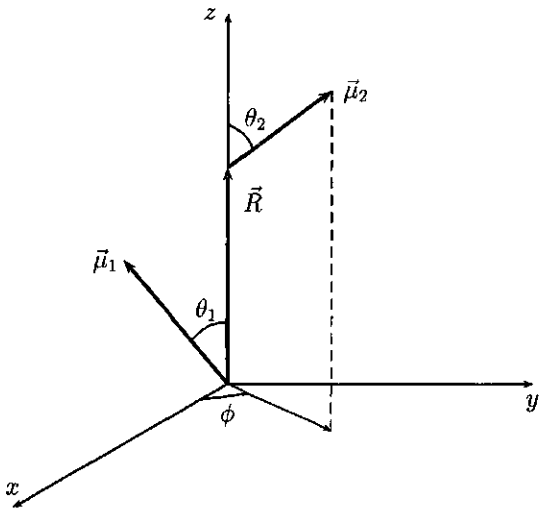

Figure 4.1: Positions and orientations of the two transition dipole moments in the dimer frame.

The hamiltonian describing the single excitations of the excitonically coupled dimer is given by the matrix

$$\mathcal{H} = \begin{pmatrix} \epsilon_1 & V \\ V & \epsilon_2 \end{pmatrix} \tag{4.1}$$

The energies ϵ_1 and ϵ_2 are the excitation energies of pigment 1 and pigment 2 respectively, and V is the excitonic interaction

$$V = \frac{1}{4\pi\epsilon_0\epsilon R^3}\vec{\mu}_1 \cdot \left(1 - 3\frac{\vec{R}\vec{R}}{R^2}\right) \cdot \vec{\mu}_2 \tag{4.2}$$

Changes in the ground state energy, and doubly excited state are neglected throughout this paper. This is justified since $V << \epsilon_{1,2}$, and such changes are second order in $V/\epsilon_{1,2}$.

The magnitude of the interaction depends on the transition dipole moments, and the distance between the pigments. We use the quantity

$$V_0 \approx 5.035 \frac{\mu^2}{\varepsilon R^3} \text{ cm}^{-1} \tag{4.3}$$

with μ in D and R in nm, to scale the interactions. For the Q_y transition of chlorophyll for instance, the transition moment is approximately 5.6 D, so that at a distance of 1 nm, the interaction energy V_0 between two chlorophyll molecules is approximately 160 cm^{-1}. The interaction can furthermore be modified by the relative dielectric constant ε, which for most systems is between 1 and 2.

We can now express the interaction energy in terms of the angles defined in Fig. 4.1:

$$V = V_0 \left[\sin\theta_1 \sin\theta_2 \cos\phi - 2\cos\theta_1 \cos\theta_2\right] \tag{4.4}$$

For random systems the angles θ_1, θ_2, and ϕ, and the distance R between the pigments is not fixed, but can vary according to a distribution function $N(R, \theta_1, \theta_2, \phi)$. Furthermore, the excitation energies of the monomers are also subject to some variation. For those parts of this paper where we take this diagonal disorder into account, we will assume that these values can be taken from a Gaussian distribution around the unperturbed value ϵ_0, with variance σ. Typical values for σ at room temperature are between 100 cm^{-1} and 300 cm^{-1} [84, 86, 87, 34].

We are primarily interested in the absorption spectrum of this dimer, and the oscillator strength of the lowest excitonic state. It is rather straightforward to diagonalize the Hamiltonian (4.1), and to find the excitonic states, and transition moments to these states [100]. The eigen values are:

$$\epsilon_\pm = \frac{1}{2}\left[\epsilon_1 + \epsilon_2 \pm \sqrt{(\epsilon_1 - \epsilon_2)^2 + 4V^2}\right] \tag{4.5}$$

We can write the corresponding excitonic states as

$$|+\rangle = c\,|1\rangle + s\,|2\rangle \quad \text{and} \quad |-\rangle = -s\,|1\rangle + c\,|2\rangle \tag{4.6}$$

where $|i\rangle$ denotes the state where the excitation is on monomer i, and $|\pm\rangle$ denote the excitonic states. The quantities s and c can be found from

$$s = \frac{t}{\sqrt{1+t^2}} \quad \text{and} \quad c = \frac{1}{\sqrt{1+t^2}} \tag{4.7}$$

with

$$t = \frac{\epsilon_2 - \epsilon_1 + \sqrt{(\epsilon_1 - \epsilon_2)^2 + 4V^2}}{2V} \tag{4.8}$$

The transition moments to the excitonic states can then be written as

$$\vec{\mu}_+ = c\vec{\mu}_1 + s\vec{\mu}_2 \quad \text{and} \quad \vec{\mu}_- = -s\vec{\mu}_1 + c\vec{\mu}_2 \tag{4.9}$$

The intensities of the transition are determined by the square of these quantities, under the assumption that the dimer can occur in any orientation with equal probability. We can write these intensities as:

$$I_+ = \mu^2 [1 + 2sc\cos\theta] \quad \text{and} \quad I_- = \mu^2 [1 - 2sc\cos\theta] \tag{4.10}$$

with θ the angle between the original transition moments, given by $\cos\theta = \cos\theta_1 \cos\theta_2 + \sin\theta_1 \sin\theta_2 \cos\phi$. This gives us the spectrum for every possible orientation, and relative position of the pigments. To find the observed spectrum, we have to average this with the distribution functions $N(R, \theta_1, \theta_2, \phi)$, and the distributions of the pigment energies. We will calculate the probability $P(I, \nu)$ of finding an intensity I at frequency ν. This quantity can be found from the expression

$$\begin{aligned} P(I,\nu) \;=\; & \frac{1}{2}\int_0^\infty dR \int_{-1}^{1} d\cos\theta_1 \in t_{-1}^{1} d\cos\theta_2 \int_0^{2\pi} d\phi\, N(R,\theta_1,\theta_2,\phi) \\ & \int_{-\infty}^{\infty} d\epsilon_1 \int_{-\infty}^{\infty} d\epsilon_2\, f(\epsilon_1) f(\epsilon_2) \left[\delta(\nu-\epsilon_+)\delta(I-I_+) + \delta(\nu-\epsilon_-)\delta(I-I_-)\right] \end{aligned} \tag{4.11}$$

The distribution f is given by:

$$f(\epsilon) = \frac{1}{\sqrt{2\pi\sigma^2}} e^{-(\epsilon-\epsilon_0)^2/2\sigma^2} \tag{4.12}$$

Eqn. (4.11) forms the basis of all our calculations. The absorption spectrum can be found as

$$\langle I \rangle_\nu \equiv I(\nu) = \int dI\, I P(I,\nu) \tag{4.13}$$

Homogeneous broadening, the result of the finite lifetime of each state, can be introduced in this description by replacing the $\delta(\nu - \epsilon_\pm)$ functions by the desired line profile.

DISTRIBUTION FUNCTIONS

The distribution functions we will use are all derived from $N(R, \theta_1, \theta_2, \phi)$. We first write it in the form

$$N(R, \theta_1, \theta_2, \phi) = W(R) N_R(\theta_1, \theta_2, \phi) \tag{4.14}$$

where $W(R)dR$ is the probability density for finding the nearest neighbor between R and $R + dR$, and $N_R(\theta_1, \theta_2, \phi)$ is the probability density for finding a set of angles $(\theta_1, \theta_2, \phi)$, given that the distance of the chromophores is R.

An expression for $W(R)$ was derived by Hertz [90, 101], and can be written as

$$W(R) = 4n\pi R^2 e^{-\frac{4}{3}n\pi R^3} \equiv 3\frac{R^2}{R_0^3}e^{-R^3/R_0^3} \tag{4.15}$$

where n is the particle density. R_0 (in nm) is related to the molarity M of the pigment concentration by

$$R_0 = \left(\frac{3 \times 10^{24}}{4\pi \times 6.025 \times 10^{23} M}\right)^{\frac{1}{3}} \approx 0.73\, M^{-\frac{1}{3}} \tag{4.16}$$

We can use this to estimate the number of quenchers in a given solution. Let us assume that a pair of pigments can act as a quencher when the distance is smaller than 1 nm. The probability of finding such a pair is given by

$$\int_0^1 dR\, W(R) = 1 - e^{-1/R_0^3} \tag{4.17}$$

with R_0 in nm. Together with eqn. (4.16), this means that for a molarity of 10^{-3} approximately 2.5×10^{-3} pigment pairs are found that are closer together than 1 nm.

Energy can be transferred at much lower concentrations, as evidenced by depolarization measurements on pigments in films, which show energy transfer at concentrations of 10^{-6}–10^{-7} M [86, 87, 102]. This also defines a radius, R_F, related to the Förster radius, of a sphere around an excited particle in which other pigment particles must be found to transfer the energy to. It is obvious that at concentrations 10^3 higher than these, every excited pigment will at least have a few quenching pairs within its Förster radius. Since these pairs only make a small contribution to the total number of pigments, it is not surprising that effects on the absorption spectrum are small.

The inverse of the indefinite integral $F(R)$ of $W(R)$ is given by

$$R = \left(\frac{3}{4\pi n} \ln \frac{1}{1-F}\right)^{1/3} \tag{4.18}$$

This makes it simple to generate the distribution $W(R)$ from a distribution of uniform deviates F [103, Ch. 7]. We will use this in the simulations in section 4.5.

The angular distribution $N_R(\theta_1, \theta_2, \phi)$ is more complicated. In general we can state that for large R all orientations are possible, an assumption used by Knox [34] to calculate the spectra. For shorter distances it obviously depends on the shape of the molecules what the preferred relative orientations are. For planar molecules as (bacterio)-chlorophylls and porphyrins a shifted coplanar orientation ("slipped deck of cards") appears to be common [87]. This can be introduced as a restriction on $\theta_1 \sim \theta_2$, *cf.* Fig. 4.1, which puts the transition dipoles in more or less parallel planes.

In the next section we first rederive Knox' result by an analytical procedure.

4.4 THE SPECTRAL PROFILE OF STATISTICAL PAIRS

In this case we make a number of additional assumptions. The excitation energies ϵ_i of both pigments are equal to ϵ_0. Furthermore the distance between the pigments is fixed at some value $\overline{R}$, and for that value all possible orientations are equally probably. The distribution function for positions and angles then becomes

$$N(R, \theta_1, \theta_2, \phi) = \frac{1}{8\pi}\delta(R - \overline{R}) \tag{4.19}$$

Note, however, that there is no conceivable limit in which eqn. (4.15) reduces to a delta function, except for the "close packing" situation, in which case the other assumptions are hardly justified, and singling out a pair of pigments from the closely packed cluster to calculate the absorption spectrum of the complete systems makes no sense. In other words, we do not expect the absorption spectrum of the complete system to even remotely resemble the absorption spectrum of a collection of random pairs. The calculation is still useful, since it can provide us with an estimate of the number of potential quenchers for this situation.

In addition eqn. (4.5) simplifies to

$$\epsilon_{\pm} = \epsilon_0 \pm V \tag{4.20}$$

and t, eqn. (4.8), becomes

$$t = \frac{|V|}{V} = \text{sign}(V) \tag{4.21}$$

Finally, the R in eqn. (4.4) has to be replaced by $\overline{R}$.

The absorption intensities reduce to the following expressions:

$$I_+ = \mu^2 [1 + t\cos\theta] \quad \text{and} \quad I_- = \mu^2 [1 - t\cos\theta] \tag{4.22}$$

The intensities, and excitation frequencies of course still depend on all the angles involved in the problem.

Eqn. (4.11) also becomes simpler:

$$P(I, \nu) = \frac{1}{16\pi}\int_{-1}^{1} d\cos\theta_1 \int_{-1}^{1} d\cos\theta_2 \int_0^{2\pi} d\phi \, [\delta(\nu - \epsilon_+)\delta(I - I_+) + \delta(\nu - \epsilon_-)\delta(I - I_-)] \tag{4.23}$$

In appendix A we show that this integral can be evaluated exactly, and be expressed in an elliptic function. In that appendix we also derive an analytical expression for the function

$I(\nu)$, which is shown to be equal to:

$$I(\nu) = \mu^2 \left[\frac{1}{2}(\nu - \epsilon_0) + (\epsilon_0 + V_0 - \nu) \frac{\text{asinh}\sqrt{3}}{2\sqrt{3}} \right] \quad \text{for} \quad |\nu - \epsilon_0| < V_0 \tag{4.24}$$

and

$$\begin{aligned} I(\nu) &= \mu^2 \left[\frac{1}{2}(\nu - \epsilon_0) - \frac{\nu - \epsilon_0}{|\nu - \epsilon_0|} \sqrt{\frac{(\nu - \epsilon_0)^2 - V_0^2}{3}} \right. \\ &+ \left. \frac{\epsilon_0 + V_0 - \nu}{2\sqrt{3}} \left(\text{asinh}\sqrt{3} - \text{asinh}\sqrt{\frac{(\nu - \epsilon_0)^2}{V_0^2} - 1} \right) \right] \quad \text{for} \quad V_0 < |\nu - \epsilon_0| < 2V_0 \end{aligned} \tag{4.25}$$

In these expressions the function asinh is the inverse hyperbolic sine.

In Fig. 4.2 we show this spectrum for a pair of Chla molecules at a distance of $\overline{R} = 1$ nm. It is identical to the one calculated by Knox [34] by Monte Carlo techniques.

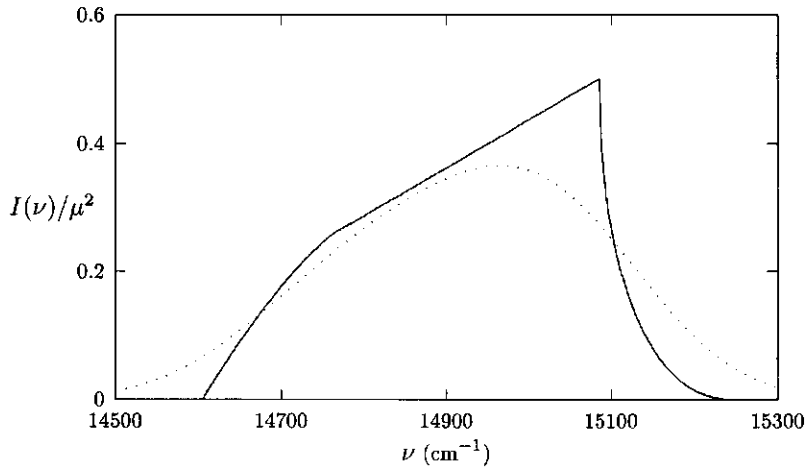

Figure 4.2: Spectrum of an ensemble of statistical pairs. The properties of the Q_y transition of chlorophyll a pigments were used to model this spectrum. The distance between the pigments is 1 nm, their transition dipole moment 5.6 D, and the transition energy was taken to be 14925 cm^{-1} (670 nm). The dashed spectrum is obtained by giving every realization a homogeneous width of 100 cm^{-1}.

The spectrum shown in Fig. 4.2 is in fact built of stick spectra. The effects of homogeneous broadening can be taken into account by dressing the sticks with a Gaussian, or

Lorentzian, lineshape. In that case we replace the terms $\delta(\nu - \epsilon_{\pm})$ by the appropriate lineshape function, and subsequently perform the integrations numerically. Homogeneous broadening is related to the lifetime of the chromophores, which for Chla in solution was measured to be ≈ 5 ns, and the width of the phonon wing, which is the main contribution. We estimate the homogeneous linewidth to be 100 cm^{-1}, at room temperature. This has important consequences for a possible quenching mechanism based on these statistical pairs. The dashed spectrum in Fig. 4.2 shows the homogeneously broadened spectrum of statistical pairs.

Quenching is supposed to take place by the following mechanism: an excited monomer loses its energy by the Förster transfer mechanism to a nearby statistical dimer. This cannot be to the lower excitonic state of that dimer, since that state is supposed to be dark, and thus cannot have a transition dipole moment, and can consequently not interact with the monomer. The upper excitonic state of the dimer thus gets excited, within a very short time loses some of its energy through interaction with the surrounding medium and reduces to the lower excitonic state. If that state is indeed dark, fluorescence will be quenched. Within this context dark of course means that it will lose its energy some other way, before it has a chance to fluoresce. This is not easy to quantify on the basis of the above picture, but let's assume all states in the lower 10% of the above spectrum are sufficiently dark to act as quenching states. A smaller number will certainly not give enough dimers with the correct geometry in the near neighborhood of our excited pigment, as our calculations of the previous section show.

What is not visible in the above spectrum is that it results from pairs of lines, and not from uncorrelated single lines. Moreover, these lines are symmetrical with respect to the unperturbed excitation energy ϵ_0. That means that the upper excitonic state corresponding to a lower excitonic dark state must occur at the very blue edge of the spectrum.

Apart from the distance and relative angles between pigments, Förster transfer also depends on the overlap between the emission spectrum of the donor, and the absorption spectrum of the acceptor. The emission spectrum of a pigment is usually to the red of the absorption spectrum due to the Stokes shift, but even if we assume that the Stokes shift is zero, the amount of overlap between a line with width 100 cm^{-1} at position 14925 cm^{-1} and a similar line at 15200 cm^{-1} is negligible: for Gaussian lines the overlap factor is 0.02.

As a consequence we may state that even if the lower excitonic state of a statistical dimer can be considered dark, an excited monomer has no possible mechanism to transfer its energy to the higher excitonic state of that same dimer.

It is not immediately obvious that there could be no quenching dimers with small exciton splitting, but a moments reflection shows that the spectrum in Fig. 4.2 gives also the correlation between lower state dipole moment and excitonic splitting: the lower half of the spectrum is the lower state dipole moment squared, and the distance to the center of

the spectrum just half the excitonic splitting, so small transition dipoles correlate directly with large exciton splitting.

Often dimers have s spectrum that is red-shifted compared to the monomer spectra, which would of course be helpful for energy transfer from monomers, since it increases the overlap between monomer emission, and highest excitonic state absorption, but on the other hand the red-shift can be taken as indicative for the coupling with a charge transfer state [104, 105, 106], so that those dimers which do get a considerable overlap are also those with the most charge transfer character.

A possible way out of this dilemma is the introduction of inhomogeneous broadening mechanisms: inhomogeneous broadening is usually much larger than homogeneous broadening, and could easily give us monomers which spectra overlap with upper excitonic states, but we will show in the next section that inhomogeneous broadening also has the effect of increasing lower excitonic state dipole strengths.

4.5 INHOMOGENEOUS BROADENING EFFECTS

Starting point is again eqn. (4.11), but now we concentrate first on the integrals over the distribution functions $f(\epsilon)$. For a given set of angles, and positions, the intensity $I(\nu)$ can be written as

$$I(\nu) = \frac{1}{2}\int_{-\infty}^{\infty} d\epsilon_1 \int_{-\infty}^{\infty} d\epsilon_2\, f(\epsilon_1) f(\epsilon_2) \left[I_+ \delta(\nu - \epsilon_+) + I_- \delta(\nu - \epsilon_-)\right] \tag{4.26}$$

We introduce the following notation [107]:

$$\Delta = \frac{1}{2}[\epsilon_2 - \epsilon_1] \quad \text{and} \quad \Sigma = \frac{1}{2}[\epsilon_2 + \epsilon_1] \tag{4.27}$$

The new transition dipoles can then be written as:

$$I_\pm = \mu^2 \left[1 \pm \frac{V}{\sqrt{\Delta^2 + V^2}} \cos\theta\right] \tag{4.28}$$

and the corresponding energies are

$$\epsilon_\pm = \Sigma \pm \sqrt{\Delta^2 + V^2} \tag{4.29}$$

Furthermore a straightforward calculation gives the distribution of Σ and Δ as:

$$P(\Sigma, \Delta) = \frac{1}{\pi\sigma^2} e^{-(\epsilon_0 - \Sigma)^2/\sigma^2} e^{-\Delta^2/\sigma^2} \tag{4.30}$$

Introducing of this result in eqn. (4.26 and subsequently performing the integration of Σ gives

$$I(\nu) = \frac{\mu^2}{2\sqrt{\pi\sigma^2}} \int_{-\infty}^{\infty} d\Delta\, e^{-\Delta^2/\sigma^2} \left[e^{-(\epsilon_0 - \nu + \sqrt{\Delta^2+V^2})/\sigma^2} \left(1 + \frac{V}{\sqrt{\Delta^2+V^2}} \cos\theta \right) \right.$$
$$\left. + \; e^{-(\epsilon_0 - \nu - \sqrt{\Delta^2+V^2})/\sigma^2} \left(1 - \frac{V}{\sqrt{\Delta^2+V^2}} \cos\theta \right) \right] \tag{4.31}$$

For $\Delta = 0$ we recover the stick spectrum, for not too large values of Δ we can approximate the integral by

$$I(\nu) = \frac{1}{2}\mu^2 e^{-(\epsilon_0 - \nu + \sqrt{\sigma^2+V^2})/\sigma^2} \left(1 + \frac{V}{\sqrt{\sigma^2+V^2}} \cos\theta \right)$$
$$+ \; \frac{1}{2}\mu^2 e^{-(\epsilon_0 - \nu - \sqrt{\sigma^2+V^2})/\sigma^2} \left(1 - \frac{V}{\sqrt{\sigma^2+V^2}} \cos\theta \right) \tag{4.32}$$

In Fig. 4.3 we have plotted the spectrum resulting from eqn. (4.31) as well as from (4.32) for an inhomogeneous broadening of 100 cm^{-1}. We took the special case where the transition dipoles are in the same direction, and perpendicular to the vector connecting them, so that for the unperturbed system the lower excitonic state is completely dark. We note that the spectrum can reasonably well approximated by eqn. (4.32), that the exciton splitting is not equal to $2V$ but to $2\sqrt{\sigma^2+V^2}$, which differs substantially from $2V$, and finally that the lowest excitonic state acquired a considerable amount of dipole strength. Realistic values of σ are often higher. For $\sigma = 200$ cm^{-1}, we find that the lower excitonic state caries about 10% of the total oscillator strength. The effect of exchange narrowing that inhomogenous broadening by diagonal disorder also shows is for a dimer not of great relevance.

In Fig. 4.4 we show the spectrum resulting from averaging expression (4.31) over all possible orientations of the transition dipoles. As in Fig. 4.2 the distance between the pigments is taken to be fixed at 1 nm. We note that in this case the diagonal disorder also has as one of its main effects a considerable increase in the intensity of the lower excitonic state. Thus we may state that although the introduction of diagonal disorder undoubtably will increase the possibility of energy transfer from a monomeric pigment to the higher excitonic state of a quenching statistical dimer, a side effect is, however, that the quenching properties of such a dimer are decreased.

Although the spectral effects of excitonic coupling on the systems studied sofar are quite distinctive, ranging from observable excitonic splitting, as in Figs. 4.3, and 4.4, to enhancement of the red side of the spectrum for higher values of (in)homogeneous broadening, we do not expect to observe those effects in real systems. After all, the proportion of statistical pairs is small to begin with compared to the total number of absorbers, at least at low concentration, and furthermore the distribution of distances also obscures the effect. Of course, when the concentration gets higher, the number of statistical pairs

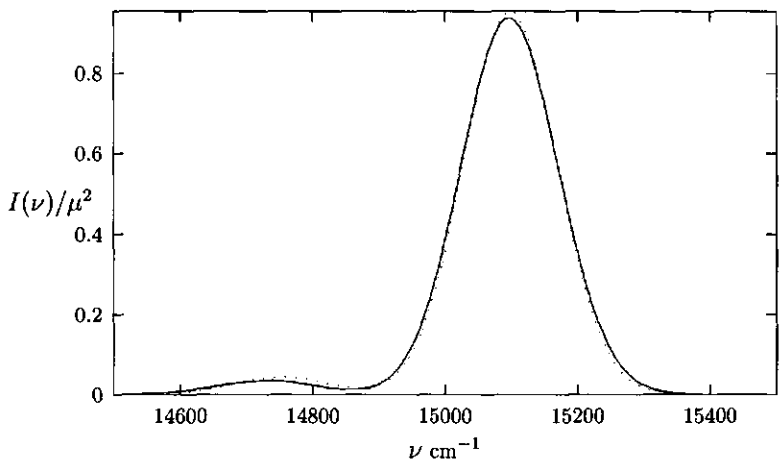

Figure 4.3: Disordered dimer spectrum calculated from eqn. (4.4) (solid line), and approximation (4.32) (dots). Parameters were chosen as follows: $\theta_1 = \theta_2 = \frac{\pi}{2}$, $\phi = 0$, $\mu = 5.6$ D, $R = 1$ nm, and $\sigma = 100$ cm^{-1}. The geometry of the dimer gives a lower excitonic state with no dipole strength in the absence of disorder. The full–width–half–maximum (FWHM) of the monomer spectrum is $2.355\sigma \approx 236$ cm^{-1}.

increases, but interaction with other pigments then also starts to play a role, since the likelihood of finding a trimer with relative distances smaller than 1 nm then also becomes appreciable. In the final section we show some calculation of spectra of more concentrated systems by taking all interactions into account, here we show that even for ordered pairs with a distance distribution the specific spectral effects are diminished. To that end we take the configuration described in the caption of Fig. 4.3, but we vary the distance according to the Hertz distribution, eqn. (4.18). The most probable distance for a given particle density is

$$\overline{R} = (2/3)^{1/3} R_0 \approx 0.87 R_0 \tag{4.33}$$

and we choose the values for the simulation such that this distance is 1 nm. This accounts for the variance still found in statistical pairs within quenching distance of an excited monomer. We note that this differs very little from the average distance for a given density, which can be written as

$$\langle R \rangle = R_0 \int_0^\infty dx\, x^{1/3} e^{-x} = R_0 \Gamma(\frac{4}{3}) \approx 0.89 R_0 \tag{4.34}$$

In Fig. 4.5 we show the spectrum resulting from a simulation where the distance was varied in accordance with the Hertz distribution, and where, in addition we assumed a homogeneous linewidth of 100 cm^{-1}, and an inhomogeneous width of 200 cm^{-1}. Also

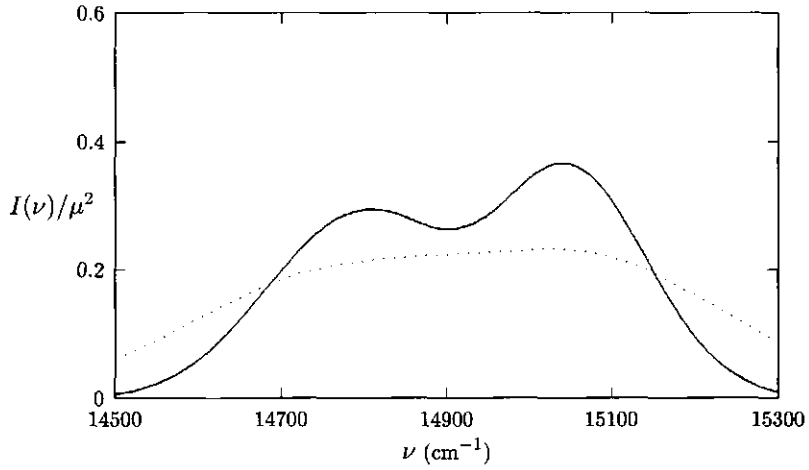

Figure 4.4: Inhomogeneously broadened spectrum of a statistical pair of chromophores. For the solid line we used an inhomogeneous linewidth of 100 cm^{-1}, for the dotted line 200 cm^{-1} was used. The latter is a more realistic value.

included is the spectrum of a monomeric pigment with the same broadening parameters. The dimer spectrum has become almost symmetrical, and compared with the monomer spectrum is shifted towards the blue, and slightly broader. Again there is considerable dipole strength at the red end of the spectrum.

In a subsequent paper [89] (Chapter 5 of this Thesis), we analyze spectra of erythrosin B in PVA film at varying concentrations, where apart from broadening a small blue shift can be observed at higher concentrations, and which can therefore be attributed to the effect described here, although formation of oligomers can also contribute significantly.

The monomer spectrum displayed in Fig. 4.5 was found by direct convolution of the Gaussian corresponding to the homogeneous broadening, and the Gaussian distribution of excitation energies. The result of this convolution is a Gaussian with width $\sqrt{\sigma^2 + \sigma_h^2}$, where σ_h is the variance of the homogeneous Gaussian. The dimer spectrum is broader, even though there is a small exchange narrowing effect, due to the distributed positions.

4.6 SPECTRAL EFFECTS

From the results of the previous section it could be concluded that the spectral effects of the presence of statistical pairs is considerable. In all cases studied the spectrum is asymmetric, and there is a considerable blue shift, even if homogeneous and inhomogeneous

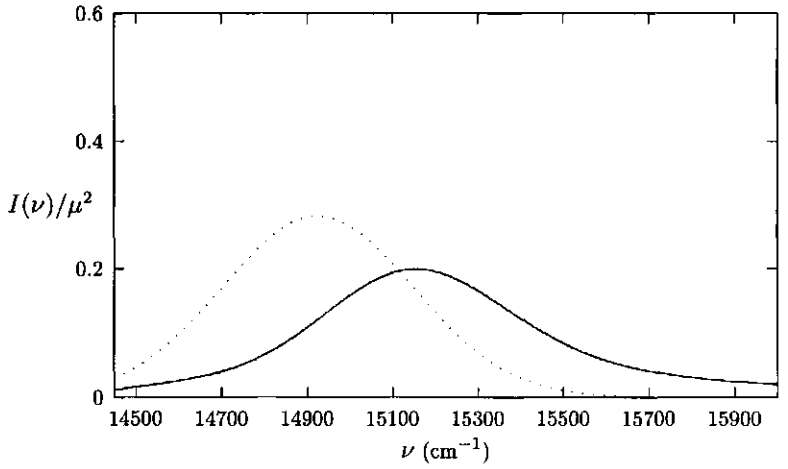

Figure 4.5: Spectrum of a statistical pair with fixed parallel orientation but positions distributed according to the Hertz distribution, eqn. (4.15). The most probable distance is chosen as 1 nm, and homogeneous (100 cm^{-1}) and inhomogeneous (200 cm^{-1}) broadening are included. Also shown (dotted) is the spectrum of a collection of monomers with the same values of homogeneous and inhomogeneous broadening parameters.

broadening are included, and if the distance distribution is taken into account. However, we also showed that the number of statistical pairs present in low concentration solution may be large enough to act as potential quenchers if an additional dark state is assumed, but the overwhelming majority of pigments will still occur in monomeric form, and dominate the absorption spectrum.

The spectrum displayed in Fig. 4.5 could be interpreted as the absorption spectrum of a collection of statistical pairs with preferred orientation. The spectral effects shown there, a blueshift, and extra broadening due to variations in relative positions could be observed for higher concentrations. However, for an average distance of 1 nm, the overall concentration is approximately 0.6 M, and consequently a larger number of pigments can be found in the immediate proximity of a statistical dimer, thus rendering the statistical pair picture incomplete. In fact on average a third neighbor will be found at a distance of $\sqrt{2} \approx 1.4$ times the nearest neighbor distance (*cf.* Fig. 4.6), which means that for a random system at a density such that the average distance is 1 nm, the interaction strength with the next nearest neighbor, which is about 40 % that of the nearest neighbor interaction, cannot be neglected. We could of course consider trimers, or tetramers, but that is hardly useful. It cannot be expected that they have lowest excitonic state that is dark, and the ground state interaction will make it very unlikely that these oligomers are statistical in nature.

In this section we show some results that could be found if systems were indeed completely random. The simulations were done on 20 randomly positioned and oriented pigments in a cubic box of length 5 nm. The value of R_0 for this setup if 1.15 nm, so that the average distance, and the most probably distance between nearest neighbors is $\approx$ 1 nm. In Fig. 4.6 we show the nearest neighbor distribution function for this situation. It differs slightly from the Hertz distribution, because of boundary effects: for particles near a wall there are fewer neighbors. The Figure shows that this does not have appreciable effects on the most probable nearest neighbor position. Obviously this could be improved using periodic boundary conditions but for our purposes that is hardly worthwhile.

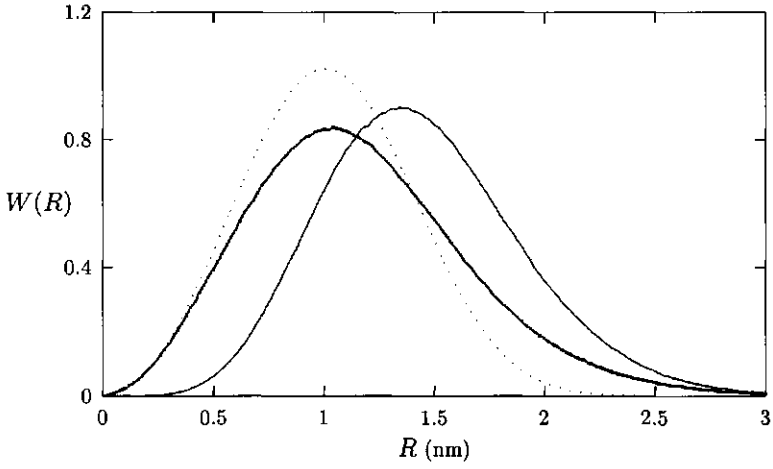

Figure 4.6: Normalized nearest neighbor distribution for randomly placed particles in a box. Also shown (dotted) is the Hertz distribution, eqn. (4.15) for $R_0 = 1.15$ nm. The thin solid line is the probability of finding a third pigment at distance R from the center of a nearest neighbor pair.

For a large number of realizations ($N = 10^4$) we calculated the average absorption spectrum of such a system by calculating all excitonic interaction energies V_{ij} (*cf.* eqn. (4.2)), diagionalizing the resulting Hamiltonian, and subsequently finding all excitonic states and their transition dipole moments. The result is displayed in Fig. 4.7 for zero inhomogeneous broadening, and for an inhomogeneous broadening of 100 cm^{-1}. We note that for zero inhomogeneous broadening there appears to be a large monomeric component to the spectrum, as evidenced by the sharp peak at the unperturbed transition frequency. There is no visible evidence for an enhancement at the blue side of the spectrum due to the presence of statistical pairs.

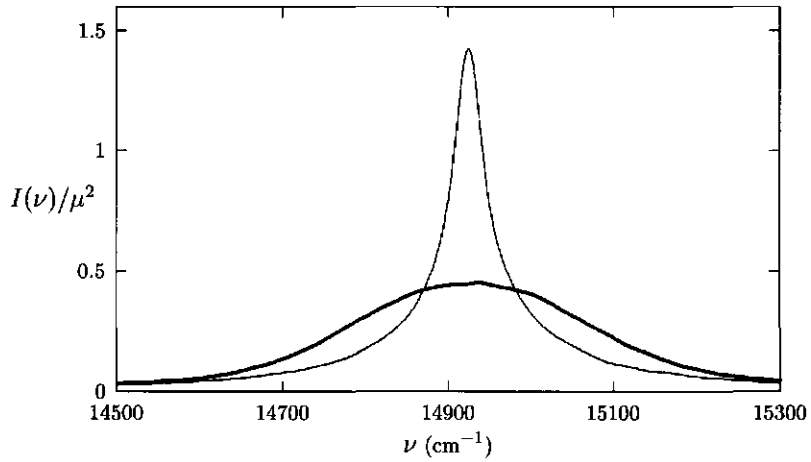

Figure 4.7: Absorption spectra for randomly distributed particles in a box. The particle density is 0.16 nm^{-3}, corresponding to a 0.27 M solution. Transition moments and excitation energies as in the other simulations. The thin solid curve is for an inhomogeneous broadening of zero, whereas the thick solid line has an inhomogeneous broadening of 100 cm^{-1}. The spectra were calculated with a small homogeneous broadening, 10 cm^{-1} to speed up convergence.

It can be inferred from Fig. 4.6 that roughly half of the nearest neighbors at the given particle density are closer than 1 nm. To see if steric hindrance has observable effects on the absorption spectrum, we also performed a simulation where all particles closer than 1 nm are given the same orientation. The results are displayed in Fig. 4.8 for a homogeneously broadened spectrum only. We used a small homogeneous broadening (10 cm^{-1}), mainly to speed up the convergence of the Monte Carlo calculation. Even for this small broadening the enhancement on the blue side can hardly be noticed. Simulations with larger homogeneous broadening, or additional inhomogeneous broadening do not show any difference with the spectra calculated without taking steric hindrance into account.

These results can easily be understood on the basis of the particle distribution function. As can be inferred from the results of the previous sections, a blueshifted spectrum, or enhancement of the blue side of the spectrum occurs for dimers with a preferred parallel orientation of the dipole moments, or statistical pairs, where the contribution of blueshifted spectra is still predominant over the redshifted spectra. A direct calculation shows that even for the relatively high concentrations considered here the number of pairs of pigments closer than 1.5 nm, (for larger distances the excitonic interaction becomes too small to give appreciable effects) still does not exceed more than 10 % of the total number of pairs. Even if we use maximal enhancement of these pairs by choosing them

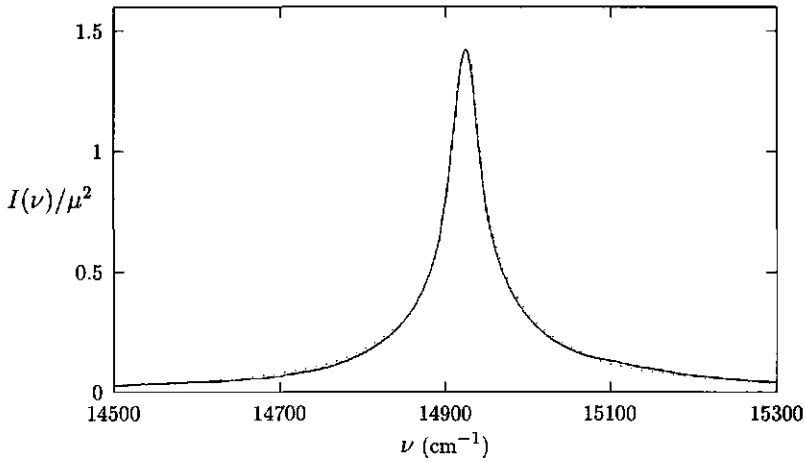

Figure 4.8: Absorption spectra for a random collection of pigments. The dotted spectrum is the same as the one displayed in the previous Figure. without inhomogeneous broadening. For the solid line spectrum the additional assumption was made that pigments closer than 1 nm have parallel transition dipole moments. There is an extremely slight decrease on the red side of the spectrum, and a corresponding slight increase on the blue side, in accordance with earlier results on statistical pairs.

to have parallel transition moment, the contribution is negligible.

4.7 CONCLUSIONS

The aim of this paper is twofold: to give an estimate of the number of potential quenchers in the neighborhood of an excited chromophore, and to show what the spectral effects of those quenchers are on the observed absortion spectrum.

Although a perfectly ordered dimer with a dark lower excitonic state could potentially act as a quencher, we have shown, on the basis of the Hertz distribution that such pairs are far too few in number if homogeneous and inhomogeneous broadening are taken into account, or (restricted) distributions over the relative orientations and distances. For higher concentrations, where the number of potential quenchers increases, the interaction with other nearby pigments starts to play a role, and the probability of finding a lowest excitonic dark state again decreases.

Spectroscopically the presence of quenching pairs will not be noticed, at least not in ordinary absorption spectroscopy. The results of the previous section indicate that the

absorption spectrum of a collection of pigments will mainly just be broadened at higher concentrations due to excitonic interactions, and the characteristic blueshift of the statistical pairs contributes insufficient to give an observable effect.

4.8 Appendix

Derivation of eqn. (4.24)

Starting point of the derivation is expression (4.23). To make the derivation more readable, we introduce the following dimersionless variables:

$$e_{\pm} = \frac{\epsilon_{\pm} - \epsilon_0}{V_0} = \pm(\sin\theta_1 \sin\theta_2 \cos\phi - 2\cos\theta_1 \cos\theta_2)\text{signV} \tag{4.35}$$

and

$$i_{\pm} = \frac{I_{\pm}}{\mu^2} - 1 = \pm(\sin\theta_1 \sin\theta_2 \cos\phi + \cos\theta_1 \cos\theta_2) \tag{4.36}$$

where we note that $|e_{\pm}| \leq 2$ and $|i_{\pm}| \leq 1$. Introducing $\cos\theta_i = x_i$ then yields:

$$e_+ = -e_- = \sqrt{1-x_1^2}\sqrt{1-x_2^2}\cos\phi - 2x_1x_2 \tag{4.37}$$

and

$$i_+ = -i_- = \sqrt{1-x_1^2}\sqrt{1-x_2^2}\cos\phi + x_1x_2 \tag{4.38}$$

Eqn. (4.23) can then be rewritten as

$$P(i,e) = \frac{1}{16\pi\mu^2 V_0}\int_0^{2\pi} d\phi \int_{-1}^{1} dx_1 \int_{-1}^{1} dx_2 (\delta(e-e_+)\delta(i-i_+) + \delta(e-e_-)\delta(i-i_-)) \tag{4.39}$$

where we also wrote $e = (\nu - \epsilon_0)/V_0$, and $i = I/\mu^2 - 1$.
Eqn. (4.13) can be expressed as

$$I(\nu) = \mu^2 \int_{-1}^{1} di\,(i+1)P(i,e) \tag{4.40}$$

Integration over ϕ is straightforward and gives:

$$P(i,e) = \frac{1}{16\pi\mu^2 V_0}\int_{-1}^{1} dx_1 \int_{-1}^{1} dx_2 \left[\frac{\delta(e-i+3x_1x_2)}{\sqrt{(1-x_1^2)(1-x_2^2)-(i-x_1x_2)^2}} + \frac{\delta(e-i-3x_1x_2)}{\sqrt{(1-x_1^2)(1-x_2^2)-(i+x_1x_2)^2}}\right] \tag{4.41}$$

where the values of i have to be such that the arguments of the square roots in these expressions are positive. Outside that range, the result is zero. Note that both terms are

in fact equal: a simple change of variables, for instance $x_2 \to -x_2$ in the second term proves this. Subsequently integrating over x_2 gives:

$$P(i,e) = \frac{1}{2\pi\mu^2 V_0} \int_0^1 dx_1 \frac{1}{\sqrt{(1-x_1^2)(9x_1^2-(e-i)^2) - x_1^2(2i+e)^2}} \tag{4.42}$$

again with the requirement that the argument of the square root is positive. This restricts the integration interval of x_1 for specific values of i and e. We also used that the integrand is symmetric in x_1.
Although it is possible to get analytical expressions in terms of elliptic functions for this integral, these are rather complicated. However, in view of eqn. (4.40) we only need

$$\langle i+1 \rangle_e = \int_{-1}^1 di\, iP(i,e) + \int_{-1}^1 di\, P(i,e) = \int_{-1}^1 di\, iP(i,e) + P(e) \tag{4.43}$$

To calculate the integrals in eqn. (4.43) we rewrite the square root in eqn. (4.42) as a function of i:

$$\sqrt{(1-x_1^2)(9x_1^2-(e-i)^2) - x_1^2(2i+e)^2} = \sqrt{ai^2+bi+c} \tag{4.44}$$

with

$$a = -3x_1^2 - 1, \quad b = -6ex_1^2 + 2e, \quad \text{and} \quad c = -9x_1^4 + 9x_1^2 - e^2 \tag{4.45}$$

First we note that

$$a \pm b + c = -[3x_1^2 \mp 1 \pm e]^2 < 0 \tag{4.46}$$

This means that at the boundaries $i = \pm 1$ the argument of the square root in eqn. (4.44) is negative for all values of x_1.
Furthermore $b^2 - 4ac$ can be written as

$$b^2 - 4ac = -36x_1^2(x_1^2-1)(3x_1^2 - e^2 + 1) \tag{4.47}$$

It is easy to see that for $|e| < 1$ this discriminant is larger than zero for all values of $0 < x_1 < 1$, whereas for $1 < |e| < 2$ it is only larger than zero in the interval $x_1 \in [\sqrt{(e^2-1)/3}, 1]$.
Eqns. (4.46) and (4.47) imply that the effective boundaries of the integration over i are $[-b \pm \sqrt{b^2-4ac}]/2a$.
Eqn. (4.43) can now be written as

$$\langle i+1 \rangle_e = \frac{1}{2\pi\mu^2 V_0} \int dx_1 \int di \frac{i+1}{\sqrt{ai^2+bi+c}} \tag{4.48}$$

The integration over i can be performed [108] and gives upon introduction of the integration boundaries and some straightforward algebraic manipulations

$$\int di \frac{i+1}{\sqrt{ai^2+bi+c}} = \pi \left[\frac{2e}{(3x_1^2+1)^{3/2}} + \frac{1-e}{(3x_1^2+1)^{1/2}} \right] \tag{4.49}$$

The remaining integral can be written as:

$$(i+1)_e = \frac{1}{\mu^2 V_0}\left[e\int_\alpha^1 dx\,(1+3x^2)^{-3/2} + \frac{1}{2}(1-e)\int_\alpha^1 dx\,(1+3x^2)^{-1/2}\right] \qquad (4.50)$$

with $\alpha = 0$ if $|e| < 1$ and $\alpha = \sqrt{(e^2-1)/3}$ if $1 < |e| < 2$. Both integrals are standard [108], the result is given in the main text as eqns. (4.24) and (4.25).

Chapter 5

A SPECTROSCOPIC STUDY OF ERYTHROSIN B IN PVA FILMS

Regien G. Stomphorst, Gert van der Zwan, Marc A.M.J. van Zandvoort, Alexander B. Sieval, Han Zuilhof, Frank J. Vergeldt and Tjeerd J. Schaafsma, J. Phys. Chem., in press.

5.1 ABSTRACT

The effects of increasing concentration (10^{-7} to 2.5×10^{-3} mol/g) of Erythrosin B (Ery B) in polyvinyl alcohol (PVA) films on its visible absorption spectrum have been investigated. In a concentration range of 2×10^{-7} to 10^{-5} mol/g no effects on the absorption spectrum are found. By contrast, within this concentration range time-resolved fluorescence experiments (fluorescence- and anisotropy decay) reveal the presence of energy transfer (ET) between Ery B molecules, followed by fluorescence at low concentrations and fluorescence quenching at higher concentrations. At a concentration of $\approx 5 \times 10^{-5}$ mol/g the absorption spectrum broadens as compared to the monomeric spectrum and fluorescence is almost completely quenched. A further increase of the concentration results in a blue shift of the absorption spectrum. Using molecular mechanics calculations it is shown that the initial broadening can be ascribed to excitonic interactions between randomly oriented molecules, whereas the blue shift at higher concentrations can be explained by the formation of oligomeric structures. At concentrations of $\geq 2.5 \times 10^{-3}$ mol/g the molecules are closely packed resulting in a contribution at the red edge of the absorption spectrum.

5.2 INTRODUCTION

Understanding the excitonic interactions between chromophores (pigment- or dye molecules) and the consequences for their spectral behavior is essential to construct artificial antenna systems [88, 109, 110]. In natural photosynthetic systems the chromophores are held in fixed relative orientations and distances, which are dictated by the proteins in which they are embedded. To create an artificial embedding for the dye molecules, one can conveniently make use of polymer matrices [32, 87]. Dye molecules in polymer films are more flexible in the way they organize themselves with respect to each other than chromophores embedded in proteins. The use of a polymer matrix avoids clustering of the dye molecules to aggregates that chromophores, such as chlorophylls or porphyrins, often display in water and organic solvents. However, in all randomly oriented systems excitation energy gets lost by fluorescence and fluorescence quenching [84]. Fluorescence quenching is mostly attributed to energy transfer from excited monomers to quenching pairs [34, 111] and already occurs at concentrations at which the majority of the molecules are still monomers as judged from the absorption spectra. Monomer to monomer energy transfer can be revealed by the fluorescence anisotropy decay of the acceptor molecules [112]. Monomer to dimer energy transfer can be investigated by fluorescence quenching. When excitonic interactions are affecting the absorption spectra, the first effect of these interactions is broadening of spectra compared to the monomeric spectra, provided the intermolecular distances are sufficiently large to exclude ground state interaction(s), resulting in preferential orientations of neighboring molecules [111] (Chapter 4 of this Thesis). When the concentration is too high to permit the chromophore molecules to be randomly oriented, intermolecular steric hindrance between the molecules dictates their orientational distribution.

This paper treats the spectral effects of increasing concentration of Erythrosin B (Ery B, Fig. 5.1) molecules in PVA films. We measured absorption spectra to investigate the behavior of Ery B molecules in PVA films, using absorption- and fluorescence spectroscopy and molecular mechanics computations to explain the spectral shifts and shapes of the absorption spectra at various chromophore concentrations. Because at low concentrations of Ery B the absorption spectra are not different from the monomeric spectra, we use the fluorescence life time and -anisotropy to investigate the intermolecular interactions between excited Ery B molecules at increasing concentration.

5.3 MATERIAL AND METHODS

5.3.1 Sample preparation

Dimethylsulfoxide (DMSO, J.T. Baker Chemicals B.V., analytical grade) was used without further purification. 100% Hydrolysed polyvinyl alcohol (PVA, Aldrich Chemie) with an average molecular weight of 100 kD was purified from side products using a modified ethanol extraction method previously described [86, 113]. Erythrosin B (Merck) was used

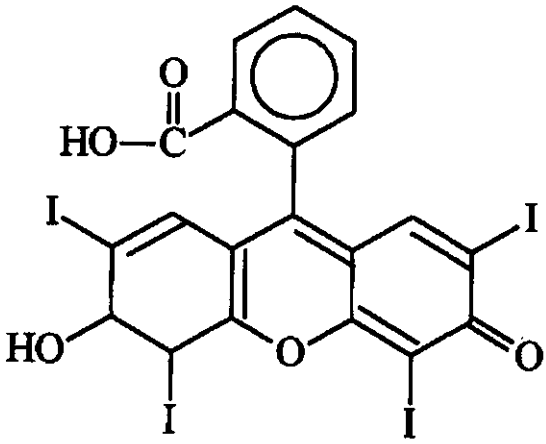

Figure 5.1: Molecular structure of Erythrosin B (Ery B)

as received. PVA solutions in DMSO were prepared by adding 1 gram of purified PVA powder to 12 ml of DMSO and heating this mixture to 353 K under continuous magnetic stirring until a clear solution was obtained. The PVA/DMSO solution was then mixed with the desired amount of the stock solution of Ery B in DMSO. For the preparation of the films, two preparation methods were used. In the first, the evaporation method, the solution was poured out on a small glass plate, followed by drying in the dark under a continuous nitrogen stream. For low concentration of Ery B this method results in $\approx 50\,\mu m$ thick films, with sufficient optical absorption (OD ≥ 0.05). At higher Ery B concentrations the films were made as thin as possible, to prevent reabsorption effects (OD ≤ 0.5). Final Ery B concentrations in the films were in the range of 10^{-7} to 2.5×10^{-3} mol/g PVA. The refractive index of PVA films was 1.52 as determined using an Abbe refractometer. No birefringence was observed. In the second method,i.e. spin coating, the solution was poured on a small glass plate and subsequently spun around on a turning table, resulting in $\approx 50\,\mu m$ layers. For time-resolved experiments the films were placed between thin glass plates using ultra-pure glycerol to assure optical contact with the glass. The glass plates were glued around the edges and masked with black tape, leaving a spot of 2 mm in diameter for illumination.

5.3.2 Experiments

Time-resolved measurements of the fluorescence- and fluorescence anisotropy decay of the films were carried out at the LENS-institute (Laboratorio di Spettroscopia Moleculare) in Florence (Italy) using the time correlated single photon-counting system [114], at an

excitation wavelength of 532 ± 1 nm. The fluorescence was observed through a band pass interference filter with peak transmission at 573 nm and bandwidth of 6 nm (Omega) and a 550 nm cut-off filter (Omega). The fluorescence was collected in a quasi-forward geometry, thus preventing the excitation beam from directly reaching the detection system. The instrumental function of the detection system was obtained for each measurement by measuring the time profile of the scattered laser light. For the present experimental conditions its full width at half maximum (FWHM) was 80 ps. Typically, decay curves were measured over 1000 channels with a width of 0.04612 ns and a maximum peak of more than 2×10^4 counts for the sum $(I_{vv} + 2I_{vh})$. Due to the possibility of degradation of Ery B on heating and long exposure to the laser light, the photochemical stability of the sample was checked after each data run by measuring the absorption spectrum. No visible decomposition was found. Unpolarized absorption spectra were measured at room temperature using a DW2000 (SLM-Aminco) or a Kontron Uvicon 810 spectrophotometer. The slit widths were 2 nm on both spectrophotometers. No differences were detected between the results obtained with the two instruments.

5.3.3 Molecular modeling

All calculations were done with the MSI program Cerius^2 [1], using the PCFF force field [115, 116, 117, 118] and applying 'high-convergence criteria' [2][3] in all minimizations. The geometry of a single Ery B molecule was optimized. Subsequently, this optimized molecule was used to construct clusters of two, three, and four Ery B molecules by copying and moving this structure. The initial positions and orientations of the Ery B molecules, which form the oligomers are important. Various interactions (e.g., $\pi - \pi$ stacking, COOH dimers, and hydrogen bonding between the OH and C=O groups of the molecules) are included in the calculations. The relative positions and orientations of the chromophores dictate the initial value of the strength of these interactions. A particular orientation of the monomer units in a dimer might give rise to a local minimum, which is not the lowest possible. The possible interactions were investigated by systematically varying the relative positions and orientations of the molecules in a cluster with respect to each other. The number of possible orientations grows rapidly with the number of molecules in a cluster, as a result of the different interactions between the monomers. Therefore it is necessary from a practical point of view to eliminate certain types of -chemically less relevant- structures from the calculations at an early stage. The more molecules need to be considered, the more of the clusters that can be designed have a local energy minimum that may be considerably higher than that of the energetically lowest situation. Since it is not clear which types of structures should be eliminated, a deductive approach was used in the early stages of the investigations. As a rule of thumb it was decided

[1] Cerius^2, version 3.8, Molecular Simulations Inc.

[2] This term is specific to the Cerius^2 program so it has in the text been put between quotes.

[3] The criteria for the high-convergence minimizationsare: Atom root mean square force 1×10^{-2} kcal mol^{-1} nm^{-1}; atom maximum force 5×10^{-2} kcal mol^{-1} nm^{-1}; energy difference 1×10^{-4} kcal/mol; root mean square displacement 1×10^{-6} nm; maximum displacement 5×10^{-6} nm.

that, if a certain orientation of the molecules gave an energy that was considerably lower (typically > 10 kcal/mol) compared to the previous, fully optimized situation (or ensemble of situations) from which it was derived, the original needed no further investigation. The newly obtained geometry was then used as the new starting point. The same principle was used if the introduction of a new type of interaction gave similar differences in the energy of the system compared to that found for other types of interactions. By applying this method several types of -chemically less realistic- orientations were eliminated at an early stage.

5.4 CALCULATION OF ABSORPTION SPECTRA

The excitonic interactions between the Ery B molecules depend on their mutual distance and orientation. Although due to ground-state interactions dimers, trimers, or even higher aggregates may be formed, the most probable distances between monomeric Ery B molecules in PVA films is calculated from their concentration. The distance between the molecules (R_0) is given by:

$$R_0(nm) = \left(\frac{3}{4\pi} \times \frac{10^{21}}{N_A \times 1.4 \times c_I} \right)^{\frac{1}{3}} \tag{5.1}$$

where N_A is Avogadro's number and c_I is the concentration of Ery B in PVA films, ranging from 10^{-7} to 2.5×10^{-3} mol/g. The density of the PVA films is 1.4 g/ml [87]. The most probable distance for a given monomer density is $\overline{R} = (2/3)^{1/3} R_0 \approx 0.87 R_0$ as follows from the nearest neighbor distribution [111] (Chapter 4 of this Thesis). The average distance of the nearest neighbor distribution (R_n) is [90]:

$$< R_n > \approx 0.89 R_0 \tag{5.2}$$

Hence, the values between the most probable distance and the average value of the nearest neighbor distribution are not very different. Table 5.1 summarizes the R_0 values for the different concentrations. The length of an Ery B molecule is ≈ 0.7 nm. Consequently, for concentrations of 10^{-3} and 2.5×10^{-3} (and probably even 5×10^{-4}) steric hindrance affects the mutual orientation of the Ery B molecules in PVA films.

To simulate the absorption spectra we use molecular exciton theory, assuming the point dipole approximation [35, 119]. The excitonic interaction energy expressed by the interaction Hamiltonian $\hat{V}$ can be written as:

$$\hat{V} = \frac{1}{4\pi\varepsilon\varepsilon_0 R^3} \hat{\vec{\mu}}_n \cdot \left(1 - 3\frac{\vec{R}_{n,m}\vec{R}_{n,m}}{R^2} \right) \cdot \hat{\vec{\mu}}_m \tag{5.3}$$

where $\hat{\vec{\mu}}_n$ is the transition dipole operator of monomer n, ε the relative dielectric constant of the solvent and $\vec{R}_{n,m}$ the center to center distance between the molecules n and m. We

Table 5.1: Average distance between Ery B molecules vs. concentration

c (mol g^{-1})	label	R_0 (nm)
10^{-7}	A	14.1
2×10^{-7}	B	11.3
5×10^{-6}	C	3.8
10^{-5}	D	3.1
5×10^{-5}	E	1.8
10^{-4}	F	1.4
5×10^{-4}	G	0.83
10^{-3}	H	0.66
2.5×10^{-3}	I	0.48

use the quantity

$$V_0 \approx 5.035 \frac{\mu^2}{\varepsilon R^3} \text{ cm}^{-1} \tag{5.4}$$

with μ in Debye units and R in nm, to scale the interactions. For Ery B molecules the single dominant dipole moment is $\approx$ 6.3 D [4]. where ε for PVA was calculated to be 2.3, from the refractive index of 1.52. The distances (R) depend on the concentration considered (see eqn. (5.1)). for a random distribution of Ery B molecules in PVA films, we can simulate the absorption spectra by assuming a distance distribution, letting the molecules adapt any mutual orientation with respect to each other and including inhomogeneous and homogeneous broadening.

To simulate the absorption spectra for the complex structures (dimers, trimers and tetramers) as obtained from the molecular mechanics calculations, we analyzed the positions and orientations of the monomers contained in these complexes and we calculated the resulting stick spectra [120] (Chapter 6 of this Thesis). For realistic spectra, distance fluctuations, inhomogeneous and homogeneous broadening should be included. For our purpose only the values of the stick spectra are relevant, because the spectral shift is our main interest.

[4]The dipole moment has been calculated using the extinction coefficient of 10^5 $mol^{-1}cm^{-1}$ and an estimate for full width half maximum of 770 cm^{-1} at peak maximum of 18300 cm^{-1}. The last two values were estimated by fitting the monomeric absorption spectra (see Fig. 5.2) with separate Gaussian line shapes for the B(0,0) band and the B(0,1) band. Only the B(0,0) band has been taken into consideration.

Table 5.2: Fluorescence- and fluorescence anisotropy decay data

c (mol g^{-1})	τ (ns)	r_0	$r(t)$ (ns)
10^{-7}	0.8 ± 0.1	0.37	-
2×10^{-7}	0.8 ± 0.1	0.37	2.0
5×10^{-6}	0.5 ± 0.1	0.37	1.0
10^{-5}	0.4 ± 0.1	0.35	-
5×10^{-5}	0.3 ± 0.1	0.33	-

5.5 RESULTS

5.5.1 Spectroscopic measurements

Table 5.2 contains the results of fluorescence- and fluorescence anisotropy decay experiments. The decay curves were analyzed using a reiterative deconvolution algorithm using a non–linear least–squares Marquardt procedure, and applying a multi-exponential function to either the separate parallel and perpendicular fluorescence anisotropy decay curves I_{vv} and I_{vh} or the total intensity decay curve $I_{vv} + 2I_{vh}$. The first column of Table 5.2 presents the fluorescence lifetime τ (ns) for different concentrations of Ery B in PVA films. The second and last column of Table 5.2 contain the initial anisotropy r(0) and the anisotropy decay time, t(ns). The absorption spectra for concentrations $\approx 5 \times 10^{-6}$ mol/g are shown in Fig. 5.2. Next to the main B(0,0) band a second vibrational band is visible. Each spectrum is normalized at the peak value and consequently the surface area is not constant. Hence, the growth of the vibrational band is relative to these normalized peaks. In Table 5.1 and Fig. 5.2 we labelled the different concentrations in alphabetic order.

5.5.2 Molecular modeling

The formation of clusters is a possible explanation for the observed broadening and shifts of the absorption spectra. Therefore clusters of Ery B molecules were investigated by molecular mechanics calculations, using the MSI program Cerius^2 and the PCFF force field. This force field has been shown to be a suitable force field for the molecular modelling of clusters of (functionalized) organic molecules. [121, 110] The optimized structures of the oligomeric clusters are shown in Fig. 5.3. Table 5.3 shows the energies of these clusters and the distances between the monomers constituting these clusters, with reference to the structures in Fig. 5.3 listed in the last column.

The results from the molecular mechanics calculations have shown that the Ery B molecules have various options for the formation of clusters or complexes. Calculations on dimeric complexes showed that the two dimers D1 and D2, in which a dimerization through the

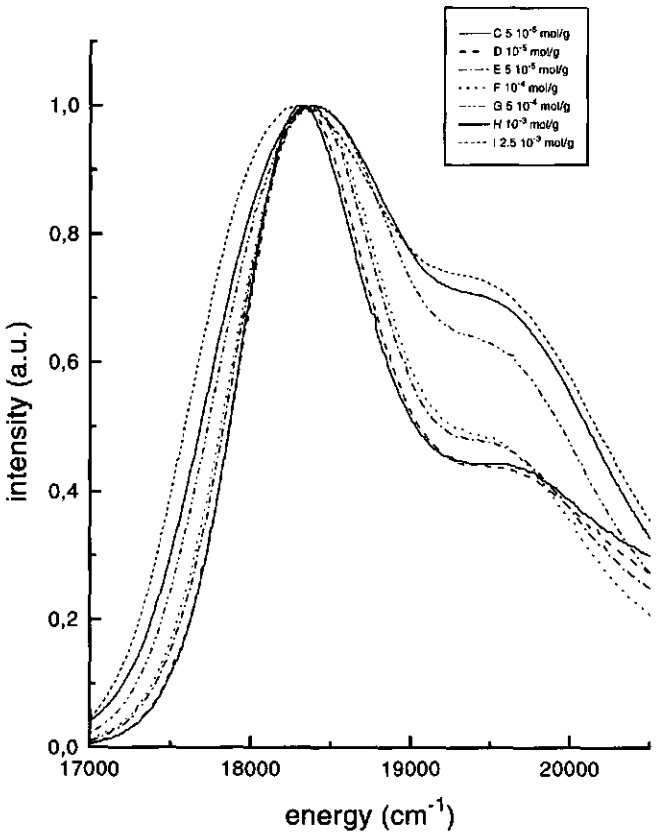

Figure 5.2: Absorption spectra for concentration range 5×10^{-6} to 2.5×10^{-3} mol Ery B/gram PVA

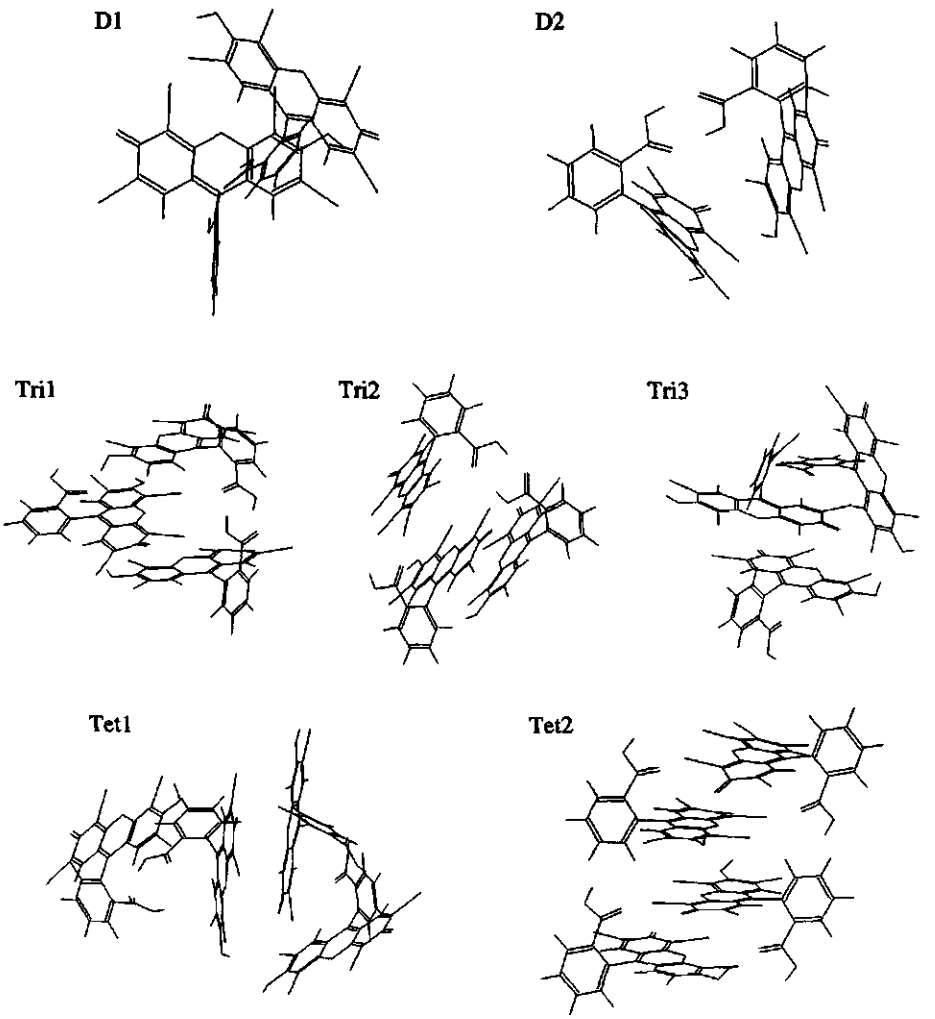

Figure 5.3: Energetically favorable optimized dimers, trimers and tetramers according to PCFF Molecular Mechanics Computations

Table 5.3: Low energy structures based on molecular mechanics calculations

oligomer[a]	energy (kcal/mol)	distances (nm)	Fig. 5.3
dimer 1	31.33	0.67	D1
dimer 2	33.76	0.60	D2
trimer 1	23.47	0.56; 0.63; 0.84	Tri1
trimer 2	23.48	0.59; 0.62; 0.78	Tri2
trimer 3	24.95	0.47; 0.71; 0.78	Tri3
tetramer 1	21.19	0.70; 0.47; 0.63[b]	Tet1
tetramer 2	21.90	0.53; 0.44; 0.57[b]	Tet2

[a] The monomer energy is 26.8 kcal/mol

[b] Nearest neighbor distances.

carboxylic acid groups occurs, are the most stable dimers. These two structures only differ in the relative orientation of the aromatic rings. The energy per Ery B molecule in these clusters (15.7 and 16.9 kcal/mol, respectively) is lower by $\approx$ 10 kcal/mol than that of a single Ery B molecule (26.8 kcal/mol). The formation of trimeric structures is enthalpically more favorable than dimerization. In the trimers Tri1 and Tri2, which are geometrically different but have the same energy per Ery B molecule (7.8 kcal/mol), the aromatic moiety of the third Ery B molecule is in between the large aromatic systems of the other two molecules, which strongly increases the $\pi - \pi$ interactions between the large aromatic rings. The 'carboxylic acid' dimer in the collection of dimeric structures is not completely destroyed by this process. In the third trimeric structure, Tri3, which is only 1.5 kcal/mol higher in energy (i.e., 0.5 kcal/mol per Ery B molecule) compared to Tri1 and Tri2, the acid dimers are partially broken and a complex three-dimensional cluster has been formed, in which both $\pi - \pi$ interactions and interactions between the OH and C=O groups of the Ery B molecules are present. In all three trimers the energy per Ery B molecule is lower, by $\approx$ 8 kcal/mol, compared to the values as found for the dimers D1 and D2. This indicates that the enthalpy for formation of these trimeric structures is more favorable than dimerization. Formation of tetrameric structures even further decreases the energy of the system, however, the gain in energy per Ery B molecule is somewhat lower than for the dimer-to-trimer transition. The two structures with the lowest energy are depicted in Fig. 5.3. For Tet1 a fourth Ery B molecule appears to bind to trimer Tri3. This molecule is at the left side in the picture of Tet1 and has formed a carboxylic acid dimer with the lowest Ery B molecule in Tri3. The structure of the former trimeric part shows only small differences compared to Tri3. In Tet2 the stacking of the aromatic moieties has become dominant and the dimers of the carboxylic acid groups have completely disappeared. The formation of larger clusters (pentameric, hexameric, etcetera) is also possible, as this will still result in a lower enthalpy per Ery B molecule, given the trend that is present in Table 5.3. However, such structures were not investigated, as

Table 5.4: Calculated spectra for structures given in Table 5.3

oligomer	energy blue shift(cm^{-1}) (intensity) [a]	energy red shift(cm^{-1})
dimer 1	270 (82)	-270 (12)
dimer 2	200 (98)	-200 (2)
trimer 1	90 (25);190 (70)	-280 (5)
trimer 2	90 (55);170 (40)	-260 (5)
trimer 3	70 (38);230 (38)	-300 (24)
tetramer 1	35 (28);400 (49)	-35 (6);-400 (17)
tetramer 2	1300(83)	-6 (9);-200 (7);-1094 (1)

[a] The relative intensity is given in parentheses

it becomes increasingly difficult to design the appropriate clusters that yield the global minimum, because the number of possible interactions and combinations increases rapidly. As a result the difference between the various situations will also become smaller, and probably too small, for these larger clusters, an effect that was already found for the tetramers. Although the formation of very large clusters might be favorable from the point of view of the enthalpy, the actual clustering may not occur as a result of entropy considerations, which are not incorporated in the calculations. For larger structures the entropy contribution to the free energy becomes increasingly important, so molecular mechanics calculations cannot predict the stability of large molecular aggregates.

The results of these molecular mechanics calculations show that enthalpy favors the formation of small Ery B clusters. Thus, it is expected that clustering will occur in the films. However, whether the clusters are actually formed, depends not only on the gain in energy for each Ery B molecule in the cluster, but also on other factors, such as the polarity of the local environment in the films and the kinetics of the complexation process, neither of which can be investigated by molecular mechanics calculations. Thus, it is not possible to predict from these results alone which clusters, dimers, trimers, or tetramers will actually be in the films. The simulated spectra for these structures are given in Table 5.4. As can be seen from this table blue shifts are dominant.

5.6 DISCUSSION

5.6.1 Concentration range 10^{-7} - 5×10^{-5} mol/g: fluorescence- and fluorescence anisotropy decay

First we discuss the results of the fluorescence- and fluorescence anisotropy decay experiments. The results given in Table 5.2 reveal the following: at the 10^{-7} mol/g concentration

the value of the initial polarization R(0) agrees with published values [122] when no energy transfer takes place. The same applies to the constant value of the fluorescence anistropy. Both the absorption- and the fluorescence spectra indicate the presence of monomers. At a concentration of 2×10^{-7} mol/g the fluorescence anisotropy decay become noticeable due to energy transfer among the monomers. The initial value of the anisotropy and the fluorescence lifetime equal those of the monomers [122]. implying that the fluorescence is not quenched by oligomers.

At a concentration of 5×10^{-6} mol/g the fluorescence anisotropy decays faster as a result of more efficient energy transfer. Another new feature at this concentration is the decrease of the fluorescence lifetime, which implies that the quantum yield of the fluorescence has decreased. This is explained by energy transfer from an excited monomer to a non-fluorescent species, which leads to a faster fluorescence decay and a shortening of the flourescence lifetime [32, 123].

In Part 1 [111] (Chapter 4 of this Thesis) we discussed the number of quenching pairs present vs. the concentration. Assuming that monomers closer together than 1 nm form quenching pairs [111] (Chapter 4 of this Thesis), the probability to encounter a quenching pair is approximately 1 %. At a concentration of 10^{-5} mol/g the fluorescence quenching is further enhanced, yielding a further lifetime shortening and giving rise to a lower initial anisotropy. Already at this concentration the anisotropy decay is too fast to be experimentally observable. At a concentration of 5×10^{-5} mol/g the probability to encounter a quenching pair has increased to 40% and the fluorescence quenching is further increased. At concentrations $\geq 5 \times 10^{-5}$ mol/g the fluorescence is quenched beyond detection.

5.6.2 Concentration range 5×10^{-5} - 10^{-4} mol/g: absorption spectra

At concentrations $\leq 5 \times 10^{-6}$ mol/g, the absorption spectra are identical to those of the monomers. Note the B(0,1) vibrational band next to the main B(0,0) band (Fig. 5.3). The noticeable growth of the B(0,1)/B(0,0) intensity ratio (Fig. 5.3) is mainly caused by broadening of the B(0,0) band, thereby lowering its intensity. In the remainder of this paragraph we concentrate on the B(0,0) band.

Between 5×10^{-5} mol/g and 10^{-4} mol/g the spectra start to exhibit a general broadening and a slight blue shift with respect to the monomeric spectra. The average intermolecular distance at these concentrations is calculated to be ≈ 1.5 nm, whereas the molecular size is ≈ 0.7 nm. This means that the majority of the molecules have sufficient freedom to adapt any mutual orientation. A fraction of $\approx 10\%$ of the molecules are closer than 0.7 nm, however, and have limited freedom to rotate. The spectral shifts of molecules with an average intermolecular distance of ≈ 1.5 nm correspond to $V_0 = 20 - 50$ cm^{-1} (eqn. (5.4))

5.6.3 Concentration range 10^{-4} - 10^{-3} mol/g: absorption spectra

Whereas excitonic interactions between randomly oriented molecules cause only spectral broadening, simulated spectra using molecular mechanics calculations show that the formation of dimeric, trimeric and tetrameric structures result in a blue shift (Table 5.4). At 5×10^{-4} mol/g the average distance between the molecules is only slightly larger than the size of the molecules. Thus, we expect a number of the complex structures, including those presented in Fig. 5.2 to be present in the films. This explains the clearly visible blue shift of the spectrum at a concentration of 5×10^{-4} mol/g. This spectrum shows that tetramer 2 does not appear to have a large contribution to the spectrum because its shift would have been located at 197500 cm^{-1}, which is the location of the B(0,1) band and apparently at that position there is no enhanced intensity. The detailed mechanism which determines the actually present structures is not clear. The energy differences between the various clusters are small, so it seems likely that a small difference in preparation conditions may change the fraction of each of the structures present in the film. This argument is supported by the results for spincoated films (see next paragraph), which produce different spectral shifts than discussed before. Also for spin coated films blue shifts remain dominant, however.

5.6.4 Concentration range 10^{-3} - 2.5×10^{-3} mol/g: absorption spectra

At concentrations of 10^{-3} mol/g and 2.5×10^{-3} mol/g the chromophores are closely packed, i.e. at a concentration of 2.5×10^{-3} mol/g, 1 g PVA contains 2.2 g of Ery B. The space to form isolated oligomer structures found at low concentrations is now considerably reduced. The resulting structures contain Ery B molecules parallel to each other and parallel to the connecting vector $\vec{R}$.

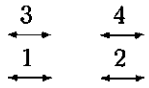

The exciton interactions between chromophore 1 and 2 cause red shifs. The same applies to chromophore 3 and 4. The angle between the connecting vector $\vec{R}$ of chromophore 1 and 4 and the chromophore transition dipole moments of these chromophores is below the magic angle and hence these combinations cause mainly red shifts. Only the combinations of 1 and 3 and 2 and 4 cause blue shifts. Hence, this very dense packing results in a spectral shift which is dominant to the red side of the spectrum.

5.6.5 Spincoating

At concentrations of 5×10^{-5} to 2.5×10^{-3} mol/g we also prepared some samples by applying spin coating instead of the drop evaporation technique (see Material and Method

section). Spincoating is frequently used to deposit thin layers ($\leq$ 500nm) on a substrate [124, 125, 126] and is carried out by spinning the sample at a constant speed during deposition of a small amount of dye solution. We expected that spin coating was an easier way to make thin films, without strongly influencing the spectra, but as can be seen from a comparison of Figs. 5.2 and 5.4 some spincoated samples have spectra which are significantly different from those prepared by casting and evaporation (Fig. 5.2). Spectra I and Is hardly differ but spectrum E, F and G (evaporation method) and spectra Es, Fs and Gs (spin coating method) are quite different.
However, the last mentioned spectra are all blue-shifted. It seems that the forces on the molecule during the spin coating process, cause differences in the orientation of the chromophores with respect to each other. Two different mechanisms, which could cause the difference between spin coated and evaporated samples are:

- The individual oligomer structures are the same (see Fig. 5.3), but the relative occurrence of each of these structures is different. To give an example, tetramer 2 seems hardly present in evaporated samples but this might be the cause of the experimental blue shift, at the location of the B(0,1) band in the spincoated sample at a concentration 5×10^{-4} mol/g.

- The strong shear forces applied on the spincoated samples cause the chromophores to align, giving them a different orientation than with casting/evaporation.

Whatever mechanism might work, it is important to realize that the spincoating and evaporation method could give different absorption spectra caused by different molecular structures. Because at the highest concentration of 2.5×10^{-3} mol/g films prepared by spincoating and casting/evaporation have the same red-shifted spectral profile, one may conclude that at this high concentration the aggregate structure is predominantly determined by the properties of the Ery B molecules themselves and not by external forces, such as occur during spincoating. At intermediate concentrations, the dye molecules have freedom to yield their orientation to the highly anisotropic forces during spincoating.

5.7 CONCLUSIONS

1. The effects of concentration on the absorption spectrum of Ery B in PVA films are not observable at low concentrations ($\leq 5 \times 10^{-5}$ mol/g), but fluorescence anisotropy decay experiments demonstrate the presence of quenching of excited monomers by concentration pairs in their immediate environment.

2. At concentrations $\geq 5 \times 10^{-5}$ mol/g excitonic interactions between Ery B molecules become noticeable in the absorption spectrum. In the concentration range 5×10^{-5} -

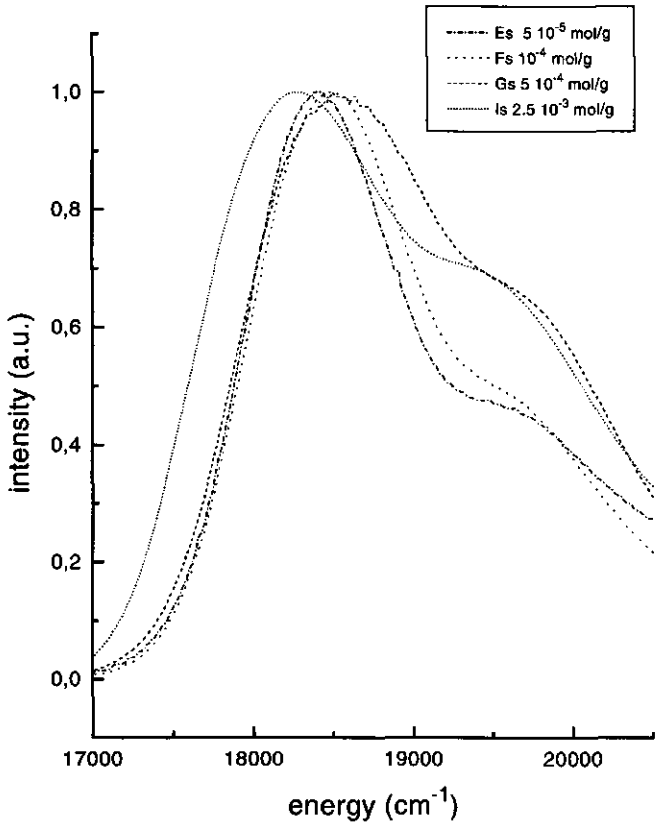

Figure 5.4: Absorption spectra for spin coated samples

2.5×10^{-3} mol/g broadening of the spectra is first observed, then a blue shift and finally a red shift of the spectra at the highest concentration.

5.8 Acknowledgements

The authors want to thank R. Torre and P. Bertolini at the LENS-institute in Florence for their help with time- resolved measurements.

Chapter 6

EXCITONIC INTERACTIONS IN COVALENTLY LINKED PORPHYRIN DIMERS WITH ROTATIONAL FREEDOM

Regien G. Stomphorst, Rob B. M. Koehorst, Gert van der Zwan, Bert Benthem and Tjeerd J. Schaafsma, Journal of Porphyrins and Phtalocyanines 3, 346-354 (1999)

6.1 ABSTRACT

Experimental and calculated absorption spectra are compared for four different porphyrin dimers covalently linked by alkyl- or phenyl bridges. Spectra of the corresponding monomers were used as a reference to determine the experimental excitonic shift(s) of the absorption spectrum in the Soret-region. The excitonic interaction was calculated using the point dipole approximation and taking into account the restricted conformational freedom of the monomeric units in the dimers, due to steric constraints. The constraints were independently verified by magnetic dipole-dipole broadening of the EPR spectra of several $(CuTPP)_2$-substituted dimers. The observed and calculated absorption spectra agree at least semi-quantitatively.

6.2 INTRODUCTION

During the last two decades considerable progress has been made in resolving the X-ray structure of two components of the photosynthetic unit, *i.e.* the bacterial reaction centre [127] and the associated antenna complex [128]. The interchromophoric interactions between the (bacterio) chlorophylls within the reaction centre and the antenna complex have been simulated by biomimetic models of various porphyrin assemblies (for reviews see, [129, 130, 131, 132, 133]) Whereas in the photosynthetic unit the chromophores are kept in a rather fixed position and relative orientations, this does not apply to many porphyrin models [134, 135, 136, 137]. To judge whether a particular porphyrin model is suitable to mimic the spectral properties of the photosynthetic unit, the conformational freedom of the model must be carefully considered.

This paper reports the results of a comparison of experimental absorption spectra in the B(0,0) Soret-band region of four different, covalently bound porphyrin dimers with numerically calculated spectra using a point dipole approximation for the excitonic interaction between both porphyrin monomers in the excited dimer, allowing these dimers to assume all accessible groundstate conformations. Oscillator strengths for the monomer Soret-bands were taken from literature. All calculations apply to one and the same solvent (toluene). Calculations of excitonic shifts in porphyrin dimers have been previously reported, without taking conformational freedom into account to explain the spectra [36, 138, 139] or with only taking the most extreme cases into consideration [135, 140].

The dimers **1** through **4**, (Fig.6.1) investigated in this work are derivatives of meso-tetraphenylporphyrin and meso-porphyrin IX dimethylester, having their conformational freedom partly restricted by steric effects and the position of the covalent link.

This work aims at answering the following questions: (i) What are the effects of (restricted) conformational freedom on their excitonic spectra? (ii) What is the range of conformations of the various dimers which can be concluded from experimental and calculated spectra? (iii) Does the use of the point dipole approximation for the excitonic interaction yield a satisfactory description for the investigated dimers?

6.3 MATERIALS AND METHODS

Free base meso $\alpha,\beta,\gamma,\delta$-tetraphenylporphyrin ($H_2$TPP) monomers and dimers, o,p-C_3−(TPP)$_2$ and p,p-C_3−(TPP)$_2$ were synthesised according to literature [141, 142] and purified by adsorption chromatography on silica gel (Merck, Kiezelgel 60) with chloroform as eluent and gel permeation chromatography (Biobeads SX2, Biorad Laboratories) with toluene. The phenyl-bridged dimer was a gift of dr. M. R. Wasielewski [143] and the meso-dimer was a gift of dr. K. Ichimura [144]. The purity was checked using absorption and fluorescence spectroscopy and thin layer chromatography [145].

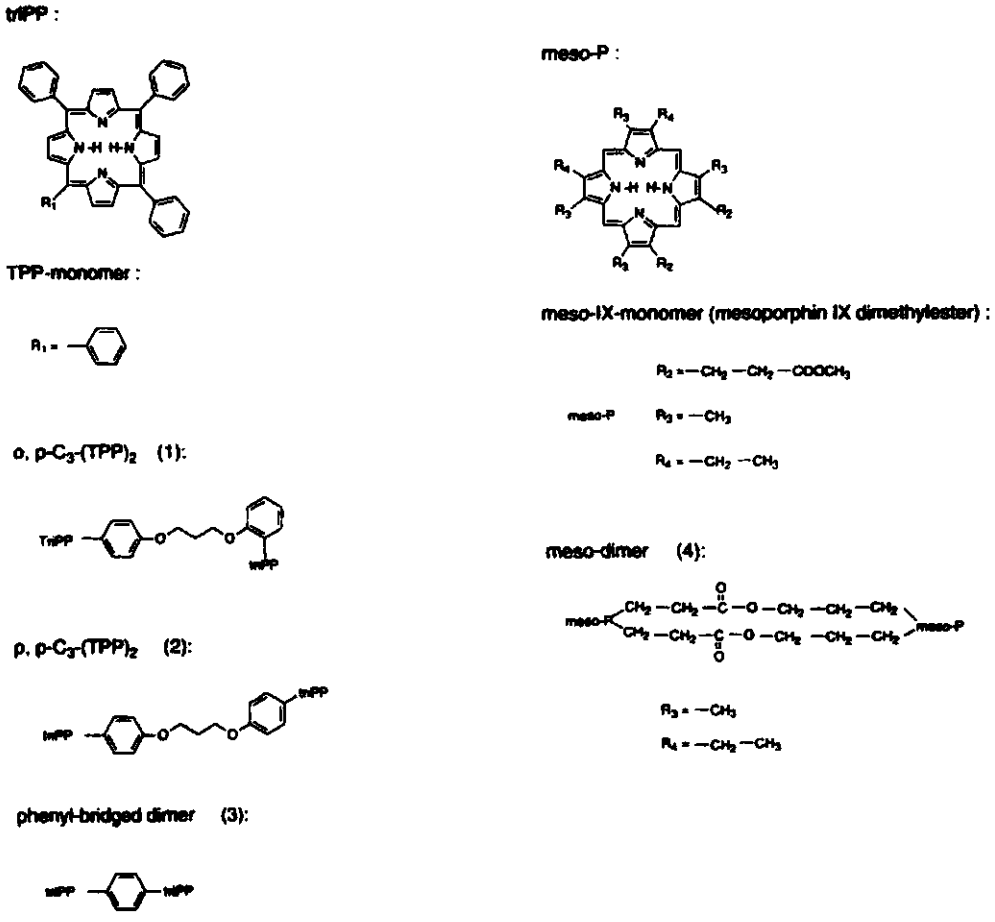

Figure 6.1: Molecular structures of dimers. The symbol -C_3- represents the five atom bridge $-O-(CH_2)_3-O-$. The symbols triPP and meso-P represent triphenylporphyrin and meso-porphyrin respectively.

Absorption spectra were recorded at room temperature using a Kontron Uvicon 810 spectrophotometer with a 2 nm slitwidth. The dimer concentration in toluene as a solvent (Merck p.a.) was approximately 10^{-5}M.

Metals were inserted into the free-base porphyrin by standard procedures [146]. Mixed metalfree base porphyrin dimers were synthesised by inserting a metal ion into either of the porphyrin monomers [141]. In the ortho-para mixed dimer the metal ion is always in the porphyrin macrocycle with the covalent link at the ortho position. Metallated porphyrin dimers were synthesised from the corresponding metallo-porphyrin monomers or by metallating both porphyrin macrocycles of a free-base porphyrin dimer. All solvents (p.a. grade) were used without further purification. EPR spectra of CuTPP monomers and -dimers and of the mixed CuTPP-H_2TPP dimers were recorded at T=125 K in a hexane/toluene (2:1) mixture or in MTHF using a Varian E-6 spectrometer.

Table 6.1: E_{max} (λ_{max}) and FWHM widths of the experimental spectra in toluene

monomer/dimer	$E_{max}(cm^{-1})$ ($\lambda_{max}(nm)$)	FWHM (cm^{-1})	rel. height	figure ref.
TPP-monomer	23910 (418.2)	550	n.a.	A1- A3
o,p-C_3−$(TPP)_2$	23740 (421.2) |23950 (417.5) [a]	650 | 1000 [b]	1:1	A1
p,p-C_3−$(TPP)_2$	23820 (419.8)	590	n.a.	A2
phenyl- bridged	23380 (427.7) |23960 (417.4) [a]	550 | 500	1:0.7	A3
meso-IX-monomer	24920 (401.2)	1100	n.a.	A4
meso-dimer	25641 (390.0) [c]	[d]	n.a.	A4

[a] Decomposition into three Gaussians.

[b] The second derivative shows two close-lying peaks close together, which can not be resolved using three Gaussian functions.

[c] Only the strongest peak was taken into account.

[d] No Gaussian distribution.

6.4 EXPERIMENTAL RESULTS

Table 6.1 summarizes the results for E_{max} (λ_{max}) and the full width at half maximum (FWHM) of the experimental spectra. Apart from the B(0,0) Soret-band there is a vibrational band B(0,1) at $\approx$ 407 nm for the TPP monomer and at $\approx$ 382 nm for the meso-IX-monomer. The intensity ratio (measured as the ratio of the peak-heights) for the B(0,0) and B(0,1) transitions is 1:0.3 for the TPP monomer and 1:0.45 for the meso-IX-monomer. A multi-Gaussian fit analysis was used to fit the spectral profiles, except for the meso-dimer, because for this compound the distance ($\vec{R}$) between the porphyrin macrocycles is not constant. The standard error of the fitted B(0,1) profile is much larger than that of the B(0,0) profile, and in view of this low intensity is not taken into consideration for calculating the spectra. To determine the position of the B(0,0) band in the experimental spectra as accurately as possible, the Gaussian B(0,1) profile

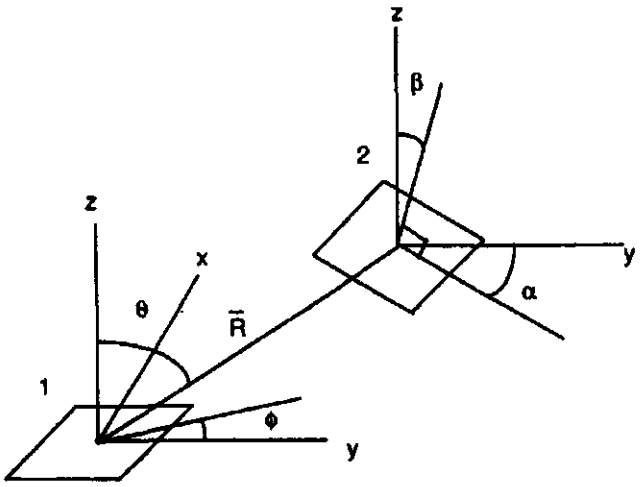

Figure 6.2: Relative orientation of porphyrin 1 with respect to porphyrin 2. $\vec{R}$ is the centre-to-centre distance between the porphyrin macrocycles. The angles ϕ and θ are the azimuth and polar angles of $\vec{R}$. The orientation of porphyrin 2 with respect to 1 is given by the Euler angles(α, β, γ)

is subtracted from the total spectrum. Table 6.1 therefore represents the data for the position of the B(0,0) band corrected in this way for the vibrational B(0,1) band.

6.5 THEORY

The monomers in each of the investigated dimers studied are free-base porphyrins, in which the B(0,0) band is not split [147]. Therefore there are two degenerate B states, which are denoted as $|n, x\rangle$ and $|n, y\rangle$ where $n = 1, 2$ labels the monomer. The ground state is denoted as $|n, 0\rangle$. The transition moments from the ground state to each of these states are equal in magnitude, and perpendicular to each other. Noting that the centre-to-centre distance between the molecules is large compared to the size of the monomers, the point dipole approximation is used to calculate the intermolecular excitonic energy.

In each of the monomers n we construct a molecular coordinate frame with the z_n-axis perpendicular to the macrocycle, and the x_n- and y_n-axes in the molecular plane. In view of the above mentioned degeneracy, the choice of these last two axes is arbitrary, and consequently all results obtained must be independent of rotations around the molecular z_n-axis. With respect to the origin of porphyrin 1, the centre of porphyrin 2 is located at position $\vec{R}$, and the orientation of the molecular frame of porphyrin 2 with respect to

the molecular frame of porphyrin 1 is given by the set of Euler angles (α, β, γ). The polar angle and azimuth of $\vec{R}$ are denoted by θ and ϕ respectively. The common choice of the Euler angles is that β and α denote the polar angle and azimuth of the molecular z_2-axis with respect to the frame of 1, whereas γ is a rotation around the molecular z_2-axis [148]. All results must be independent of γ (see Fig. 6.2).

The monomer Hamiltonian can be written as:

$$\mathcal{H}_n = \epsilon_B \left(|n,x\rangle \langle n,x| + |n,y\rangle \langle n,y| \right) \tag{6.1}$$

where the excited state energy ϵ_B (relative to the ground state) is assumed to be identical for both monomers.

The interaction Hamiltonian $\hat{V}$ can now be written as:

$$\hat{V} = \frac{1}{4\pi\epsilon R^3} \hat{\vec{\mu}}_1 \cdot \left(1 - 3\frac{\vec{R}\vec{R}}{R^2} \right) \cdot \hat{\vec{\mu}}_2 \tag{6.2}$$

where $\hat{\vec{\mu}}_n$ is the dipole operator of monomer n, and ϵ the dielectric constant. An explicit representation of the dipole operator in the basis given above is:

$$\hat{\vec{\mu}}_n = \mu \vec{e}_{nx} \left(|n0\rangle \langle nx| + |nx\rangle \langle n0| \right) + \mu \vec{e}_{ny} \left(|n0\rangle \langle ny| + |ny\rangle \langle n0| \right) \tag{6.3}$$

In this expression μ is the magnitude of the transition dipole moment, and $\vec{e}_{nx}$ and $\vec{e}_{ny}$ are unit vectors along the molecular x_n- and y_n-axes, respectively.

To obtain the dimer absorption spectrum we need to diagonalize the Hamiltonian

$$\mathcal{H} = \mathcal{H}_1 + \mathcal{H}_2 + \hat{V} \tag{6.4}$$

and express the new eigenstates (excitonic states) $|k\rangle$ in terms of the original states:

$$\mathcal{H} |k\rangle = \epsilon_k |k\rangle \quad \text{with} \quad |k\rangle = \sum_{n=1}^{2} \sum_{\mu=x,y} C_{n\mu}^k |n,\mu\rangle \tag{6.5}$$

The absorption intensity at energy ϵ_k is then, for dimers in solution, proportional to:

$$I_k \propto \mu^2 \sum_{n,m=1}^{2} \sum_{\mu,\nu=x,y} C_{n\mu}^k C_{m\nu}^{k*} \; vece_{n\mu} \cdot \vec{e}_{m\nu} \tag{6.6}$$

A straightforward calculation shows that to find the eigenvalues and eigenvectors, *i.e.* the coefficients $C_{n\mu}^k$ of the above Hamiltonian we need to diagonalize the following 4×4 matrix:

$$\begin{pmatrix} \epsilon_B & 0 & V_{xx} & V_{xy} \\ 0 & \epsilon_B & V_{yx} & V_{yy} \\ V_{xx} & V_{yx} & \epsilon_B & 0 \\ V_{xy} & V_{yy} & 0 & \epsilon_B \end{pmatrix} \tag{6.7}$$

where

$$V_{\mu\nu} = \frac{\mu^2}{4\pi\epsilon R^3}\vec{e}_{1\mu} \cdot \left(1 - 3\frac{\vec{R}\vec{R}}{R^2}\right) \cdot \vec{e}_{2\nu}, \quad \mu, \nu = x, y \tag{6.8}$$

Explicit expressions for I_k and $V_{\mu\nu}$ in terms of the Euler angles (α, β, γ) and the spherical components of $\vec{R}$ can be found in appendix A of ref. [100].

The interaction energy is scaled by the factor

$$V = \frac{\mu^2}{4\pi\epsilon R^3} \tag{6.9}$$

which depends on the magnitude of the transition dipole moments, the distance between the monomers and the dielectric constant of the medium.

The calculational procedure is furthermore as follows: for each possible realisation of the parameters $\alpha, \beta, \gamma, \theta, \phi, R$ the matrix (6.7) is diagonalized numerically. Subsequently all intensities are added, at the correct energy (wavelength), for all allowed geometry's. The conformation of the four dimeric molecules is given in Table 6.2.

For the phenyl-bridged dimer, two cases were analysed: $\beta = \frac{1}{2}\pi$ and $\beta = \frac{1}{3}\pi$ in view of a discussion in the literature about the existence of two (or more) conformers [149]. The meso-dimer could theoretically unfold, corresponding to a maximum of $\theta = \frac{1}{2}\pi$, but the probability of this conformation is estimated to be low.

Table 6.2: Dimer conformations

dimer	distance (nm)	$\vec{R}$	angular range
o,p-C_3–$(TPP)_2$	2.0 [a]	$\phi = 0;\ \theta = 0.38\pi$	$\alpha = 0 \rightarrow 2\pi;\ \beta = \frac{1}{2}\pi$
p,p-C_3–$(TPP)_2$	2.7 [b]	$\phi = 0;\ \theta = 0$	$\beta = 0 \rightarrow 2\pi$
phenyl- bridged	1.25 [c]	$\phi = 0;\ \theta = 0$	$\beta = 0$ and ($\beta = \frac{1}{2}\pi$ or $\beta = \frac{1}{3}\pi$)
meso-dimer	1.1-0.4	$R = R_0 \sin\theta^d;\ \phi = \frac{1}{2}\pi$	$\theta = \frac{1}{4}\pi \rightarrow \frac{1}{12}\pi;\ \alpha = 0;\ \beta = \frac{1}{2}\pi + 2\theta$

[a] Average of EPR measurements and space filling models (see Table 6.5).
[b] value obtained from space filling models.
[c] value obtained from literature [150].
[d] R_0=1.5 nm.

6.6 RESULTS OF CALCULATIONS

For the four differently connected porphyrin dimers mentioned in the Introduction the spectra were calculated. According to literature [151] the extinction coefficient of TPP in benzene is 4.7 10^5 $M^{-1}cm^{-1}$. The extinction coefficient of meso-IX-monomer in $CHCl_3$ is

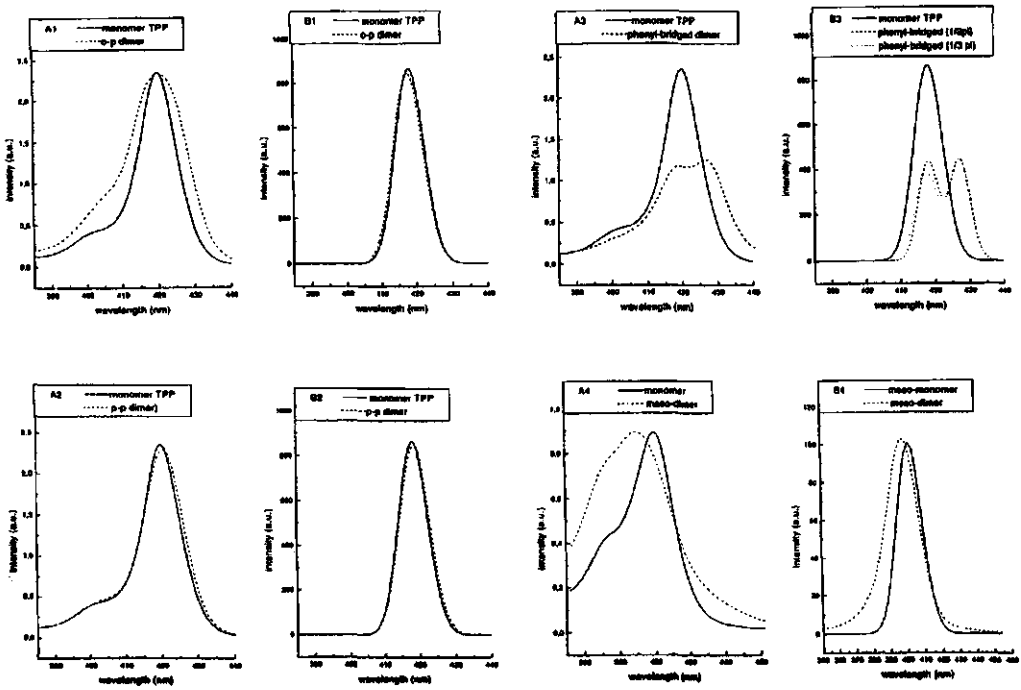

Figure 6.3: Experimental and calculated spectra of TPP-monomer (solid lines), o,p-C_3−$(TPP)_2$ (A1, B1), p,p-C_3−$(TPP)_2$ (A2, B2), phenyl- bridged (A3, B3), meso-IX-monomer (solid line) and meso-dimer (A4, B4). (for corrections of the B(0,1) band see Table 6.1)

Table 6.3: Calculated results for absorption spectra of monomers and dimers

monomer/dimer	$V(cm^{-1})$	calculated features	figure ref.
TPP-monomer	n.a.	n.a.	B1- B3
o,p-C_3−$(TPP)_2$	62.2	slight blue shift	B1
p,p-C_3−$(TPP)_2$	25.3	red shift to 419.1	B2
phenyl- bridged ($\frac{1}{2}\pi$)	254.9	monomeric 418.2; red shift to 427.3	B3
phenyl-bridged ($\frac{1}{3}\pi$)	254.9	blue shift to 416.0; red shift to 427.3	B3
meso-IX-monomer	n.a.	n.a.	B4
meso-dimer	251-8383	broad blue shift	B4

1.66 $10^5 M^{-1}cm^{-1}$ [152], which is of the same order as for a similar compound in CH_2Cl_2 [153]. Since the difference between the solvents toluene used in this work and benzene and $CHCl_3$ as in previous studies is negligible the literature values are used to calculate μ for TPP and the meso-IX-monomer. Using the square of the high frequency refraction index [154] for the relative dielectric constant $\epsilon_r = n^2 = 2.2$ of toluene, μ is calculated to be 14.7 D for TPP and 12.1 D for meso-IX-monomer. The maximum of the Soret band of monomeric TPP in toluene is at 23910 cm^{-1} (418.2 nm) and this value is used as a reference for compound **1**, **2** and **3**. (The difference between $C_{1.5}$ substituted TPP and the parent compound TPP is negligible). For the meso-dimer we use the meso-IX-monomer as a reference with a Soret band maximum at 24920 cm^{-1} (401.2 nm).

The results of the calculations are given as V (cm^{-1}) (see Table 6.3). After scaling (see equation (6.9)), the angle dependent function, equation (6.8) ranges from -2 to 2. The dependence of the energy shifts and the corresponding intensities on the angular distribution were calculated ignoring the vibronic B(0,1) band, because of its uncertain position. The calculated stickdiagram was convoluted with a Gaussian distribution with a FWHM width of 550 cm^{-1}, which means $2 * \sigma^2 = 110000$ cm^{-1} for the TPP-monomer, o,p-C_3−$(TPP)_2$ and p,p-C_3−$(TPP)_2$. For the phenyl-bridged dimer half this value is taken due to exchange narrowing. The FWHM widths of the meso-IX-monomer and the meso-dimer are taken as 1100 cm^{-1}

6.7 DISCUSSION

The interaction energy is dependent on the size of the transition dipole moments of the molecules concerned, the dielectric constant of the medium, the distances between the monomers and the relative orientation of the monomers in the dimer. In the next paragraphs the model, the dielectric constant and the distance between the monomers used in our calculations are discussed. Finally, the experimental and calculated spectra are compared to elucidate the influence of rotational freedom on the spectra and the range of conformations of the various dimers.

Table 6.4: λ_{max} of monomers and dimers in acetone and toluene

monomer/dimer	λ_{max}(nm) in acetone	λ_{max}(nm) in toluene
TPP-monomer	413.7	418.2
o,p-C_3–$(TPP)_2$	417.6 [a]	417.5 | 421.2
p,p-C_3–$(TPP)_2$	415.9	419.8
phenyl-bridged dimer	413.8 | 424.0	417.4 | 427.7
meso IX monomer	396.8	401.2
meso-dimer	385.3	390.0

[a] The two peaks are too close together to be resolved.

6.7.1 Point dipole model

In most of the examples there is a good agreement between the experimental spectra and those calculated using the point dipole model. Therefore, the assumption of the point dipole model that the centre to centre distance between the molecules is large compared to the size of the molecules seems reasonable except for the meso-dimer. Since the distance between the two macrocycles of the meso-dimer in its completely folded form is 0.4 nm, *i.e.* shorter than the monomer diameter. To calculate spectra for the meso-dimer requires therefore more refined models e.g. CNDO/S [149], the transition-monopole treatment [155] or the extended dipole model [140].

Note that the Kasha model [35] is a point dipole model describing the excitonic interactions in dimers consisting of two monomeric units with a single, non-degenerate transition dipole moment. Therefore, this model can not be applied to dimers of porphyrins having two perpendicular degenerate transition dipole moments, as is sometimes done [156].

6.7.2 Dielectric constant

The influence of the dielectric constant of the solution on the excitonic interaction has been previously reported [157]. In our calculations we used the relative high-frequency dielectric constant ϵ_r= 2.2 for toluene, whereas the relative static dielectric constant ϵ_s= 2.4 [158]. Since both dielectric constants are not very different, it is not *a priori* clear, whether ϵ_r or ϵ_s should be used in the calculations. Therefore, the dimers were also measured in acetone instead of toluene. The relative static dielectric constant for acetone ϵ_s= 21 whereas ϵ_r= 1.8. In Table 6.4 the values of the shift of λ_{max} of the four dimers in acetone compared to those in toluene. The Soret maxima for the TPP-monomer in acetone are considerably shifted to 414 nm (418 nm in toluene) and for the meso-IX-monomer to 397 nm (401 nm in toluene).

The shifts given in Table 6.4 for acetone and toluene are only slightly different, implying that their dielectric constants are very similar, justifying the use of ϵ_r.

Table 6.5: (Differential) first derivative peak-to-peak EPR linewidths (G) and porphyrin centre-to-centre distances of $(CuTPP)_2$ and CuTPP-H_2TPP dimers; solvents: toluene/hexane (1:2) (A) and MTHF (B); T=125K

dimer	ΔH_{pp}(Cu-H_2)[a]		ΔH_{pp}(Cu-H_2)		ΔH_{pp}		r_{cc}^b		r_{cc}^c
configuration	(G)		(G)		(G)		(nm)		(nm)
	A	B	A	B	A	B	A	B	
para-para	8.3	–[d]	9.2	–[d]	0.9	–[d]	2.7	–[d]	2.7
ortho-para	8.0	6.1	9.7	7.5	1.7	1.5	2.2	2.2	1.9

[a] Same configuration as the corresponding $(CuTPP)_2$ dimer.
[b] Error estimated from inaccuracy of EPR linewidths ($\pm 0.1G$) : ± 0.1 nm.
[c] From space filling models.
[d] Not quoted due to large line broadening.

6.7.3 Distance

Considering the internal rotational freedom of some of the investigated dimers it is not certain whether reliable values of the average centre-to-centre distance r_{CC} between the porphyrin macrocycles can be obtained from space-filling models. Therefore, we have employed the broadening of EPR transitions in fully Cu^{2+}-substituted dimers as an independent means to estimate the average value of r_{CC}. Dipolar interactions between both paramagnetic centres result in broadening of the EPR spectra depending r_{CC} as $< r_{CC}^{-3} >$ [159]. CuTPP-H_2TPP dimers with the same configurations are used as a reference.

EPR spectra for the p,p-$(CuTPP)_2$ and o,p-$(CuTPP)_2$ dimers are compared with the reference spectra of p,p-CuTPP-H_2TPP and o,p-CuTPP-H_2TPP respectively . The superhyperfine lines in the Cu-Cu dimers are noticeably broadened in the 3300-3400 G region. The net dipolar broadening in a particular dimer due to the magnetic dipolar interaction was obtained by subtracting the peak-to-peak linewidth ΔH_{pp} of a selected superhyperfine line in the reference compound from that for the corresponding Cu-Cu dimer, yielding an estimate of the effective average Cu-Cu distance in the dimer, and thus the centre-to-centre distance r_{CC} between the porphyrin macrocycles in the various dimers, see Table 6.5. This Table also shows a solvent dependence of r_{CC}, presumably due to increased folding of the dimer in the more polar environment, *i.e.* of MTHF as compared to toluene/hexane.

The dipolar broadening, expressed as the second moment of the Cu-Cu dimer EPR linewidths can be related to r_{CC} by

$$(\Delta\bar{\nu})^2 = \frac{3\mu_0^2\gamma^2}{1024\pi^4}h^2S(S+1)\frac{(1-3\cos^2\theta)^2}{r_{cc}^6} \tag{6.10}$$

in SI units, where $(\Delta\bar{\nu})^2$ is the mean square linewidth (in Hz); μ_0 is the magnetic perme-

ability of vacuum (H m^{-1}); $\gamma = g_e\gamma_e$ with g_e the free electron g-factor and γ_e magnetogyric ratio of the free electron; h is Planck's constant; S=$\frac{1}{2}$ for Cu^{2+}; θ is the angle between r_{cc} and the direction of the external magnetic field.

The resolved superhyperfine components are found to have a Gaussian lineshape, as a result of unresolved proton superhyperfine structure. Then, formula (6.10) can be rewritten as

$$r_{cc}(nm) = 1.23(\delta H_{pp})^{\frac{1}{3}} \tag{6.11}$$

with the differential peak-to-peak linewidth δH_{pp} defined as

$$\delta H(mT) = \Delta_{pp}(dimer) - \Delta_{pp}(ref) \tag{6.12}$$

In Table 6.5 the distances r_{CC} from equation (6.11) have been compared with those from space filling models. Whereas the agreement is good for the p,p dimer, it is less satisfactory for the o,p dimer. Also no solvent effect on r_{CC} is observed for this dimer. Both results are probably due to dominant steric effects of the phenyl substituents.

From a comparison of the values of r_{CC} from EPR data and space-filling models, respectively, we may conclude that the latter give a good estimate of the average centre-to-centre distance between the porphyrin macrocycles to be used in calculations of the excitonic interactions.

6.7.4 Comparison of experimental and calculated spectra

Comparison of the spectra in Fig. 6.3 shows good agreement between the experimental and calculated spectra. The figures in Table 6.1 and Table 6.3 show even better agreement because of the correction for the vibronic B(0,1) band. Intramolecular rotational freedom can give rise to significant differences between the spectra. Comparison of the p,p-C_3–$(TPP)_2$ and the meso-dimer indicates that stretched dimers show a completely different spectrum due to their rotational freedom either around the y-axis (resulting in mainly redshifted spectra) or the x-axis (resulting in mainly blueshifted spectra). The range of conformations chosen for o,p-C_3–$(TPP)_2$ does not account for the experimental net red shift, which was not found for the calculated spectrum. This red shift may be caused by folding of the dimer, which would also explain the larger red shift than calculated, as a result of the shortening of the distance between the porphyrin rings.

For the phenyl-bridged dimer spectra were calculated for two different cases (see Fig. 6.3). Comparison of the spectra shows that the experimental spectrum resembles the $\theta = \frac{1}{3}\pi$ case more closely than for $\theta = \frac{1}{2}\pi$. Note, however, that the phenyl-bridged dimer has been investigated in toluene as a solvent and that different solvents may result in different ground state conformations. The two above mentioned cases should be distinguishable by the absence and presence, respectively of circular dichroism. We plan to perform such experiments in the near future.

Because of its two links the meso-dimer has entirely lost its rotational freedom about the y-axis, as applies to p,p-C_3−$(TPP)_2$. The short double links between both parts of the meso-dimer allow folding, *i.e.* rotation about the x-axis, which affects the distance R. The average distance is ≈ 0.7 nm.

BIBLIOGRPHY

Bibliography

[1] P.C.W. Davies and J.R. Brown. *The Ghost in the Atom.* Cambridge University Press, 1986.

[2] G. Gamow. *Mr. Tompkins in paperback (Mr. Tompkins in wonderland (1940) and Mr. Tompkins explores the atom (1945)).* Cambridge University Press, 1993.

[3] R. Penrose. *The Emperor's New Mind.* Oxford University Press, 1989.

[4] P. Pourveur. *Noorderlicht.* De Tijd Antwerpen, 1998.

[5] M. Frayn. *Copenhagen.* M. Blackmore (director), London, 1998.

[6] J.T. Cushing. *Quantum Mechanics (Historical Contingency and the Copenhagen Hegemony).* University of Chicago Press, 1994.

[7] S. Weinberg. *Dreams of a Final Theory.* Vintage London, 1993.

[8] T.S. Kuhn. *The Structure of Scientic Revolutions.* University of Chicago Press, 1962.

[9] J.W. McAllister. *Beauty and Revolution in Science.* Cornell University Press, 1996.

[10] P. Gibbins. *Particles and Paradoxes (the limits of quantum logic).* Cambridge University Press, 1987.

[11] A. Pais. *Subtle is the Lord... The Science and Life of Albert Einstein.* Oxford University Press, 1982.

[12] A. Whitaker. *Einstein, Bohr and the Quantum Dilemma.* Cambridge University Press, 1996.

[13] W. Heisenberg. *The physical principals of quantum theory (translated form German (1949)).* Dover Publications, 1930.

[14] M. Jammer. *The Philosophy of Quantum Mechanics (The Interpretations of Quantum Mechanics in Historical Perspective).* A Wiley-Interscience Publication, 1974.

[15] Von Neumann. *Mathematical Foundations of Quantum Mechanics (translated by R.T. Beyer).* Princeton University Press, 1955.

[16] M.L. de Broglie. Nouvelle Dynamique des Quanta. In *Electrons et Photons, Raports et Discussions du Cinqième Conseil de Physique tenu 'a Bruxelles du 24 au 29 Octobre*, pages 105–141. Gauthier-Villars, Paris, 1928.

[17] D. Bohm and B.J. Hiley. *The Undivided Universe.* Routledge, 1993.

[18] D. Deutsch. *Proc. R. Soc. Lond. A.*, 400:97–117, 1985.

[19] D.Z. Albert. *Quantum Mechanics and Experience.* Harvard University Press, 1992.

[20] R.B. Griffiths. *Phys. Rev. Lett.*, 70(15):2201–2204, 1993.

[21] R. Omnés. *The Interpretation of Quantum Mechanics.* Princeton University Press, 1994.

[22] L.E. Bellantine. *Phys. Rev. Lett.*, 42(4):358–380, 1970.

[23] R.P. Holland. *The quantum theory of motion.* Cambridge University Press, 1993.

[24] L. de Broglie. *Non-Linear Wave Mechanics (a causal interpretation).* Elsevier Publishing Company, 1960.

[25] D. Bohm. *Phys. Rev.*, 85:166–197, 1952.

[26] J.S. Bell. *Reviews of Mod. Phys.*, 38:447–452, 1966.

[27] R. van Grondelle, J.P. Dekker, T. Gillbro, and V. Sundstrom. *Biochimica et Biophysica Acta*, 1187:1–65, 1994.

[28] R. A. Marcus and N Suntin. *Biochimica et Biophysica Acta*, 723:265–322, 1985.

[29] M. Bixon and J. Jortner. *J. Phys. Chem*, 90:3795–3800, 1986.

[30] R.E. Blankenship. *Photosynthetic. Res.*, 22:3, 1989.

[31] D. DeVault. *Photosynthetic. Res.*, 22:5–10, 1980.

[32] M.A.M.J. van Zandvoort. Pigment-polymer matrices as model systems for energy transfer processes between photosynthetic piments. *Ph.D Thesis*, University of Utrecht, 1994.

[33] D. Mugnai, A. Ranfagni, and L.S. Schulman. *Tunneling and its Implications (Proceedings of the Adriatico Research Conference).* World Sientific Publishers, 1997.

[34] R.S. Knox. *J. Phys. Chem.*, 98(30):7270–7273, 1994.

[35] M. Kasha, H.R. Rawls, and M. Ashraf El-Bayoumi. *Pure Appl. Chem.*, 11:371, 1965.

[36] A. Osuka and K. Maruyama. *J. Am. Chem. Soc.*, 110:4454–4456, 1988.

[37] T.P. Spiller, P.S. Spencer, T.D. Clark, J.F. Ralph, H. Prance, R.J. Prance, and A. Clippingdale. *Foundation of Physics Letters*, 4(6):507–521, 1991.

[38] T.P. Spiller. Trajectories of particles interacting with environments. In A. van der Merwe and A. Garuccio, editors, *Wave and Particles in Light and Matter*, pages 447–461. Plenum Press New York, 1994.

[39] A. Terenzi and F. Cannata. *Foundation of Physics Letters*, 10(4):347–356, 1997.

[40] A.M. Steinberg. *Superlattices and Microstructures*, 23(3/4):823–832, 1998.

[41] J.T. Cushing. The Causal Quantum Theory Program. In J.T. Cushing, A. Fine, and S. Goldstein, editors, *Bohmian Mechanics and Quantum Theory : an Appraisal.* Kluwer Academic Publishers, 1996.

[42] C.R. Leavens. Bohmian Mechanics and the Tunneling Time Problem for Electrons. *Procedings of the Adriatico Research Conference on Tunneling and its Implications*, ed. D. Mugnai and A. Rafani and L.S. Schulman:100–120, 1996.

[43] J.T. Cushing. *Found. Phys.*, 25(2):269–280, 1995.

[44] W.Pauli. Die Allgemeinen Prinzipien der Wellenmechanik. In R. Kronig and V.F.Weisskopf, editors, *Collected Scientific Papers, Volume 1.* John Wiley and Sons Inc., 1964.

[45] H. Salecker and E.P. Wigner. *Phys. Rev.*, 109(2):571–577, 1958.

[46] G.R. Allcock. *Ann of Phys.*, 53:253–285, 1969.

[47] G.R. Allcock. *Ann of Phys.*, 53:286–310, 1969.

[48] G.R. Allcock. *Ann of Phys.*, 53:311–348, 1969.

[49] P. Busch. *Found. Phys.*, 20(1):1–43, 1990.

[50] J. Hilgevoord. *Am. J. of Phys.*, 64(12):1451–1456, 1996.

[51] Y. Aharonov and B. Reznik. *Phys. Rev. Letters*, 84(7):1368–1370, 2000.

[52] X. Oriols, F. Martin, and J. Su ne. *Phys. Rev. A*, 54(4):2594–2604, 1996.

[53] E.H. Hauge and J.A. Stovneng. Tunneling Times: A Critical Review. *Reviews of Mod. Phys.*, 61(4):917–936, 1989.

[54] V.S. Olkhovsky and E. Recami. *Phys. Reports*, 214(6):339–356, 1992.

[55] R. Landauer and Th. Martin. *Reviews of Mod. Phys.*, 66(1):217–228, 1994.

[56] M. Büttiker. *Phys. Rev. B*, 27(10):6178–6188, 1983.

[57] F.T. Smith. *Phys. Rev.*, 118(1):349–356, 1960.

[58] C.R. Leavens and G.C. Aers. Bohm trajectories and the Tunneling Time Problem. In R. Wiesendanger and H.J. Guntherrodt, editors, *Scanning Tunneling Microscopy III*, pages 105–140. Springer, New York, 1993.

[59] J.G. Muga, S. Brouard, and R. Sala. *Phys. Lett. A*, 167:24–28, 1992.

[60] N. Grot, C. Rovelli, and R.S. Tate. *Phys. Rev. A*, 54(6):467–64690, 1996.

[61] V. Delgado. *Phys. Rev. A*, 59:1010–1020, 1999.

[62] J.G. Muga, R. Sala, and J.P. Palao. *Superlattices and Microstructures*, 23(3/4):833–842, 1998.

[63] J. Kijowski. *Phys. Rev. A*, 59(1):897–899, 1999.

[64] R.S. Dumont and T.L. Marchioro II. *Phys. Rev. A*, 47(1):85–97, 1993.

[65] C.R. Leavens and W. R. McKinnon. *Phys. Let. A*, 194:12–20, 1994.

[66] C.R. Leavens. *Superlattices and Microstructures*, 23(3/4), 1998.

[67] C. Dewdney and B.J. Hiley. *Found. Phys.*, 12(1):27–48, 1982.

[68] C.R. Leavens. *Phys. Let. A*, 178:27–32, 1993.

[69] T.P. Spiller, T.D. Clarck, R. J. Prance, and H. Prance. *Europhys. Letters*, 12(1):1–4, 1990.

[70] C.R. Leavens, G. Iannaccone, and W.R. McKinnon. *Phys. Let. A*, 208:17–24, 1995.

[71] A. Challinor, A. Lasenby, S. Somaroo, C. Doran, and S. Gull. *Phys. Let. A*, 227:143–152, 1997.

[72] K. Bedard. *Found. Phys. Letters*, 10(2):183–187, 1997.

[73] J.T. Cushing and G.E. Bowman. Bohmian mechanics and chaos. In J. Butterfield and C. Pagonis, editors, *From physics to philosophy*, pages 90–107. Cambridge University Press, 2000.

[74] J.T. Cushing, A. Fine, and S. Goldstein. *Bohmian Mechanics and Quantum Theory : an Appraisal.* Kluwer Academic Publishers, 1996.

[75] V.A. Benderskii, D.E. Makarov, and C.A. Wight. *Adv. Chem. Phys.*, 88:15–53, 1994.

[76] M. Bixon and J. Jortner. *Chem. Phys. Letters*, 159(1), 1989.

[77] D. DeVault. *Quantum-mechanical tunnelling in biological systems.* Cambridge University Press, 1984.

[78] W.H. Press, S.A. Teukolsky, W.T. Vetterling, and B.P. Flannery. *Numerical Recipes in C.* Cambridge University Press, 1992.

[79] C.R. Leavens. *Solid State Communications*, 74(9):923–928, 1990.

[80] A.O. Caldeira and A.J. Leggett. *Ann. Phys.*, 149:374–456, 1983.

[81] W. Kühlbrandt, D.N. Wang, and Y. Fujiyoshi. *Nature*, 367:614–621, 1994.

[82] H. Gerhardt. Continuous-wave dye lasers. In F.P. Schäfer, editor, *Dye Lasers*, pages 121–137. Springer-Verlag, Berlin, 1999.

[83] W.. Watson and R. Livingston. *J. Chem. Phys.*, 18:802–809, 1951.

[84] G.S. Beddard and G. Porter. *Nature*, 260:366–367, 1976.

[85] J.P. Ide, D.R. Klug, W. Kühlbrandt, l. Georgi, and G. porter. *Biochim. Biophys. Acta*, 983:384–394, 1987.

[86] M.A.M.J. van Zandvoort, D. Wöbel, A.J. Scholten, D. de Jager, G. van Ginkel, and Y. Levine. *Photochem. Photobiol.*, 58:600–606, 1993.

[87] M.A.M.J. van Zandvoort, D. Wöbel, P Lettinga, G. van Ginkel, and Y. Levine. *Photochem. Photobiol.*, 62:279–289, 1995.

[88] J.M. Kroon, E.J.R. Südholter, J. Wienke, R.B.M. Koehorst, T.J. Savenije, and T.J. Schaafsma. In *Proceedings of the 13th European Photovoltaic Solar Energy Conference*, pages 1295–1298. 1995.

[89] R.G. Stomphorst, M.A.M.J. van Zandvoort, A.B. Sieval, H. Zuilhof, F.J. Vergeldt, G. van der Zwan, and T.J. Schaafsma. *Accepted by J. of Phys. Chem.*, 2000.

[90] P. Hertz. *Math. Ann.*, 67:387–398, 1908.

[91] L.M. Beekman, M. Steffen, I. van Stokkum, C.N. Hunter, S.G. Boxer, and R. van Grondelle. *J. Phys. Chem. B*, 101:7284, 1997.

[92] L.M. Beekman, R.N. Frese, G.J.S. Fowler, I. van Stokkum, C.N. Hunter, and R. van Grondelle. *J. Phys. Chem.B*, 101:7293, 1997.

[93] S.G. Boxer. In J. Amesz and A.J. Hoff, editors, *Biophysical techniques in photosynthesis*, pages 177– 189. Kluwer Academic Publishers, Amsterdam, 1996.

[94] F. Remacle and R.D. Levine. *J. Phys. Chem.A*, 104:2341, 2000.

[95] G. van der Zwan and J.T. Hynes. *J. Phys. Chem.*, 89:4181–4188, 1985.

[96] H.J. Kim and J.T. Hynes. *J. Phys. Chem.*, 93:5194–5210, 1990.

[97] H.J. Kim and J.T. Hynes. *J. Phys. Chem.*, 93:5211–5223, 1990.

[98] H.J. Kim and J.T. Hynes. *J. Phys. Chem.*, 96:5088–5110, 1992.

[99] J.N. Gehlen, D. Chandler, H.Y. Kim, and J.T. Hynes. *J. Phys. Chem.*, 96:1748–1753, 1992.

[100] M.H.C. Koolhaas, G. van der Zwan, F. van Mourik, and R. van Grondelle. *Biophysical J.*, 72:1828–1841, 1996.

[101] S. Chandrasekhar. Stochastic pronblems in physics and astronomy. In N. Wax, editor, *Selected papers on noise and stochastic processes*, pages 2–88. Dover publications, Inc., New York, 1954.

[102] S. Georgakopoulou, R.N. Frese, M.H.C. Koolhaas, R. Cogdell, R. van Grondelle, and G. van der Zwan. *Submitted Biophysical J.*, 2000.

[103] W.H. Press, S.A. Teuloski, W.T. Vetterling, and B.P. Flannery. *Numerical Recipes in C.* Cambridge University Press, 1992.

[104] A. Warshel and W.W. Parson. *J. Am. Chem. Soc.*, 109:6143, 1987.

[105] W.W. Parson and A. Warshell. *J. Am. Chem. Soc.*, 109:6153, 1987.

[106] H.Laguitton-Pasquier, R.Pansu, J.-P. Chauvet, A. Collet, J. Faure, and R. Lapouyade. *Chem. Phys.*, 212:437, 1996.

[107] M.H.C. Koolhaas, F. van Mourik, G. van der Zwan, and R. van Grondelle. *Journal of Luminescence*, 60/61:515–519, 1994.

[108] I.S. Gradhsteyn and I.M. Ryzhik. *Tables of Itegrals, Series and Products.* Academic Press Inc. London, 1980.

[109] G. Calzaferri. *Proc. Indian Acad Sci-Chem Sci*, 109(6):429–446, 1997.

[110] C.W. Struijk, A.B. Sieval, J.E.J Dakhorst, P. Kimkes, H. Zuilhof, E.J.R. Sudhölter, R. B. M Koehorst, H. Donker, T.J. Schaafsma, S.J. Picken, A.M. Van de Craats, and J. M. Warman. *J. Am. Chem. Soc.*, in press.

[111] R.G. Stomphorst, T.J. Schaafsma, and G. van der Zwan. *Accepted by J. of Phys. Chem.*

[112] M.P. Lettinga, H Zuilhof, and M.A.M.J. van Zandvoort. *Phys. Chem. Chem. Phys.*, 2:3697–3707, 2000.

[113] H.C. Haas, H. Husek, and L.D. Taylor. *J. Polymer. sci.*, A(1), 1963.

[114] A. Arcioni, M.A.M.J. van Zandvoort, P. Bartolini, R. Torre, R. Tarroni, R. Righini, and C. Zannoni. *J. Phys. Chem. B*, 102:1624–1631, 1998.

[115] H. Sun, S. Mumby, J.R. Maple, and A.T. Hagler. *J. Phys. Chem.*, 99:5873–5882, 1995.

[116] H. Sun. *Macromolecules*, 28:701–712, 1995.

[117] J. R. Hill and J. Sauer. *J. Phys. Chem.*, 98:1238–1244, 1994.

[118] M.J. Hwang, T.P. Stockfisch, and A.T. Hagler. *J. Am. Chem. Soc.*, 116:2515–2525, 1994.

[119] E.G. McRae and M.J. Kasha. *Chem. Phys.*, 28:721, 1958.

[120] R.G. Stomphorst, R.B.M. Koehorst, G. van der Zwan, B. Benthem, and T.J. Schaafsma. *J. Porphyrins and Phtalocyanines*, 3:346–354, 1999.

[121] A.B. Sieval, B. van Hout, H. Zuilhof, and E.J.R. Südholter. *Langmuir*, 16:2987–2990, 2000.

[122] M.P. Lettinga, M.A.M.J. van Zandvoort, C.M. van Cats, and A.P. Philipse. *Langmuir*, 16(15):6156–6165, 2000.

[123] J. Knoester. Incoherent energy transfer in disordered systems. *PhD thesis*, Utrecht University, 1987.

[124] H. Kerp, H. Donker, R.B.M. Koehorst, T.J. Schaafsma, and E.E. van Fraassen. *Chem. Phys. Lett.*, 298:302-308, 1998.

[125] S.M. Critchley, M.R. Willis, J. Cook, J.McMurdo, and Y.Maruyama. *J. Mat. Chem*, 2(2):157–159, 1992.

[126] B.A. Gregg. *Chem. Phys. Lett.*, 258:376–380, 1996.

[127] J. Deisenhofer, O. Epp, K. Huber, and H. Michel. *J. Mol. Biol.*, 180:385–398, 1984.

[128] G.McDermott, S.M. Prince, A.A. Freeler, A.M. Hawthornthwaite-Lawless, M.Z. Papiz, R.J. Cogdell, and N.W. Isaacs. *Nature*, 374:517–521, 1995.

[129] M. R. Wasielewski. *Mol. Biol., Biochem. Biophys.*, 35:234–276, 1982.

[130] M. R. Wasielewski. *Photochem. Photobiol.*, 47:923–929, 1988.

[131] M. R. Wasielewski. *Chem. Rev.*, 92:435–461, 1992.

[132] D. Gust, T. Moore, and A. L. Moore. *Acc. Chem. Res.*, 26:198–, 1993.

[133] D. Dolphin, J. Hiom, and J. B. Paine III. *Heterocycles*, 16:417–447, 1981.

[134] R. L. Brookfield, H. Ellul, A. Harriman, and G. Porter. *Chem. Soc., Faraday Trans. II*, 82:219–233, 1986.

[135] R. Selensky, D. Holten, M. W. Windsor, J. B. Paine, D. Dolphin, M. Gouterman, and J.C. Thomas. *Chem. Phys.*, 60:33–46, 1981.

[136] E. Scamporrino and D. Vitalini. *Macromolecules*, 25:1625–1632, 1992.

[137] T. Nagata, A. Osuka, and K. Maruyama. *J. Am. Chem. Soc.*, 112:3050–3059, 1990.

[138] Y. Won, R. A. Friesner, M. R. Johnston, and J. L. Sessler. *Photosynth. Res.*, 22:201–210, 1989.

[139] V. S.-Y. Lin, S. G. DiMagno, and M. J. Therien. *Science*, 264:1105–1111, 1994.

[140] B. von Maltzan. *Z. Naturforsch.*, 40a:389–420, 1985.

[141] R. G. Little. *J. Heterocyclic Chem.*, 15:203–208, 1978.

[142] A.D. Adler, F.R. Longo, J. D. Finarelli, J. Goldmaster, J. Assour, and L.A. Korsakoff. *J. Org. Chem.*, 32:476, 1967.

[143] D. Heiler, G. L. McLendon, and P. Rogalskyj. *J. Am. Chem. Soc.*, 109:604, 1987.

[144] K. Ichimura. *Chem.Lett.*, pages 641–644, 1977.

[145] L. Benthem. Tetraphenylporphyrin dimers. an optical and magnetic resonance study. *PhD Thesis. Agricultural University*, 1984.

[146] A. D. Adler, F. R. Longo, F. Kampas, and J. Kim. *J. Inorg. Nucl. Chem.*, 32:2443–2445, 1970.

[147] M. Gouterman. Optical spectra and electronic structure of porphyrins and related rings. In D. Dolphin, editor, *The Porphyrins, vol III*, pages 1–156. Academic Press, 1978.

[148] M. Rose. *Elementary Theory of Angular Momentum (chapter IV)*. John Wiley and Sons, 1957.

[149] S. Eriksson, B. Källebring, S. Larsson, J. Märtensson, and O. Wennerström. *Chem. Phys.*, 146:165–177, 1990.

[150] P. Jaegermann, M. Plato, B. von Maltzan, and K. Möbius. *Mol. Phys.*, 78(50:1057–1074, 1993.

[151] G. M. Badger, R. Alan Jones, and R. L. Laslett. *Aust. J. Chem.*, 17:1028–1035, 1964.

[152] R. M. C. Dawson, Daphne C. Elliott, W. H. Elliott, and K. M. Jones. *Data for Biochemical Research.* Oxford (2 nd. ed.), 1969.

[153] Y. F. A. Chow, D. Dolphin, J. P. Paine III, D. McGarvey, R. Pottier, and T.G. Truscott. *J. Photochem. Photobiol., B: Biology*, 2:253–263, 1988.

[154] P. Debeye. *Polar Molecules.* The Chemical Catalog Company, Inc., Dover Publications, inc. N. Y., 1929.

[155] C. A. Hunter, J. K. M. Sanders, and A. J. Stone. *Chem. Phys.*, 133:395–404, 1989.

[156] A. Osuka and K. Maruyama. *J. Am.Chem. Soc.*, 110:4454, 1988.

[157] T. H. Tran-Thi, J. F. Lipskier, P. Maillard, M. Momemteau, J.-M. Lopez-Castillo, and J.-P. Jay-Gerin. *J. Phys. Chem.*, 96:1073–1082, 1992.

[158] Ed. R. C. Weast. *Handbook of Chemistry and Physics.* C. R.C. Press, USA, 1974.

[159] A. Carrington and A. D. McLachlan. *Introduction to Magnetic Resonance.* Harper and Row, New York, 1969.

SUMMARY

Tunneling times and excited state interactions between chromophores

Summary

This Thesis consists of two related parts. The first part (Chapters 2 and 3) presents the results of a fundamental theoretical study of the interpretation of quantum mechanics, and particularly of tunneling processes. Part two (Chapters 4, 5, and 6) describes the experimental results of spectroscopic investigations of quantum mechanical interactions between chromophores, which may play a role in electron transport by means of tunneling.

The formulation of the quantum theory at the beginning of the twentieth century resulted in a scientific revolution. The impact of this theory on our physical world picture is still visible today. The quantum theory is impressively successful in its predictions of the outcomes of experiments, but the interpretation of the theory is still shaky. The predictions of quantum mechanics about the outcome of experiments are detailed and testable, but the meaning of the theory for quantum systems, in which no measurement has taken place is not clear. Various interpretations exist. Two of these are compared in Chapter 2. The first is the orthodox or Copenhagen interpretation, which was advocated by the Copenhagen-based Niels Bohr. His followers claimed that, in the orthodox interpretation, nothing can be said about the properties of systems if no suitable measurement has been carried out. The alternative is the causal interpretation of quantum mechanics, in which a particle, e.g. an electron, has a well-defined position and velocity at each instant of time independent of a measurement act. The causal theory does not assign a special role to the observer. In the causal interpretation the location as a function of time amounts to trajectories. The two interpretations are empirically equivalent, i.e. they predict the same experimental outcomes.

In Chapter 2 the meaning of the two interpretations is clarified by the notion of tunneling time. Tunneling is the quantum mechanical phenomenon that a particle can cross a barrier even if its energy is less than the barrier energy. The time a particle takes to tunnel is the tunneling time. Time is a confusing concept: quantum theory appears not to know how to handle this topic. Time appears in the quantum mechanical formulae as a parameter, and not as an operator that corresponds to an observable quantity. Since an unambiguous time operator is missing, it is interesting to see what different interpretations have to say about tunneling times. It is strictly speaking impossible to define tunneling times in the orthodox interpretation because of the lack of a clear time operator, of which the expectation value can be observed by experiment. In the causal interpretation, every trajectory corresponds to a possible path of an electron. The density functions determine the probability that particles move on particular trajectories. This is how the stochastic character of quantum mechanics is accounted for in this interpretation. The transmission time is defined as the time spent inside the barrier by the electrons that eventually cross the barrier. The average transmission time can be defined by means of the trajectories, both in the case of stationary wave functions and in that of time-dependent, Gaussian wave packets. The Gaussian wave packets travel from minus infinity to plus infinity. On the way they meet potential barriers, which cause them to be reflected or transmitted.

The process by which an electron moves from one chromophore to another can be described as tunneling because of the high potential barrier formed by the medium between the chromophores. In this Thesis the experimental media used are polymer films and apolar solutions. The model described in Chapter 2 is generally used in the literature but appears not to be applicable for a system of two chromophores and a tunneling electron, because electrons belonging to chromophores neither start in infinity nor go to infinity. A better model, a double potential well, is used in Chapter 3. The conclusion of Chapter 2 is that the transmission time can be defined in the causal interpretation when time-dependent wave packets are used.

Chapter 3 illustrates the preceding by tunneling of a particle from one potential well to another passing a potential barrier. This model is the so-called double potential well. Examples are primary charge separation in the photosynthetic reaction center and in artificial model systems of chromophores in solutions and polymer films. The latter two cases are investigated spectroscopically in this Thesis. In these molecular systems, effective electron transport between chromophores after absorption of light takes place, yielding charge separation, i.e. the formation of chromophore cations. During their transport between natural or artificial chromophores, the released electrons often have to pass weak conducting media, corresponding to high potential barriers. If the energy of the electron exceeds the energy of the potential barrier, electron transport can be explained by classical theories. However, if the energy of the electron falls below the energy of the potential barrier, this is no longer possible. The transport mechanism is then understood as quantum mechanical tunneling. Experimental proof of tunneling has been found at low temperatures in photosynthesis.

In Chapter 3 the chromophores and the tunneling electrons are described by double potential wells. Each well represents a chromphore and the space between the molecules a potential barrier. The formalism of the causal interpretation is applied to define a transmission time. The transmission time can be found using trajectories. An alternative method provides the average transmission time without calculating the trajectories. Arrival time distribution functions are defined and these are used to determine the average arrival time of the tunneling electrons at the entrance and at the exit of the barrier. Because arrival time distribution functions and hence both average arrival times and transmission times are not determined in an experimental context, we conclude that these definitions of transmission times are meaningless in the orthodox interpretation. The question posed at the end of Chapter 3 is whether, and if so how, these transmission times are experimentally accessible.

The theoretical models developed in Chapters 2 and 3 are too simple to be extrapolated to real systems, such as electron transport between an electron donor and an acceptor, one of which is excited by light. Intermolecular interactions between excited electron donor molecules and ground state surrounding molecules cannot be neglected in chromophore films and solutions with relatively high concentrations of chromophores. These excitonic

interactions should be included in adequate descriptions of electron transfer. Chapters 4, 5, and 6 describe these interactions using absorption and emission spectroscopy. In Chapter 4 a theoretical description of the absorption characteristics of chromophores in disordered films is given. At low concentrations, chromophores in films are mainly monomers. On statistical grounds, however, we conclude that some molecules are close enough together to form dimer-like structures, concentration pairs with characteristic absorption spectra. The presence of these concentration pairs influences the emission characteristics of chromophore films as well. When monomer electrons are excited by the absorption of photons, the electrons might return to the ground state, giving off their energy as fluorescence. Light energy can also be transferred to neighboring concentration pairs, in which case the fluorescence is quenched.

The aim of Chapter 4 is to estimate the influence of potential quenchers in the vicinity of excited monomers and to predict the influence of these quenchers on the absorption spectra. The transfer of energy from monomers to concentration pairs, the so-called Förster transfer, takes place over quite large distances (1-5 nm). Statistics can be used to calculate the number of quenchers in particular concentrations of chromophores. In the literature it is assumed that two monomers that form a concentration pair are randomly oriented with respect to each other. If these pairs consisted of randomly oriented monomers and all fluctuations are taken into account, it appears on theoretical grounds that there would not be enough quenchers to describe the experimental changes. Because most chromophores are elongated or pancake-like, they are not randomly oriented but exhibit preferential orientations. These preferential orientations increase the efficiency of fluorescence quenching and theory and experiment are thereby reconciled. An analytical expression of the spectral changes compared to monomeric spectra of randomly oriented dimers is presented. To describe the interaction between chromophores that have one dominant transition dipole moment, a point dipole exciton model is used. To enhance the description of the spectral changes, homogeneous and inhomogeneous line broadening and monomer-to- monomer distance fluctuations should be taken into account. Inclusion of these factors in the model gives rise to the conclusion that the dimer spectra are broadened compared to the monomeric spectra and that the broadening is stronger at the blue end than at the red end of the spectra. However, to detect the blue-shifted spectral profile of randomly oriented dime-like samples, the concentration needs to be so high that isolated dimers cannot be observed. Then, simulation of the dimers becomes impossible, and all mutual interactions must be taken into account. Modeling of these interactions shows that the blue shift is not visible, and that only a broadening of the absorption spectra with respect to the monomeric spectra remains.

Chapter 5 describes spectral changes that result from changes in the concentration changes of elongated Erythrosin-B (Ery B) chromophores in polyvinylalcohol (PVA) films. At low concentrations, monomers are numerous,giving monomeric absorption spectra. At higher concentrations, measurements of fluorescence quenching show formations of pairs, which are not visible in the absorption spectra. At higher concentrations still, a broadening

of the absorption spectra is observed, as predicted by the theory developed in Chapter 4. Further increase of the concentrations induces order of the chromophores. Preferential orientations for dimers, trimers, and tetramers are determined by use of molecular mechanics. Structures that are energetically favorable according to these calculations are selected. The mutual orientations of these oligomers are used to simulate absorption spectra using an exciton model. All structures show dominant blue-shifted spectra, like the experimental spectra. At very high concentrations, the experimental peak shifts to the red end of spectra. Red shifts can be explained theoretically, by simulation of very densely packed molecules.

Chapter 6 describes absorption spectra of four porfyrin dimers in toluene solutions. Porphyrines are pancake-like molecules containing two perpendicular transition dipole moments. The experimental absorption spectra are explained with the aid of simple exciton models. To account for the two perpendicular transition dipole moments, the exciton model presented in Chapter 5 is extended. The orientations and rotational freedom of the monomers comprising a dimer explain the spectral changes in the absorption spectra.

This Thesis uses the quantum theory at various levels. Both tunneling and the excitonic interactions between molecules involved in tunneling processes can be described only by the quantum theory. This theory is well equipped to explain experimental data but at the same time appears to yield more questions than answers. This Thesis reports on the fascinating interplay of question and answer between the quantum mechanics of molecular processes and our knowledge of observable processes

SAMENVATTING

Tunneltijden en excitonic interacties tussen kleurstofmoleculen

Samenvatting

Dit proefschrift bestaat uit twee met elkaar verband houdende delen. Het eerste deel (de hoofdstukken 2 en 3) beschrijft de resultaten van een fundamenteel-theoretische studie van de interpretatie van de kwantummechanica en met name van tunnelprocessen. Het tweede deel (de hoofdstukken 4 t/m 6) geeft de experimentele resultaten weer van spectroscopisch onderzoek van de kwantummechanische wisselwerking tussen kleurstoffen, die bij electronenoverdracht door middel van tunneling een rol kunnen spelen.

De formulering van de kwantumtheorie aan het begin van de 20e eeuw wordt niet voor niets een wetenschappelijke revolutie genoemd, waarvan de gevolgen voor ons fysische wereldbeeld tot op heden merkbaar zijn. De kwantummechanica heeft weliswaar indrukwekkende successen geboekt met betrekking tot het voorspellen van de uitkomsten van experimenten, maar de interpretatie van de theorie is nog altijd omstreden. De kwantummechanica doet weliswaar gedetailleerde en toetsbare voorspellingen over de resultaten van experimenten maar het is lang niet altijd duidelijk wat deze theorie betekent voor systemen, die zich kwantummechanisch gedragen, als er geen meting heeft plaatsgevonden. Er bestaan daarom meerdere interpretaties van de kwantummechanica, waarvan er twee in hoofdstuk 2 met elkaar worden vergeleken, te weten (i) de orthodoxe interpretatie, die ook wel de Kopenhaagse interpretatie wordt genoemd omdat deze gepropageerd werd door de zogenaamde Kopenhaagse school rond Niels Bohr en die inhoudt dat de kwantummechanica geen enkele uitspraak kan doen zolang er niet gemeten is en (ii) de causale interpretatie die inhoudt dat een deeltje, ongeacht of een meting heeft plaatsgevonden, een zekere plaats en snelheid heeft. In de causale interpretatie van de kwantummechanica is er geen speciale rol weggelegd voor de experimentator. Binnen deze interpretatie kunnen 'trajectories' of paden uitgerekend worden, die de plaats als functie van de tijd weergeven. De beide interpretaties zijn empirisch gelijkwaardig, d.w.z. zij voorspellen dezelfde experimentele uitkomsten.

In hoofdstuk 2 wordt de betekenis van de beide bovengenoemde interpretaties toegelicht aan de hand van het begrip 'tunneltijd'. Tunnelen is het kwantummechanische fenomeen dat een deeltje niet voldoende energie bezit om over een potentiaalbarrière heen te gaan en toch aan de andere kant verschijnt. Tunneltijd vraagt naar de tijd die een deeltje erover doet om te tunnelen. Nu is tijd in de kwantummechanica een lastig begrip omdat deze grootheid in de kwantummechanica alleen als parameter fungeert, en niet als operator, die met een waarneembare grootheid correspondeert. Het is daarom interessant om te kijken wat de beide verschillende kwantummechanische interpretaties te zeggen hebben over de tunneltijd. Binnen de orthodoxe interpretatie is het strikt gesproken niet mogelijk om over tunneltijd te spreken omdat er geen éénduidige tijdsoperator bestaat met een verwachtingswaarde, die via een experiment geobserveerd kan worden. In de causale interpretatie geeft ieder pad een mogelijk traject voor een tunnelend deeltje weer. De kans dat een deeltje zich langs een bepaald pad beweegt, wordt bepaald door de bijbehorende dichtheidsfunctie. Op deze manier uit zich in deze interpretatie het stochastische

karakter van de kwantummechanica. De transmissietijd is dan gedefinieerd als de tijd die een elektron in de potentiaalbarrière verblijft, d.w.z. de tijd tussen het moment, dat het deeltje de potentiaalbarrière binnengaat en het moment, waarop het aan de andere kant ervan verschijnt. M.b.v. de paden kan nu een gemiddelde transmissietijd worden gedefinieerd, gebruikmakend van stationaire golffuncties en tijdafhankelijke, Gausische golfpakketjes. De golfpakketjes komen aan vanuit het oneindige, gaan naar het oneindige, en ontmoeten onderweg een potentiaalberg, waardoor ze gereflecteerd of doorgelaten worden. Als een elektron van één kleurstofmolecuul naar een ander kleurstofmolecuul gaat, kan dat proces ook als tunneling worden beschreven omdat het medium tussen de kleurstofmoleculen een hoge potentiaalbarrière vormt. In dit proefschift zijn de media, die gebruikt zijn in de experimenten polymeer films en apolaire oplosmiddelen. Het in hoofdstuk 2 beschreven model is in de literatuur gangbaar maar niet toepasbaar op het systeem van twee kleurstofmoleculen waartussen electronenoverdracht plaatsvindt, omdat de elektronen die bij de kleurstofmoleculen behoren niet uit het oneindige aankomen en evenmin naar het oneindige gaan. Een beter model, een dubbele potentiaalput, wordt daarom in het volgende hoofdstuk behandeld. De conclusie van hoofdstuk 2 is dat binnen de causale interpretatie een transmissietijd gedefinieerd kan worden, als er gebruik gemaakt wordt van tijdsafhankelijke golfpakketjes.

Hoofdstuk 3 illustreert het voorgaande aan de hand van het tunnelen van een deeltje door een potentiaalbarrière tussen twee potentiaalputten, de z.g.n 'dubbele put'. Voorbeelden daarvan zijn de primaire ladingsscheiding in het fotosynthetisch reactiecentrum, en in synthetische modelsystemen daarvan in de vorm van kleurstoffen, zowel in oplossing als in polymeerfilms. De laatste twee zijn in dit proefschrift spectroscopisch nader onderzocht. In deze moleculaire systemen vindt effectieve elektronenoverdracht plaats tussen natuurlijke pigmenten of synthetische kleurstoffen na absorptie van licht, leidend tot ladingsscheiding, d.w.z. vorming van electronen en pigment- of kleurstofkationen. Voor het transport van de vrijgekomen electronen tussen de verschillende natuurlijke of synthetische kleurstoffen moeten de electronen meestal een slecht of niet geleidend medium passeren, overeenkomend met een potentiaalbarrière. Zolang het electron een hogere kinetische energie heeft dan de hoogte van de barrière , kan de elektronen overdracht met een klassieke theorie worden beschreven. Is de kinetische energie van de electronen echter lager dan de hoogte van de barrière, dan kan de elektronen overdracht niet meer klassiek worden beschreven en moet het transport-mechanisme kwantummechanisch als 'tunneling' worden opgevat, Deze tunneling is bijvoorbeeld in de fotosynthese bij lage temperatuur experimenteel aangetoond.

Hoofdstuk 3 beschrijft het systeem van de kleurstofmoleculen en het tunnelende elektron met een dubbele potentiaal put. Elke put stelt een kleurstofmolecuul voor en de ruimte tussen de moleculen een potentiaalberg. Het formalisme van de causale interpretatie wordt toegepast om de transmissietijd te definiëren, die uit de paden kan worden berekend. Er wordt ook een methode aangegeven om die transmissietijd te berekenen zonder dat de paden behoeven te worden uitgerekend. Er wordt een distributiefunctie

voor de aankomsttijden gedefinieerd, waaruit de gemiddelde aankomsttijd van de tunnelende elektronen aan het begin en het eind van de barrière berekend kan worden. Omdat de distributiefunctie voor de aankomsttijden en dus de gemiddelde aankomsttijden en daarom ook de transmissietijd gedefinieerd zijn zonder dat er metingen worden verricht, is de conclusie van hoofdstuk 3 dat de definitie van transmissietijd alleen betekenis heeft binnen de causale interpretatie. De vraag aan het eind van hoofdstuk 3 is óf, en eventueel hoe, de gemiddelde transmissietijden experimenteel bepaald kunnen worden.

De in de hoofdstukken 2 en 3 ontwikkelde theoretische modellen zijn in feite te simplistisch om zonder meer toegepast te kunnen worden op reële systemen, waarin electronenoverdracht plaatsvindt tussen een electrondonor en een acceptor, waarvan één van de twee met licht wordt aangeslagen. In kleurstoffilms en oplossingen met een relatief hoge kleurstofconcentratie kunnen de intermoleculaire excitonische interacties tussen een aangeslagen, electron donerend molecuul met omringende moleculen in de grondtoestand niet worden verwaarloosd. Voor een correcte beschrijving van de electronenoverdracht in een dergelijk systeem moeten deze exciton interacties worden meegenomen. In de hoofdstukken 4 t/m 6 wordt beschreven hoe deze interacties m.b.v. absorptie- en emissiespectroscopie zijn bepaald.

In hoofdstuk 4 wordt een theoretische beschrijving gegeven van de effecten van exciton interacties op het absorptiespectrum van kleurstofmoleculen in ongeordende films. Bij een lage concentratie zijn deze als monomeer aanwezig, maar op statistische gronden zijn er ook moleculen die zo dicht bij elkaar zitten dat ze dimeerachtige structuren vormen, aangeduid als 'concentratie paren' met een karakteristiek absorptiespectrum. De aanwezigheid van concentratieparen beinvloedt ook de emissie eigenschappen van de kleurstoffilms. Als daarin een monomeer licht absorbeert, komt het molecuul in een aangeslagen toestand en kan onder uitzending van fluorescentie terugvallen naar de grondtoestand. De excitatie kan ook worden overgedragen naar een nabijgelegen concentratie paar, waardoor de fluorescentie wordt gedoofd (Engels: 'quenched'). Het doel van hoofdstuk 4 is het voorspellen van de invloed van concentratieparen in de buurt van een geëxciteerd monomeer op het absorptiespectrum en de fluorescentie van films en geconcentreerde oplossingen van kleurstoffen. De energieoverdracht van monomeer naar concentratie paar d.m.v. het z.g.n. Förster mechanisme kan over vrij grote afstanden plaatsvinden (1-5 nm). M.b.v. statistiek kan berekend worden hoeveel concentratieparen aanwezig zijn bij een bepaalde concentratie van kleurstof moleculen. In de literatuur gaat men ervanuit dat de twee monomeren, die een concentratie paar vormen ten opzichte van elkaar willekeurig georiënteerd. Als de paren willekeurig georinteerd zouden zijn en alle afstands- en oriëntatiefluctuaties worden meegenomen, blijken er theoretisch niet genoeg paren te zijn om deze spectraal te kunnen waarnemen. Omdat de meeste kleurstoffen langgerekt of pannekoekvormig zijn zullen de paren niet willekeurig georinteerd zijn maar ten opzichte van elkaar een voorkeursorintatie hebben, waardoor de efficiëntie van de fluorescentiedoving toeneemt. De theoretisch voorspelde spectrale veranderingen als gevolg van de aanwezigheid van concentratieparen komen goed overeen met de experimenteel gevonden resultaten. Er is een analytische

uitdrukking ontwikkeld voor de veranderingen van het absorptiespectrum ten opzichte van die van het monomeer als gevolg van de aanwezigheid van willekeurig georiënteerde dimeren. De interacties tussen de kleurstofmonomeren, uitgaande van één dominant overgangsdipoolmoment, in een dimeer worden m.b.v. een exciton model beschreven. Voor een realistischer beschrijving moeten homogene en inhomogene lijnverbreding en fluctuaties in de monomeer-monomeer afstand meegenomen worden. Uit de simulaties van de vorm van het absorptiespectrum kan worden geconcludeerd dat het dimeer spectrum verbreed is met een grotere verschuiving naar kortere dan naar langere golflengte ten opzichte van het monomeer spectrum. Er is echter een behoorlijk hoge concentratie kleurstoffen nodig om het spectrale profiel met een dominante blauwverschuiving van deze willkeurig georiënteerde dimeren te kunnen waarnemen, maar bij dergelijke concentraties is er geen sprake meer van geïsoleerde dimeren,, dan moeten alle onderlinge intermoleculaire interacties in ogenschouw genomen worden. Modellering daarvan geeft alleen een verbreding van het spectrum te zien ten opzichte van dat van het monomeer.

Hoofdstuk 5 beschrijft de veranderingen van het absorptiespectrum als gevolg van concentratie veranderingen van sigaarvormige erythrosine-b (Ery B) kleurstofmoleculen in een polyvinylalcohol (PVA) polymeerfilm. Bij lage concentratie zijn vooral monomeren aanwezig, resulterend in monomeer absorptiespectra. Meting van de fluorescentiedoving laat de vorming van concentratieparen zien bij verhoging van de concentratie, maar deze zijn niet te zien in de absorptiespectra. Verdere verhoging van de concentratie leidt tot verbreding van het absorptiespectrum, in overeenstemming met de theorie uit hoofdstuk 4. Bij nog verdere concentratieverhoging gaan de kleurstofmoleculen zich ten opzichte van elkaar ordenen. Voorkeursoriëntaties voor dimeren, trimeren en tetrameren zijn berekend met behulp van moleculaire mechanica, en structuren, die op grond van deze berekeningen energetisch voordelig zijn, zijn daaruit geselecteerd. De onderlinge oriëntaties van deze oligomeren worden gebruikt om spectra te simuleren volgens het exciton model. Deze structuren blijken alle een dominante blauwverschuiving hebben, die ook in de experimentele spectra wordt gevonden. Bij hoge concentraties verschuift het experimentele spectrum naar het rode gebied in overeenstemming met de theoretische voorspelling van de verschuiving als de moleculen zich op zeer korte afstand van elkaar bevinden.
Hoofdstuk 6 beschrijft de absorptiespectra van vier verschillende porfyrinedimeren in tolueen oplossing. Porfyrines zijn pannekoekvormige moleculen met twee onderling loodrechte overgangsdipoolmomenten in het vlak van het molecuul. De experimentele absorptiespectra kunnen met behulp van een eenvoudig exciton model worden verklaard. Om rekening te houden met de twee loodrecht op elkaar staande overgangsdipoolmomenten is het exciton interactie model uit de vorige hoofdstukken uitgebreid. De spreiding van de oriëntaties en de daarvoor beschikbare bewegingsvrijheid van de monomeren in de verschillende dimeren kunnen de veranderingen in de absorptie spectra vrij goed verklaren.

Het werk, dat in dit proefschrift wordt beschreven maakt op verschillende niveaus gebruik van de kwantummechanica. Zowel tunneling als de exciton interacties tussen de moleculen waartussen de tunneling optreedt, zijn alleen kwantummechanisch te beschri-

jven. De ontwikkelde theorie kan veel experimentele gegevens goed verklaren, maar heeft zoals gewoonlijk meer vragen opgeroepen dan dat het antwoorden gegeven heeft. Dit proefschrift is een verslag van het fascinerende vraag- en antwoordspel tussen de kwantummechanica van moleculaire processen en wat wij van die processen (menen) waar te nemen.

Na vele studies en vele jaren werkervaring begon ik (Regina Geerta Stomphorst) in 1995 op partime basis aan het onderzoek, dat leidde tot dit proefschrift. De eerste helft van dit onderzoek, vooral het fysisch chemische werk, heb ik aan de Universiteit in Wageningen verricht (quantum mechanica op de werkvloer). De tweede helft van het onderzoek verbleef ik aan de Vrije Universiteit in Amsterdam en werkte ik nauw samen met dr. G. van der Zwan (de wiskundige kant van de quantum mechanica). Dr. J. Uffink uit Utrecht werd mijn tweede copromotor omdat ik enorm geboeid raakte door de interpretatie mogelijkheden van de quantum mechanica (grondslagen van de quantum mechanica). Op het ogenblik ben ik als toegevoegd docent verbonden aan de Wageningen Universiteit om het college 'chemische binding' te verzorgen.

DANKWOORD

Tenslotte.....

wil ik verschillende mensen bedanken.

Laat ik beginnen in Wageningen. De eerste helft van mijn promotietijd speelde zich daar af onder begeleiding van Tjeerd Schaafsma. Tjeerd, jij hebt de hele promotie tijd een vinger aan de pols gehouden en daarom wil ik je bedanken voor je begeleiding als promotor. Van de vakgroep moleculaire fysica wil ik verder nog een paar mensen met name noemen: Frank Vergeldt, ik vond het prachtig dat ik mocht mee genieten van je enorme voorraadschuur aan programmeer en andere 'tomba la bomba'. Rob Koehorst, dank je voor de zorg waarmee je de experimenten hebt uitgevoerd. Shirley van der Wiel, omdat door jou alles zo soepel kon verlopen. Ook anderen van de vakgroep moleculaire fysica en de vakgroep organische chemie: bedankt voor de samenwerking.

Het hoogte punt uit mijn Wageningse tijd was het woongenot bij de VERZAMELING. Daarom: Emiel, Frank, Iris, Janine, Rienke, Menno, Jasper, Michael: 'Ik vond het relaxed om koe 31 in hema tenue met griep tussen de oren en een Australisch dreadlockhoofd op zeezicht te zien knutselen'.

Het tweede gedeelte van mijn promotie tijd speelde zich in Amsterdam af. Dit is tevens de zetel van Gert van der Zwan, mijn copromotor. Gert, ik heb genoten van je fundamentele aanpak. Bedankt dat je je enorme wiskundige ervaring met mij wilde delen. Ik vond het prettig dat jij (en met jou, de vakgroepen waartoe je behoor(de)t) me halverwege mijn promotietijd de gelegenheid bood om naar Amsterdam te komen.

De vakgroep moleculaire biofysica in Utrecht wil ik bedanken voor de mogelijkheid om bij hen experimenten uit te voeren. Marc van Zandvoort (Utrecht en Maastricht) wil ik bedanken. 'Wij werken samen, noem mij nooit, nooit begeleider' (citaat). Ik vond de samenwerking leuk, maar helaas is koken nog steeds niet mijn hobby.

Om Jos Uffink, mijn tweede copromotor te bedanken, weet ik niet goed waar te beginnen. Jos, door jou ging er een nieuwe wereld voor me open: filosofische implicaties van theorieën, mooi taalgebruik en nog veel meer. Je introduceerde mij bij de quantum club. Dit illustere gezelschap verzorgt iedere maand een intellectueel uitdagende avond. Maar bovenal heb ik heel veel van je geleerd. Veel daarvan hoop ik lang te onthouden maar de voorschriften voor het dinee in het keurige Oxford ben ik nu al vergeten!

Van het thuisfront wil ik eerst mijn vader en moeder noemen. Pa en ma jullie hebben mij genen en een goede opvoeding gegeven. Dat geeft zo'n soort boekje, maar om jullie niet helemaal de schuld te geven, zal ik toegeven dat er ook een beetje van mezelf bijzit.

Wouter heeft mijn belangstelling voor natuurkunde aangewakkerd, pa zag dat er filosofie aan ontbrak en Roswita heeft met haar krantenknipsels mij een duw in de goede richting gegeven: bedankt.

Thea, vaardig met de pen: dank je dat je dapper gepoogd hebt mij journalistiek verantwoord te laten schrijven. Ook bedankt voor het ontwerpen van de voorkant.

Met Hans, Ina, Swanny en Ton leef ik in de waan van een goed 'hei en wij' gevoel. Dat helpt altijd, ook voor een proefschrift.

Mijn paranimfen, Richard en Joke zijn beiden van grote invloed geweest op de voortgang van dit proefschrift.

Richard, we hebben al veel samen gedaan: lachen om deltafuncties en voortbewegende golfpakketjes volgens de achterwaartse methode in Algol60. Verdrietig zijn om Gon. In jouw auto (de cockroach) rondgereden door het prachtige, uitgestrekte afrikaanse landschap. Veel van de tekst in dit boekje heb ik bij jou op de vloer in Oshakati geschreven. Bedankt en op naar een volgend project.... .

Joke, het voorwoord heb ik voor jou geschreven, ter bevordering van de dialoog.
Het proefschrift is klaar, zodat we dit onderwerp van ons lijstje 'voor tijdens de wandelingen' af kunnen strepen. Je hebt me goed op de been gehouden!